


A New Classification of Existing Techniques for Error/Defect Detection in Image Processing

Haider Abdulzahra Saad Alsaide¹, Mohammad Reza Soltanaghaei², Wael Hussein Zayer Al-Lami³, Razieh Asgarnezhad⁴

1- Department of Computer Engineering, Isfahan (Khorasgan) Branch, Islamic Azad University, Isfahan, Iran.
Email: headerabd917@gmail.com

2- Department of Computer Engineering, Isfahan (Khorasgan) Branch, Islamic Azad University, Isfahan, Iran.
Email: sultan@khuisf.ac.ir (Corresponding author)

3- Electronic Department, Amara Technical Institute, Southern Technical University, Missan, Iraq.
Email: wael.zayer@stu.edu.iq

4- Department of Computer Engineering, Aghigh Institute of Higher Education Shahinshahr, 8314678755, Isfahan, Iran.
Email: r.asgarnezhad@aghigh.ac.ir

ABSTRACT:

The detection of defects is important in quality control in manufacturing. These defects raise the costs incurred by enterprises, compress the service life of simulated products, and result in the expansive destruction of resources, thereby significantly harming people and their safety. Defect detection and classification need to be feasted as unique problems associated with the field of artificial vision. We categorize the defects like electronic components, pipes, welded parts, textile materials, etc. We express artificial visual processing techniques aimed at comprehending the charged picture in a mathematical/analytical manner. Recent mainstream and deep-learning techniques in defect detection are studied with their features, stability, and weaknesses explained. We resume with a survey of textural defect detection based on statistical, structural, and other methods. We investigate the application of ultrasonic testing, filtering, deep learning, machine vision, and other technologies utilized for defect detection to offer a new classification. In addition, high precision, high positioning, fast detection, and small objects through examination are the biggest challenges in applying quality detection.

KEYWORDS: Machine Learning, Deep Learning, Defect Detection.

1. INTRODUCTION

Due to failure in design and machine production equipment, the defect of the complex industrial processes, like internal holes, pits, abrasions, and scratches arise unfavorable working conditions. Products easily disintegrate and be inclined to weariness because of daily application. These defects raise the costs incurred by enterprises, compress the service life of simulated products, and result in an expansive destruction of resources, thereby generating significant harm to people and their safety [1]. Therefore, catching defects is a center competency that companies possess to enhance the quality of the simulated products without influencing production. Automated defect detection technology evident benefits over manual detection. It adjusts to an inappropriate environment and achieves with high precision and efficiency. The earlier research on this scope decreases the production cost enhance production efficiency and product quality for the intelligent transformation in industry.

Defect detection and classification need to be feasted as unique problems associated to the field of artificial vision. The general purpose of mimicking human vision is to determinate and organize a subject. These two objectives bonded together. We handle both classes and concentrate on the precise solutions that intensely associated to visual processing

Paper type: Research paper

<https://doi.org/>

Received: 19 April 2024; revised: 11 May 2024; accepted: 27 June 2024; published: 1 September 2024

How to cite this paper: H. A. Saad Alsaide, M. R. Soltanaghaei, W. H. Zayer Al-Lami, and R. Asgarnezhad, “A New Classification of Existing Techniques for Error/Defect Detection in Image Processing”, *Majlesi Journal of Telecommunication Devices*, Vol. 13, No. 3, pp. 117-136, 2024.

methods, particularly on inspection techniques in industrial applications. Quality control is an essential characteristic in the industrial production line. Some approaches employed to evaluate the quality of a process. Relying on the method used to determine a defect on a surface/volume, quality control strategies categorized as destructive or non-destructive (See Fig. 1). Non-destructive testing aims at observing an element to detect a defect without extracting samples from it or perpetually impairing it.

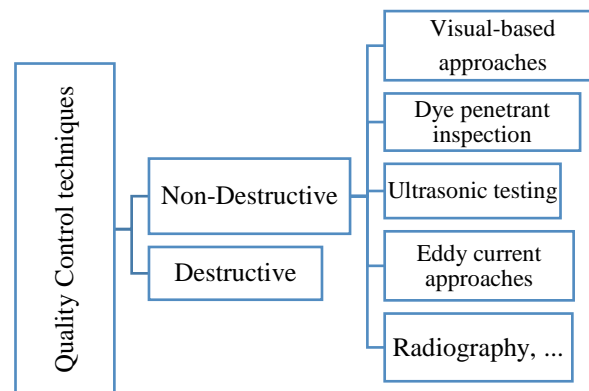


Fig. 1. Categorization of the quality control techniques.

Many researchers reviewed defect detection technologies to supply references for the application and research of defect detection technology. We outlined the application of hyperspectral [2], pulsation spectrum, infrared [3], etc. For surface defect detection, Xianghua Xie [4] contemporary advancements in surface detection utilizing computer vision and image processing techniques. By approximating of the findings of past investigations, it revealed that surface defect detection based on image processing needs high real-time performance in industrial applications. For fabric defect detection, researchers [5]-[6] investigated the application and development of defect detection methods typically employed in the textile fabrics from the standpoint of defect detection development of the textile industry production. Thermal imaging technologies employed in many industrial areas. I. Jorge Aldave [7] concentrated on the comparison of consequences received with commercially general non-experimental IR techniques to supply references for non-destructive defect detection. Defect detection technology is a hot topic in the enterprise. Defect detection technology is a desirable topic in the enterprise. Nevertheless, researchers categorize product defect types [8], the main detection techniques, summary of applications of defect detection technology, existing equipment for defect detection, etc. The review of the research status of relevant technologies have yet to be realized.

The visual based approach is one of the most common defect detection procedures in industry. Nevertheless, the traditional visual assessment is a non-measurable process with unstable and subjective outcomes. It caused authors to devise new automated defect detection systems with challenging requirements because of the complexity and individuality of any specific problem to decode. Nevertheless, a system relies on the fabric effects of the surfaces to observe the environmental requirements.

The definition of a defect and its categorization is a manner that effects on series of subjective decisions. The main features of a defect depend on the desired precision and resolution of the detection approach; the size of defects vary among industrial applications. It recommended to specify a quality criterion of the outcome in every industrial application before organizing and executing the automated system.

This study organizes the common defects of electronic elements, pipes, welding regions, and fabric textiles. It outlines the mainstream deep learning technology for defect detection with its application status to analyze the application situation of the major defect detection equipment, to supply reference for defect detection technology in approach and useful application.

This study contained as follows. In Sect. 2, we present a taxonomy of defects that appear on metal surfaces. In Sect. 3, we represent the defect detection technologies. In Sect. 4 and Sect. 5, we reviewed the existing machine learning and deep learning methods for defect detection. In Sect. 6, we express the challenges and finally concluded the conclusion.

2. TAXONOMY OF DEFECTS

In the industrial exhibition area, quality control strives at maintaining a quality level or at localizing the defects for

further repair. Conventional detection techniques deal with regular, macro-sized and complex deviations of surface defects. Basically, every artificial optical defect detection method strived to detect defect and classified them for additional processing. For a reasonable classification, industrial applications require well-structured databases of the possible defect types. Due to the randomness and essence of the defects that can appear in the operation scenarios, showing such a general and complete database for a classifier is challenging way.

In this area, basically every application utilizes a material-based defect classifier. The proposed taxonomy of defects organized to two major groups: visible and palpable. It is worth mentioning that the categorization is basically and not sufficient for systems with specific conditions. It delivered a strong and reliable basis for a classification with artificial intelligence system. The essential assumption of this defect categorization is a hardly subjective decision. This decision is based on a threshold and a logical-based illustration of the size ratio of both the element and the defect. Thus, the structure of the proposed taxonomy organized by size ratios and spatial features.

3. DEFECT DETECTION TECHNOLOGIES

Product defect detection technology detects the surface and internal defects of outcomes. The defect detection technology guides to the detection technology of spot, pit, scratch, and color differences. Internal defect detection technology contains internal flaw detection, hole detection and crack detection [9]. Some techniques used to detect product quality. These consists deep [10], magnetic powder [11], eddy current testing [12], ultrasonic testing [13], and machine vision [14] detection methods. Moist magnetic particle detection combines the magnetic powder in all liquid media. Magnetic powder observes the location of defects via liquid force and the interest of the superficial magnetic domain [15]. The moisture detection technique has high sensitivity [16]. Dry Magnetic powder testing [17] connects magnetic powder onto the cover of the magnetized workpiece for defect detection. This technique employed for the local examination of defects in large casting, welding parts, and other features that are inappropriate for moist detection.

The constant magnetic particle detection method notices defects in magnetic break or powder under the external magnetic field [18]. This method employed to monitor the defects in the external magnetic field. Some elements effect on the precision of magnetic powder testing contain roughness and the profile of the test piece, the geometrical features of defects, the specified magnetization approach, and the quality of operators [19]. The factors that affect the sensitivity of testing are imaging reagents, the performance of fluid, the quality of operators, and the impact of defects. Factors that affect the accuracy of the detection of vortex current are the parameters of material and the shape of the test piece [20].

The ultrasonic testing product influenced by the angle between the defect surface and the ultrasonic propagation direction [21]. If the angle is vertical, the signal produced is strong and the defect is efficiently detected. If the angle is horizontal, the signal returned is weak in which detecting make a leak straightforward. Thus, choosing the proper detection sensitivity and corresponding search to decrease leakage detection is necessary [22]. The factors influence ultrasonic testing contain projection direction, investigation effectiveness, sound connection quality, and instrument operating frequency [23].

Machine vision detection consists of image acquisition, defect detection, and classification. Because of accurate, non-destructive, and low-cost characteristics, machine vision is employed. Machine vision recognizes objects based on the color, texture and geometric features of objects. The quality of image acquisition defines the difficulty of image processing. The quality of the image processing algorithm impacts the accuracy, error detection rate of defect detection, and classification [24]. The deep learning approach is likewise a defect detection approach that is based on image processing, which utilized to acquire proper features in massive data [25]. Table 1 displays a comparison of employed product defect detection approaches.

Table 1. Comparison of standard defect detection techniques

Method	Advantage	Disadvantage
Ultrasonic testing	Easy to use Strong penetration High sensitivity Automatic detection Portable equipment	Unsuitable for complex work pieces
Machine vision detection	High precision Automatic detection Many applications	Surface detection only
Magnetic powder testing	Visualization in shape, size, and position Suitable for any size High precision Low cost	Difficult automatic detection Influenced by geometric shape and test pieces Limited to ferromagnetic materials

Osmosis testing	High sensitivity Affectless on shape and material type	Difficult detection for porous materials and automatically Slow detection speed
Eddy current testing	Non-contact detection Fast detection speed High sensitivity Automatic detection Suitable for high temperature environments	Low detection accuracy Difficult detection for deep detection Limitation for applicable materials Not-visualization for shape and size
X-ray testing	Non-destructive detection Strong penetration Affectless on material and structure Easy operation	Radiation affects

The traditional defect detection methods and the popular deep learning defect detection methods have their benefits. These methods are positively concentrated. Osmosis testing technology [26] is an applicable for detecting defects in highly absorbent and non-porous materials.

Most of the traditional detection techniques need to depend on manual assistance to complete, the equipment product cost increased, which is not adaptable and defined by the equipment life and manufacturing accuracy. Creative defect detection methods, especially machine vision and deep learning techniques [27], have evolved as one of the important technologies for automating defect detection due to their versatility and lack of support on human assistance.

Corresponded to traditional defect detection techniques, the new technologies present more useful examination results and decrease costs. Though these nevertheless depend on large amounts of known data to guide model updates and enhance inspection accuracy.

3.1. Artificial Visual Processing Techniques

The primary purpose of visual-based approaches is to comprehend the world both natural and artificial illustrations. The procedure in the latter is to recognize images to look for a mathematical/logical connection between the input and representations. This connection is a change from the input to the model to reduce the information included in the image to appropriate information for the application domain.

Image representation approximately separated into four levels, as depicted in Figure 3. The order of image presentation and the background functions/algorithms facilitated as low and high-level image processing. Low-level processing techniques do not employ prior knowledge about the content of the image. It means that the techniques that belong to this group applied to every image. This group contains: (1) image compression; (2) pre-processing; (3) sharpening; and (4) edge extraction techniques.

The higher-level processing techniques are complicated and work above the mathematical model of the image by selecting classifiers and where imitating the human understanding is required.

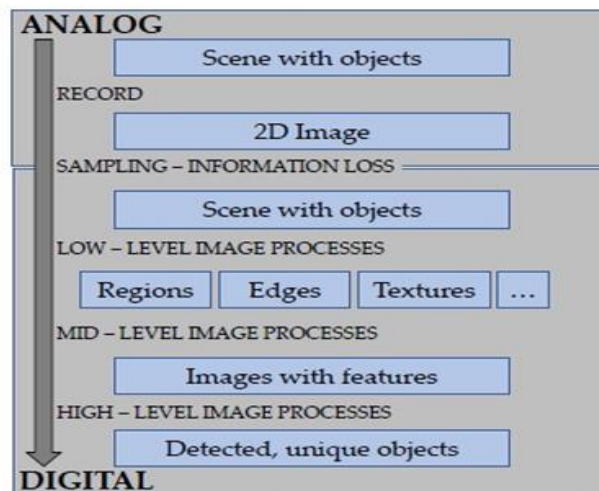


Fig. 2. The hypothetical levels of image presentation for image analysis. The modification from the analog to the digital domain consequences in some information loss.

As illustrated in Fig. 2, to achieve the level of the picture with content, several features of the image have to be conveyed. Two different principles devote for unaffectedly emerging visual statements. The one achieved about the object to be found. The second performed with no given information about the object; but with knowledge on the environment. Most non-destructive visual examination techniques to find surface irregularities apply textures, performed by low-level processes. These principles can be replicated in artificial systems, but utilizing distinct methods. To identify particular defects on a surface, a descriptor database of the possible defects must be installed.

Textural Defect Detection: Surfaces supply unique information for artificial visual detection. The latter utilize various types of texture analysis because the general task of defect detection is a surface analysis problem. The favorable and accurate method to represent a texture is to extract its unique features, although this turns out to be a demanding task.

3.2. The Traditional Method for Defect Detection Technology

Non-destructive defect detection of outcomes is utilized in manufacturing to analyze the advantages and disadvantages of diverse algorithms and enable to comprehension of the algorithms. We concentrate on the application status by the combination of classical defect detection and different algorithms. Figure 3 illustrates the diverse defect detection techniques and their affiliated performance results or outlines for non-destructive defect detection.

The ultrasonic defect detection techniques utilized to detect the defects in the internal structure of the sample. Thus, the results contemplated in the performance of the ultrasonic signal [28]. The results, as illustrated in [29], indicates that the ultrasonic defect detection techniques have the advantages of fast detection speed and simple operability. They also have special advantages in detecting defects in the internal material and structure as well as the size of the product. However, this method is unsuitable for workpieces with complicated structures with low detection efficiency.

Ultrasonic methods are ineffective for catching defects on the upper surface of the sample since a nonlinear relationship exists between the defect position and the signal obtaining the time, which shows to the defect to be arranged to the unaffected pass lock end [30].

The denser the allocation of the real position of the effect, the higher the confidence of the “trailing” spectacle of the direct access wave signal on the map. The machine vision-based defect detection techniques are appropriate for the detection of surface defects in products, which has reached up to 88.60% accuracy in binary defect detection problems [31]. The accuracy of defect detection over scratches, gaps, hierarchies, pitting, edge cracks, crusting, and inclusions achieve 95.30% [32]. The defect detection techniques based on filtering has a strong ability to explain the disruption signal and detection of the tool defect inside the machine.

To the categories of defect detection techniques for mechanical products, several other technologies are unrestricted like the X-ray image defect detection technology [33], Pulse magnetoresistance approach [34], and Acoustic emission technology [29].

Statistical Approaches: Statistical methods concentrate on study the spatial allocation of pixel values in a registered image. In this classification, it is achievable to calculate numerous publications and methods, varying from low-level to higher-order statistics, like histogram statistics, autocorrelation, local binary patterns (LBP) and others. Histogram effects and statistics support for both higher and low procedures with low computational cost. These functions include operations from statistics. It contains other histogram comparison statistics utilized for texture features, like L1 and L2 norm, EMD distance, divergence, Chi-square, and the normalized correlation coefficient. The technique catches defects by reviewing whether the distribution of the monitored data is distinct from a baseline recorded allocation in an adaptive manner.

$$\text{Sensitivity} = \frac{TP}{(TP + FN)} \quad (1)$$

$$\text{Speciticity} = \frac{TN}{(TN + FP)} \quad (2)$$

$$\begin{aligned} \text{Detection Success Rate} \\ = \frac{(TP + TN)}{(TP + FN + TN + FP)} \end{aligned} \quad (3)$$

where TP, TN, FN and FP devoted for true positive, true negative, false negative and false positive, respectively.

Structural Approaches: Structural Approaches (SA) concentrate on the spatial location of the texture components. These extracted from the texture and defined as texture primitives. Using spatial setup rules to texture primitives result in a dynamic texture model. The texture primitives are simple grey-scale regions, line features or individual pixels. These elements used in a mixture with placement rules which emanated from the geometric associations or spatial statistics of these primitives.

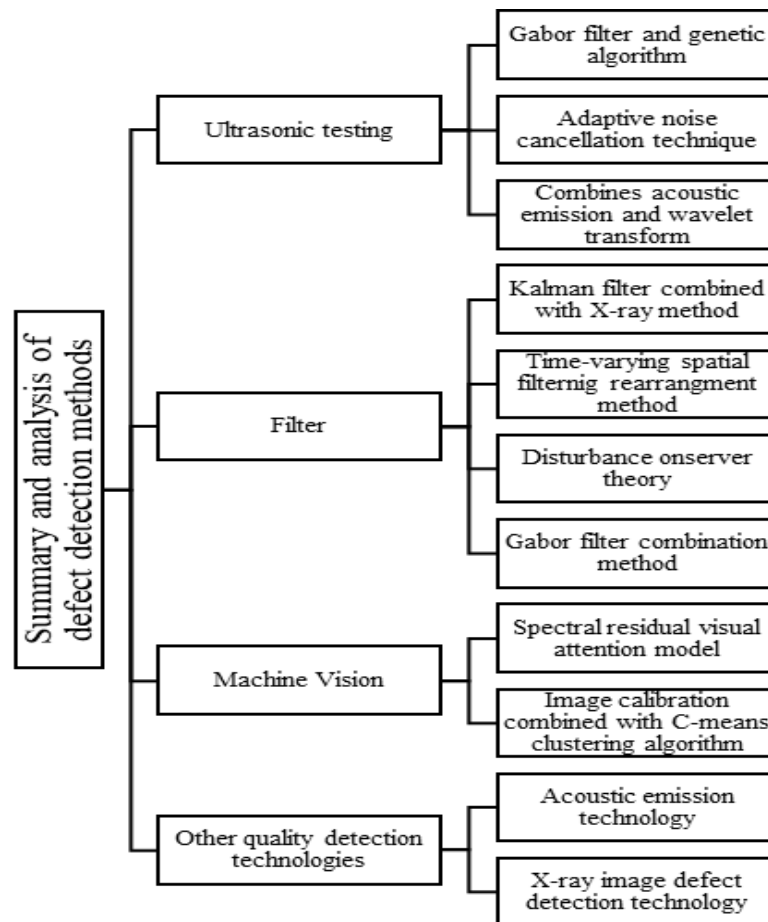


Fig. 3. Overview and analysis of defect detection techniques.

Filter-Based Approaches: Images represented by glimpsed features like edges, textures and regions (Fig. 3). Purifying these characteristics is one of the preliminary steps in image processing scope. It is a low-level process, and the edges diagnosed as spatial premature phase modifications in the image [35]. To drag edges, it employed some filters in the spatial part, like Sobel, Robert, Canny, Deriche, Laws and Laplacian filters. In most issues, working in this part implicates noise and difficulties to discover a plain kernel. Thus, converting the images into the frequency part with Fourier Transformation (FT) provides the power to efficiently filter the noise as represented in [35]. The fundamental logics converted the image into Fourier part and then filtered. After it, these logics reconverted into the spatial scope. The contrasts between the initial and processed images regarded as possible faults based on the involved procedure in the conversion [36].

The Fourier conversion relies on the whole image. These effects yielded it incapable to localize defects in the spatial part. The considerable solution is to use a FT for spatial reliance. If the window function be Gaussian, it results in the Gabor transform. The Gabor transform (GT) tries the optimal combined localization in these parts [37]. Two types of methods are of concerned. First one when some filters stowed in predetermined frequencies and directions to protect all conceivably emerging frequencies in the image and compute the correlation [38]. Nevertheless, this method is intensive to gain high distinction quality. Second one involves the performance of the optimal filters to associate with the selected recognition region, whereas acquiring the optimal sets is difficult [39].

With equivalent effects to the Gabor transform, Wavelet Transform (WT) illustrations employed as defect detectors [40]. WTs established on short waves of changing frequency and restricted period reached wavelets and supply provincial information from any directions on any input image [41].

Model-Based Approaches: Techniques based on model organized into three groups: (1) fractal, (2) autoregressive, and (3) random field models. Fractals recreate an effective role in the characterization of the natural surfaces, these firstly conveyed by Mandelbrot [42]. The primary idea of the autoregressive model (AR) is to describe texture characteristics based on the linear dependences of pixels [43].

Markov random fields techniques integrate both statistical and structural information of context conditional

commodities like pixels relying on their neighbor pixels [44] and classification problems [45].

Table 2. A preference of most typically used textural defect detection approaches.

Approach	Method	Reference
Statistical	Histogram	[46] [47]
	Co-occurrence matrix	[48] [49]
	Local binary pattern	[50]
	Other gray level statistics	[50] [51]
	Auto-correlation	[49] [52]
	Registration-based	[53] [54]
Structural	Primitive measurement	[55]
	Edge features	[56]
	Skeleton representation	[57] [58]
	Morphological operations	[59]
Filter based	Spatial domain filtering	[60]
	Frequency domain analysis	[61] [62]
	Joint spatial/spatial frequency	[63] [64]
Model based	Fractal model	[65]
	Random field model	[66]
	Texem model	[67]
	Auto-regressive	[68]
Other	Color texture analysis	[67] [63] [55]

4. MACHINE LEARNING FOR DEFECT DETECTION TECHNOLOGY

Here, the main direction is the emerging authority of the machine learning techniques. These techniques employed in all fields of product defect detection. The defect detection technology split into two major types: surface defect detection [69] and internal fault diagnosis [70]. Surface defect detection is equivalent to 'visual' detection, understanding from the target characteristics in an image with the benefit of deep learning image processing technology to organize and discover product defects, whereas internal defect diagnosis is equivalent to 'Auditory' detection, the diagnosis of defects in rotating parts like directions by means of modal analysis utilizing digital signals in the time or frequency part. We discovered the defect detection procedures and improved feature extraction [71]. Because Tool Condition Monitoring is a challenging, authors proposed a new ML-based method to describe failure symptoms of cutting tools in the time-frequency domain in 2024. This investigation concerns five cutting tools, and the results validated utilizing the Fast Fourier Transform, Short-time Fourier Transform, Empirical Mode Decomposition, and Variation Mode Decomposition methods. These methods applied to demonstrate that the suggested methodology better recognizes failure symptoms corresponded to other methods. One benefit of the suggested method is to regrade a lower order of the system results in time–frequency domain [72]. The canonical correlation analysis (CCA) is an issue for the lack of robustness against outliers. The authors in 2024 suggested a method to overcome this issue. The rendition and benefits of the suggested methods illustrated with two case studies. The results of two case analyses demonstrate that the RCCA and RSCCA methods have high robustness against outliers, and the robust FDD method is able to produce reliable results even if using the low-quality training data with outliers [73].

5. DEEP LEARNING FOR DEFECT DETECTION

Deep learning technology evolved to completed success in object detection, intelligent robot, and other fields. Deep learning has a type of neural network structure with multiple convolutions layer.

By integrating low-level characteristics to construct a conceptual high-level presentation of attribute, the data were sufficiently advanced in abstract ways like edge and shape to enhance the significance of the deep learning algorithm [74].

Thus, many researchers attempt to employ deep learning technology to defect detection of product and enhanced the product quality [75]- [76].

Table 2 outlines the benefits and drawbacks of deep learning techniques typically employed in product defect detection. It especially contains convolutional neural network (CNN) [77], autoencoder neural network [78], deep residual neural network [79], full convolution neural network [80], and recurrent neural network [81].

Table 3. Deep learning defect detection techniques.

Method	Advantage	Disadvantage
Convolutional neural network	Strong learning ability High-dimensional data High-order features	Increase the network depth
Auto encoder neural network	Good representation ability Good robustness	Consist the dimension of the input
Depth residual neural network	Better classification performance Not-overfitting	Cooperate with deeper depth
Full Convolutional neural network	Extracting the feature with any size image Obtaining the high-level semantic prior knowledge	Low speed of model
Recurrent neural network	Learning the essential features with fewer sample data	Overfitting phenomenon due to increasing the number of iterations

Deep learning is one of the quickest developing fields in computer sciences due to its capability to translate approvingly complex problems [82]. The decadent collection of classic machine learning methods resulted in the expansion of deep learning that earned its motivation from statistical learning. Most of the methods noted in the earlier sections regarded as traditional solutions, where the emphasis is on the explicitly planned features which can be contesting to represent in complex issues.

Nevertheless, deep learning utilizes data presentation learning to accomplish tasks and convert data into abstract expressions that promote the features learned for systems. This capability of deep learning overwhelms the condition of complex characteristics. Both deep and traditional machine learning exist data-driven artificial intelligence methods capable to successfully model deterministic directions, which are impossible to humans and connections between input and output. Deep learning disposes the capability of executing feature learning, model structure and model training by choosing various kernels and optimizing parameters.

A number of suitable investigations issued on defect detection explanations utilizing deep learning [83]- [84].

In 2015 Ren et al. [85] presented a technique by integrating the region proposal network (RPN) and Faster Region-based Convolutional Neural Network (Faster R-CNN) for object detection to develop about cost-free region suggestions. In [86], the authors employed a Faster R-CNN-based visual inspection approach to notice and categorize five defect classes with 90.6%, 83.4%, 82.1%, 98.1%, and 84.7% average precisions.

Their procedure completed the task especially faster than a traditional CNN based approach, which is essential for real-time implementation. Wang et al. [87] conceived a more rapid R-CNN algorithm to translate the speed problem of CNNs and to find short defects in complex products where they gained 72% detection and 81% classification accuracy. Liu et al. [88] presented a defect detection approach based on semantic segmentation. They employed a development and elongation of CNN called Fully Connected Networks (FCN). They converted the comprehensively combined layer of a CNN into a convolution layer. They acquired 99.6% accuracy on the German DAGM 2007 dataset. Lately, Kumar et al. [89] employed a deep convolutional neural network (DCNN) to catch and organize defect in tailors and performed and average of 86.2% testing accuracy, 87.7% precision and 90.6% recall.

Li et al. [90] connected Gabor filters and Pulse Coupled Neural Network (PCNN) for fabric defect detection and reached 98.6% accuracy. This factor is one of the most important factors by utilizing CNNs. To decrypt this problem, Yang et al. [91] designed a profitable and strong approach as virtual defect rendering to decode the problem of small datasets.

In a current study, Yang et al [27], designed a DCNN based system to catch and categorize defects to appear during laser welding in battery manufacturing. But they offered a novel model contacted Visual Geometry Group (VGG) model to enhance the efficiency of defect classification. Their examination on 8000 examples with a 99.87% accuracy confirmed that the pre-trained VGG model has small model size, lower defect positive rate and shorter training time and foretelling time. It is recognized that their model is favorably appropriate for quality assessment in an industrial environment.

CNN is a feedforward neural network. CNN consists of one or more convolutional layers and related layers and associated weights and pooling layers [92]. Publications is a famous LeNet convolution neural network configuration. LeNet network configuration utilized to detect defects in two conditions: (1) develop a complex multi-layer CNN structure, employ various network configuration to additional image content characteristics, and comprehensive end-to-end training to detect defects in images [93]- [94]; (2) integrate CNN with CRF model, prepare CNN with CRF energy

function as restriction or optimize network prediction results with CRF.

Autoencoder network primarily contains two steps: coding and decoding. In the first step, the input signal transformed into a coding signal for feature extraction; in the second step, the feature information is converted into a reconstruction signal. After it, the reconstruction error is underestimated by modifying the weight and bias to discover the defect detection [95]. The contrast between autoencoder networks and other machine learning algorithms is that the learning objective of the autoencoder network is not for classification, whereas for characteristic learning [96]. It has a powerful capability of autonomous learning and favorably nonlinear mapping. It learn nonlinear metric procedures to translate the problem of segmentation of difficult background and foreground regions [97].

The deep residual network counts a residual module on the basis of the convolutional neural network. The residual network is represented by effortless optimization and enhances the accuracy by improving the network depth [98], CNN, Generative Adversarial Networks [99], etc. As the depth of the network grows, the extraction characteristic grows, whereas it is effortless to yield the activation function not to combine.

The purpose of the deep residual network is to optimize the increasing number of network layers with residual while improving the network structure. The output and input segment dimensions of the convolution layer in the residual unit are identical. Then via the activation function, the loss is decreased.

The completely connected layer is a relation between any two nodes between two bordering layers. A thoroughly connected neural network employs a completely connected operation. There are more additional weight values, which indicate that the network takes up more memory and calculations [100]. During the analysis of the totally connected neural network, the feature map developed by the convolution layer mapped into a fixed-length feature vector. The entire convolution neural network obtains the input image of any size, and utilizes the deconvolution layer to sample the feature map of the last convolution layer. It retrieves to the same size of the input image. In that case, a prediction developed for each pixel, while maintaining the spatial information in the original input image. Eventually categorizes the feature map of the upper sampling pixel by pixel.

The recurrent neural network utilizes the recurrent convolution process to substitute the convolution operation on CNN. The contrast is that the recurrent neural network does not achieve the pooling layer operation to remove the features behind the recurrent operation for removing the input layer features. While it utilizes the recurrent convolution operation to process the features of the samples.

For error detection in this scope, some works are of concern. Table 2 shows the comparison of the related works. In [101], Clathrate hydrates find diverse significant applications including, but not limited to, future energy resources, gas storage and transport, gas separation, water desalination, and refrigeration. Studies on the nucleation, growth, dissociation, and micro/nanoscale properties of clathrate hydrates that are of utmost importance for those applications are challenging by experiments but can be accessible by molecular simulations. By this method, however, the identification of cage structures to extract useful insights is highly required. Herein, we introduce a hierarchical topology ring (HTR) algorithm to recognize cage structures with high efficiency and high accuracy. The HTR algorithm can identify all types of complete cages and is particularly optimized for hydrate identification in large-scale systems composed of millions of water molecules. Moreover, topological isomers of cages and $n \times \text{guest@cage}$ can be uniquely identified. Besides, we validate the use of HTR for the identification of cages of clathrate hydrates upon mechanical loads to failure.

In 2022, the prompt detection of early decay in the pavement could be an auspicious technique in road maintenance. Admittedly, early crack detection allows preventive measures to be taken to avoid damage and possible failure. With regards to the advancement in computer vision and image processing in civil engineering, traditional visual inspection has been replaced by semi-automatic/automatic techniques. The process of detecting objects from the images is a fundamental stage of any image processing technique since the accuracy rate of the classification will depend heavily on the quality of the results obtained from the segmentation step. The major challenge of pavement image segmentation is the detection of thin, irregular dark lines cracks that are buried into the textured backgrounds. Although the pioneering works on image processing methodologies have proven great merit of such techniques in detecting pavement surface distresses, there is still a need for further improvement. The academic community is already working on image-based identification of pavement cracks, but there is currently no standard structure. This literature review establishes the history of development and interpretation of existing studies before conducting new research; and focuses heavily on three major types of approaches in the field of image segmentation, namely thresholding-based, edge-based, and data driven-based methods. With comparison and analysis of various image segmentation algorithms, this research provides valuable information for researchers working on enhanced segmentation strategies that potentially yield a fully automated distress detection process for pavement images with varying conditions [102].

In [103], Laser processing of cutting tool materials particularly cemented carbides can induce many surface defects including porosity, balling, and micro-cracks. When present in the microstructure of cutting tools, micro-cracks can lead to chipping and early failure. The detection and identification of cracks can be used to predict tool performance post

laser processing. To develop a method for crack identification scanning electron microscopy (SEM) images were used. The manual review of SEM images is subjective and time consuming. This study presents a method to identify and quantify cracks from an SEM microstructure of tungsten carbide (WC) in MATLAB. Image processing algorithms were used to segment crack regions from other surface defects and the background microstructure; and subsequently to extract crack geometry and information. The results show successful segmentation of cracks from SEM images with an identification accuracy greater than 95 % across a range of different laser processing parameters.

In [104], the construction of a building involves tremendous investments of time, money, and emotion. Therefore, every stakeholder involved in the process starting from construction companies to the tenants wants to make sure that a structure is built well and that it can serve its purpose without any safety hazards. While the majority of factors concerning a building's safety are evaluated manually, there are factors like detecting visible structural damage that might incur a severe investment of time via manual inspection. Therefore, the need of the hour is to engineer automated systems that with the help of computer vision techniques will detect visually discernible defects in buildings. The paper proposes two approaches, namely digital image processing-based and deep learning-based that deal with creating surface crack inspection systems and attempt to showcase their performances in perspective by comparing their results across four different types of surface crack image datasets.

In [105], one of the major challenges in the construction industry is the detection of cracks in concrete structures and identification of failure types of these structures that lead to their degradation. Manual quality checks are prone to human error, and require longer response time and specialist experience and knowledge. Therefore, visualizing the cracks and identifying failures in concrete structures using computer techniques is now a preferred option. The present work focuses on identifying the cracks using image processing and failure pattern recognition technique by employing suitable machine learning algorithms, and validating the techniques using Python programming. For this purpose, M30 grade geopolymer and conventional concrete beams were cast using Basalt Fiber Reinforced Polymer/Glass Fiber Reinforced Polymer and Steel bars. The beams were subjected to four-point static bending test by varying the shear span to the effective depth ratio. The experimental images were used for image processing and failure pattern recognition in Python language. Employing six machine learning classifiers, the failures in the structures were classified into three classes namely, flexure, shear, and compression. The machine learning classifiers were also adopted to determine the confusion matrix, accuracy, precision, and recall scores. It was found that among the six classifiers used, the support vector classifier gave the best performance with 100% accuracy in identifying the failure patterns.

In [106], annually, millions of dollars are spent to carry out defect detection in key infrastructure including roads, bridges, and buildings. The aftermath of natural disasters like floods and earthquakes leads to severe damage to the urban infrastructure. Maintenance operations that follow for the damaged infrastructure often involve a visual inspection and assessment of their state to ensure their functional and physical integrity. Such damage may appear in the form of minor or major cracks, which gradually spread, leading to ultimate collapse or destruction of the structure. Crack detection is a very laborious task if performed via manual visual inspection. Many infrastructure elements need to be checked regularly and it is therefore not feasible as it will require significant human resources. This may also result in cases where cracks go undetected. A need, therefore, exists for performing automatic defect detection in infrastructure to ensure its effectiveness and reliability. Using image processing techniques, the captured or scanned images of the infrastructure parts can be analyzed to identify any possible defects. Apart from image processing, machine learning methods are being increasingly applied to ensure better performance outcomes and robustness in crack detection. This paper provides a review of image-based crack detection techniques which implement image processing and/or machine learning. A total of 30 research articles have been collected for the review which is published in top tier journals and conferences in the past decade. A comprehensive analysis and comparison of these methods are performed to highlight the most promising automated approaches for crack detection.

In [107], cracks considerably reduce the life span of pavement surfaces. Currently, there is a need for the development of robust automated distress evaluation systems that comprise a low-cost crack detection method for performing fast and cost-effective roadway health monitoring practices. Most of the current methods are costly and have labor-intensive learning processes, so they are not suitable for small local-level projects with limited resources or are only usable for specific pavement types. This paper proposes a new method that uses an adapted version of the weighted neighborhood pixels' segmentation algorithm to detect cracks in 2-D pavement images. The method uses the Gaussian cumulative density function (CDF) as the adaptive threshold to overcome the drawback of fixed thresholds in noisy environments. The proposed algorithm was tested on 300 images containing a wide range of noise representative of various pavement noise conditions. The method proved to be time and cost-efficient as it took less than 3.15 s per 320×480 pixels' image for a Xeon (R) 3.70 GHz CPU processor to generate the detection results. This makes the proposed method a perfect choice for county-level pavement maintenance projects requiring cost-effective pavement crack detection systems. The validation results were promising for the detection of medium to severe-level cracks (precision = 79.21%, recall = 89.18%, and F1 score = 83.90%).

In [107], in addition to causing damage to vehicles, road defects are one of the main causes of vehicle accidents which lead to loss of human lives. Many methods of detecting defects have been introduced over the years to reduce the consequences of these defects. One of these methods is image processing. Use of image and video processing has many applications in medicine, science, agriculture, and defect detection in structures. It has been used for defect detection on roads because timely detection and analysis of defect is very important for road serviceability and safety of the people. Detection of a defect by image processing broadly follows some of the basic steps which include feature extraction, edge detection, morphological operators, and training of data. Different approaches are used for various kinds of defect detection and analysis which have replaced the manual inspection method of roads saving time and resources. This chapter discusses the basic steps involved in defect detection using image processing along with existing systems that use machine learning and artificial intelligence for the detection of defects from a distance. To write this chapter, papers on the topic of image and computer vision-based defect detection systems have been consulted.

In [108], image processing is a subset of digital signal processing that has different applications and benefits in different fields. Digital processing is in fact the digital image processing that can be performed with the help of computer science, programming, and artificial intelligence. Image processing is one of the applications and subsets of artificial intelligence that, as its name suggests, processes digital images and displays a certain output with specific information based on predefined training. Nowadays, the applications of image processing technology in various fields of science, technology have caused a lot of attention in order to expand the capabilities of artificial intelligence in different engineering challenges. This paper presents recent development and applications in image processing systems in order to move forward the research field by reviewing and analyzing recent achievements in the published papers. As a result, advanced image processing systems in different applications can be developed and new techniques in the image processing systems can be introduced.

In [109], the widespread popularity of unmanned aerial vehicles enables an immense amount of power lines inspection data to be collected. How to employ massive inspection data especially the visible images to maintain the reliability, safety, and sustainability of power transmission is a pressing issue. To date, substantial works have been conducted on the analysis of power lines inspection data. With the aim of providing a comprehensive overview for researchers who are interested in developing a deep-learning-based analysis system for power lines inspection data, this paper conducts a thorough review of the current literature and identifies the challenges for future research. Following the typical procedure of inspection data analysis, we categorize current works in this area into component detection and defect detection diagnosis. For each aspect, the techniques and methodologies adopted in the literature are summarized. Some valuable information is also included such as data description and method performance. Further, an in-depth discussion of existing deep-learning-related analysis methods in power lines inspection is proposed. Finally, we conclude the paper with several research trends for the future of this area, such as data quality problems, small object detection, embedded application, and evaluation baseline.

In [110], the material extrusion (ME) process is one of the most widely used 3D printing processes, especially considering its use of inexpensive materials. However, the error known as the “spaghetti-shape error,” related to filament tangling, is a common problem associated with the ME process. Once occurring, this issue, which consumes both time and materials, requires a restart of the entire process. In order to prevent this, the user must constantly monitor the process. In this research, a failure detection method which uses a webcam and deep learning is developed for the ME process. The webcam captures images and then analyzes them by machine learning based on a convolutional neural network (CNN), showing outstanding performance in both image classification and the recognition of objects. Sample images were trained based on a modified Visual Geometry Group Network (VGGNet) model and the trained model was evaluated, resulting in 97% accuracy. The pre-trained model was tested on a 3D printer monitoring system for its ability to recognize the “spaghetti-shape-error” and was able to detect 96% of abnormal deposition processes. The proposed method can analyze the ME process in real-time and inform the user or halts the process when abnormal printing is detected.

In [111], mass spectrometry imaging (MSI) and histology are complementary analytical tools. Integration of the two imaging modalities can enhance the spatial resolution of the MSI beyond its experimental limits. Patch-based super-resolution (PBSR) is a method where high spatial resolution features from one image modality guide the reconstruction of a low-resolution image from a second modality. The principle of PBSR lies in image redundancy and aims at finding similar pixels in the neighborhood of a central pixel that is then used to guide reconstruction of the central pixel. In this work, we employed PBSR to increase the resolution of MSI. We validated the proposed pipeline by using a phantom image (micro-dissected logo within a tissue) and mouse cerebellum samples. We compared the performance of the PBSR with other well-known methods: linear interpolation (LI) and image fusion (IF). Quantitative and qualitative assessment showed advantage over the former and comparability with the latter. Furthermore, we demonstrated the potential applicability of PBSR in a clinical setting by accurately integrating structural (i.e., histological) and molecular (i.e., MSI) information from a case study of a dog liver.

In [112], machine fault diagnosis and remaining service life prognosis provide the basis for condition-based maintenance and are key to operational reliability. Accurate assessment of machine health requires effective analysis of vibration data, which is typically performed by examining the change in frequency components. One limitation associated with these methods is the empirical knowledge required for fault feature selection. This paper presents an image processing approach to automatically extract features from vibration signals, based on visual word representation. Specifically, a time-frequency image of vibration signal is obtained through wavelet transform, which is then used to extract “visual word” features for recognizing fault-related patterns. The extracted features are subsequently fed into a sparse representation-based classifier for classification. Evaluation using experimental bearing data confirmed the effectiveness of the developed method with a classification accuracy of 99.7%.

In [113], the advent of the 3G communications era has led to a trend of digital media information being transmitted through wireless networks. The variability and high error rate of the wireless communications environment often cause loss of information. Images transmitted in a noisy channel environment tend to be obstructed by unexpected information, which decreases the quality of the image. Therefore, it is an intensive research topic to repair error images and increase their post-transmission quality. Image authentication technique is a mechanism to deal with the malicious image modification problem. However, it can also be used to solve the problem of error image transmission. In this paper, a new image authentication technique is proposed to embed the image block directions as the verification information. At the receiver, the information is then extracted to detect transmission error and incorporated with a newly interleaving prediction method to repair the erroneous regions of the image. In this way, it can not only repair the image, but also detect the image blocks that are erroneous, thus enhancing the post-transmission quality of the image.

In [114], image processing has two main branches: image enhancement and machine vision. Improving images includes methods such as using a blur filter and increasing contrast to improve the visual quality of images and ensure that they are displayed correctly in the target environment, such as a printer or computer monitor. While machine vision deals with methods that can be used to understand the meaning and content of images to be used in tasks such as robotics and image axis.

In [115], robots first detect the number of banana bunches when making judgements on sterile bud removal and estimating weight for harvest in the field environment. Banana bunches are complex in shape, arranged in a nonlinear helical curve along the stalk, and have different growth states in different periods, with bunches widely spaced in the early period and densely arranged in the harvest period. Deep Learning nor classical image-processing algorithms alone can detect and count bunches in both periods. Therefore, these algorithms were combined to calculate the number of bunches in the two periods. For counting bunches in the debudding period, the convolutional neural network Deeplab V3 + model and classic image-processing algorithm were combined to finely segment bunches and calculate bunch numbers, providing intelligent decision-making for judgment on the timing for debudding. To count bunches during harvest, based on deep learning to identify the overall banana fruit cluster, the edge detection algorithm was employed to extract the centroid points of fruit fingers, and the clustering algorithm was used to determine the optimal number of bunches on the visual detection surface. An estimation model for the total number of bunches, including hidden ones, was created based on their helical curve arrangement. The results indicated a target segmentation MIoU of 0.878 during the debudding period, a mean pixel precision of 0.936, and a final bunch detection accuracy rate of 86%. Bunch detection was highly challenging during the harvest period, with a detection accuracy rate of 76% and a final overall bunch counting accuracy rate of 93.2%. Software was designed to estimate banana fruit weight during the harvest period. This research method provided a theoretical basis and experimental data support for automatic sterile bud removal and weight estimation for bananas.

In [116], leaf spot disease, which causes 10 – 50% loss in sugar beet yield, causes great damage on the leaves. This disease physiologically appears as individual circular spots on the sugar beet leaves and over time spreads to the entire leaf, resulting in complete death of the leaf. Therefore, in our study, Faster R-CNN, SSD, VGG16, Yolov4 deep learning models were used directly, and Yolov4 deep learning model with image processing was used in a hybrid way for automatic determination of leaf spot disease on sugar beet and classification of severity. The proposed hybrid method for the diagnosis of diseases and identifying the severity were trained and tested using 1040 images, and the classification accuracy rate of the most successful method was found to be 96.47%. The proposed hybrid approach showed that the combined use of image processing and deep learning models yield more successful results than the analysis made using only deep learning models. In this way, both the time spent for the diagnosis of leaf spot disease on sugar beet will be reduced and human error will be eliminated, and the relevant pesticides will be sprayed to the plant at the right time.

In [117], the authors present for the first time a method for detecting label errors in image datasets with semantic segmentation, i.e., pixel-wise class labels. Annotation acquisition for semantic segmentation datasets is time-consuming and requires plenty of human labor. In particular, review processes are time consuming and label errors can easily be overlooked by humans. The consequences are biased benchmarks and in extreme cases also performance degradation of deep neural networks (DNNs) trained on such datasets. DNNs for semantic segmentation yield pixel-wise predictions,

which makes detection of label errors via uncertainty quantification a complex task. Uncertainty is particularly pronounced at the transitions between connected components of the prediction. By lifting the consideration of uncertainty to the level of predicted components, we enable the usage of DNNs together with component-level uncertainty quantification for the detection of label errors. We present a principled approach to benchmark the task of label error detection by dropping labels from the Cityscapes dataset as well as from a dataset extracted from the CARLA driving simulator, where in the latter case we have the labels under control. Our experiments show that our approach is able to detect the vast majority of label errors while controlling the number of false label error detections. Furthermore, we apply our method to semantic segmentation datasets frequently used by the computer vision community and present a collection of label errors along with sample statistics [118].

The Problem of Photovoltaic (PV) defects detection and classification has been well studied. Several techniques exist in identifying the defects and localizing them in PV panels that use various features, but suffer to achieve higher performance. An efficient Real-Time Multi Variant Deep Learning Model (RMVDM) is presented in this article to handle this issue. The method considers different defects like a spotlight, crack, dust, and micro-cracks to detect the defects as well as localizes the defects. The image data set given has been preprocessed by applying the Region-Based Histogram Approximation (RHA) algorithm. The preprocessed images are applied with Gray Scale Quantization Algorithm (GSQA) to extract the features. Extracted features are trained with a Multi Variant Deep learning model where the model trained with a number of layers belongs to different classes of neurons. Each class neuron has been designed to measure Defect Class Support (DCS). At the test phase, the input image has been applied with different operations, and the features extracted passed through the model trained. The output layer returns a number of DCS values using which the method identifies the class of defect and localizes the defect in the image. Further, the method uses the Higher- Order Texture Localization (HOTL) technique in localizing the defect. The proposed model produces efficient results with around 97% in defect detection and localization with higher accuracy and less time complexity.

6. CHALLENGES

High precision, high positioning, fast detection, and small object through examination are the most challenges in the application of quality detection [119]- [85] (See Table 4).

7. CONCLUSION

Industrial product quality is a significant portion of product production. The research on defect detection technology has excellent functional significance to guarantee product quality. This article supplies a complete outline of the research status of product defect detection technology in complicated industrial processes. We approximated and studied traditional defect detection and deep learning techniques and completely outlined the empirical results of defect detection methods. Integrated with the actual application conditions and the result of artificial intelligence technology, the defect detection tools examined and studied. Via analysis, we discovered that 3D object detection, high precision, high positioning, and rapid detection are the challenges of industrial research. We suggested that implanted sensor equipment, online product defect detection, 3D defect detection, etc. are the evolution directions in the field of industrial product defect detection. We consider that the study will aid industrial businesses and researchers comprehend the research progress of product defect detection technology in the field of deep learning and traditional defect detection.

This article provides a review of defect detection methods represented in more than 100 scientific assistances. A substantial part of works is based on statistical statements and employs statistical or filter-based procedures. The Gabor filter is one of the utilized techniques. Nevertheless, most of the investigations offer detailed restrictions, being heavily conditional on the pattern, material and texture. Cracking the segmentation and windowing problems of coinciding objects is a ponderous topic closed by some investigators. Images having color features reproduce the complexity of these problems.

Neural networks are a strong approach utilized in artificial image processing. These almost decode every classification problem. Nonetheless, the major disadvantage is the needed large amount of training samples. In artificial image processing, this issue effortlessly cracked with labeled datasets. Regardless, in other fields like robotics, it is a challenging problem. Enhancing the training efficiency and intersection qualification of neural networks is a continuous research area. It is noted that large neural networks employed for deep learning need considerable computational resources, which direct to an inevitable parallelization of the challenges [120].

In artificial image processing, various textural databases are known for testing. Although some investigations do not supply sufficient results due to the scarcity of testing samples and regular inconsistency of such databases, there is a tremendous demand for designing general defect detection techniques able to deal with any type of defect on every kind of material and able to show a general and dedicated defect description system. To this purpose, deep learning is the emerging field that decodes the generality need and hyper-complexity of problems without drastically increasing computational costs.

REFERENCES:

- [1] T. Wang, Y. Chen, M. Qiao, and H. Snoussi, "A fast and robust convolutional neural network-based defect detection model in product quality control," *The International Journal of Advanced Manufacturing Technology*, vol. 94, pp. 3465-3471, 2018.
- [2] B. Li, M. Cobo-Medina, J. Lecourt, N. Harrison, R. J. Harrison, and J. V. Cross, "Application of hyperspectral imaging for nondestructive measurement of plum quality attributes," *Postharvest Biology and Technology*, vol. 141, pp. 8-15, 2018.
- [3] P. Li, I. Dolado, F. J. Alfaro-Mozaz, F. Casanova, L. E. Hueso, S. Liu, *et al.*, "Infrared hyperbolic metasurface based on nanostructured van der Waals materials," *Science*, vol. 359, pp. 892-896, 2018.
- [4] X. Xie, "A review of recent advances in surface defect detection using texture analysis techniques," *ELCVIA: electronic letters on computer vision and image analysis*, pp. 1-22, 2008.
- [5] H. Y. Ngan, G. K. Pang, and N. H. Yung, "Automated fabric defect detection—A review," *Image and vision computing*, vol. 29, pp. 442-458, 2011.
- [6] P. Mahajan, S. Kolhe, and P. Patil, "A review of automatic fabric defect detection techniques," *Advances in Computational Research*, vol. 1, pp. 18-29, 2009.
- [7] I. J. Aldave, P. V. Bosom, L. V. González, I. L. De Santiago, B. Vollheim, L. Krausz, *et al.*, "Review of thermal imaging systems in composite defect detection," *Infrared Physics & Technology*, vol. 61, pp. 167-175, 2013.
- [8] W. Zhang, C. Ye, K. Zheng, J. Zhong, Y. Tang, Y. Fan, *et al.*, "Tensan silk-inspired hierarchical fibers for smart textile applications," *ACS nano*, vol. 12, pp. 6968-6977, 2018.
- [9] E. Moulin, L. Chehemi, J. Assaad, J. De Rosny, C. Prada, E. Chatelet, *et al.*, "Passive defect detection in plate from nonlinear conversion of low-frequency vibrational noise," *The Journal of the Acoustical Society of America*, vol. 140, pp. 3002-3002, 2016.
- [10] Y. Li, W. Zhao, and J. Pan, "Deformable patterned fabric defect detection with fisher criterion-based deep learning," *IEEE Transactions on Automation Science and Engineering*, vol. 14, pp. 1256-1264, 2016.
- [11] A. L. Elrefai and I. Sasada, "Magnetic particle detection system using fluxgate gradiometer on a permalloy shielding disk," *IEEE Magnetics Letters*, vol. 7, pp. 1-4, 2016.
- [12] G. D'Angelo, M. Laracca, S. Ramponi, and G. Betta, "Fast eddy current testing defect classification using Lissajous figures," *IEEE Transactions on Instrumentation and Measurement*, vol. 67, pp. 821-830, 2018.
- [13] M. Kusano, H. Hatano, M. Watanabe, S. Takekawa, H. Yamawaki, K. Oguchi, *et al.*, "Mid-infrared pulsed laser ultrasonic testing for carbon fiber reinforced plastics," *Ultrasonics*, vol. 84, pp. 310-318, 2018.
- [14] J. Yang, S. Li, Z. Gao, Z. Wang, and W. Liu, "Real-time recognition method for 0.8 cm darning needles and KR22 bearings based on convolution neural networks and data increase," *Applied Sciences*, vol. 8, p. 1857, 2018.
- [15] J. Li, G. Wang, and Z. Xu, "Environmentally-friendly oxygen-free roasting/wet magnetic separation technology for in situ recycling cobalt, lithium carbonate and graphite from spent LiCoO₂/graphite lithium batteries," *Journal of Hazardous Materials*, vol. 302, pp. 97-104, 2016.
- [16] T. Rymarczyk, K. Szumowski, P. Adamkiewicz, P. Tchórzewski, and J. Sikora, "Moisture Wall Inspection Using Electrical Tomography Measurements," *Przegląd Elektrotechniczny*, vol. 94, pp. 97-100, 2018.
- [17] G. Shelikhov and Y. A. Glazkov, "On the improvement of examination questions during the nondestructive testing of magnetic powder," *Russian Journal of Nondestructive Testing*, vol. 47, pp. 112-117, 2011.
- [18] A. García-Arribas, F. Martínez, E. Fernández, I. Ozaeta, G. Kurlyandskaya, A. Svalov, *et al.*, "GMI detection of magnetic-particle concentration in continuous flow," *Sensors and Actuators A: Physical*, vol. 172, pp. 103-108, 2011.
- [19] J. Chen, Z. Liu, H. Wang, A. Núñez, and Z. Han, "Automatic defect detection of fasteners on the catenary support device using deep convolutional neural network," *IEEE Transactions on Instrumentation and Measurement*, vol. 67, pp. 257-269, 2017.
- [20] G. Y. Tian and A. Sophian, "Defect classification using a new feature for pulsed eddy current sensors," *Ndt & E International*, vol. 38, pp. 77-82, 2005.
- [21] H. Yang and L. Yu, "Feature extraction of wood-hole defects using wavelet-based ultrasonic testing," *Journal of forestry research*, vol. 28, pp. 395-402, 2017.
- [22] S. Gholizadeh, "A review of non-destructive testing methods of composite materials," *Procedia structural integrity*, vol. 1, pp. 50-57, 2016.
- [23] Y. Fang, L. Lin, H. Feng, Z. Lu, and G. W. Emms, "Review of the use of air-coupled ultrasonic technologies for nondestructive testing of wood and wood products," *Computers and electronics in agriculture*, vol. 137, pp. 79-87, 2017.
- [24] H.-D. Lin and H.-L. Chen, "Automated visual fault inspection of optical elements using machine vision technologies," *Journal of Applied Engineering Science*, vol. 16, pp. 447-453, 2018.
- [25] F. Jia, Y. Lei, J. Lin, X. Zhou, and N. Lu, "Deep neural networks: A promising tool for fault characteristic mining and intelligent diagnosis of rotating machinery with massive data," *Mechanical systems and signal processing*, vol. 72, pp. 303-315, 2016.
- [26] M. A. Habib, C. H. Kim, and J.-M. Kim, "A crack characterization method for reinforced concrete beams using an acoustic emission technique," *Applied Sciences*, vol. 10, p. 7918, 2020.
- [27] Y. Yang, L. Pan, J. Ma, R. Yang, Y. Zhu, Y. Yang, *et al.*, "A high-performance deep learning algorithm for the automated optical inspection of laser welding," *Applied Sciences*, vol. 10, p. 933, 2020.

- [28] M. Meng, Y. J. Chua, E. Wouterson, and C. P. K. Ong, "Ultrasonic signal classification and imaging system for composite materials via deep convolutional neural networks," *Neurocomputing*, vol. 257, pp. 128-135, 2017.
- [29] M. G. Droubi, N. H. Faisal, F. Orr, J. A. Steel, and M. El-Shaib, "Acoustic emission method for defect detection and identification in carbon steel welded joints," *Journal of Constructional Steel Research*, vol. 134, pp. 28-37, 2017.
- [30] W. M. Alobaidi, E. A. Alkuam, H. M. Al-Rizzo, and E. Sandgren, "Applications of ultrasonic techniques in oil and gas pipeline industries: A review," *American Journal of Operations Research*, vol. 5, p. 274, 2015.
- [31] N. Boaretto and T. M. Centeno, "Automated detection of welding defects in pipelines from radiographic images DWDI," *Ndt & E International*, vol. 86, pp. 7-13, 2017.
- [32] B. Masserey and P. Fromme, "Surface defect detection in stiffened plate structures using Rayleigh-like waves," *Ndt & E International*, vol. 42, pp. 564-572, 2009.
- [33] I. G. Kazantsev, I. Lemahieu, G. Salov, and R. Denys, "Statistical detection of defects in radiographic images in nondestructive testing," *Signal Processing*, vol. 82, pp. 791-801, 2002.
- [34] J. W. Wilson and G. Y. Tian, "Pulsed electromagnetic methods for defect detection and characterisation," *NDT & E International*, vol. 40, pp. 275-283, 2007.
- [35] D. Marr and E. Hildreth, "Theory of edge detection," *Proceedings of the Royal Society of London. Series B. Biological Sciences*, vol. 207, pp. 187-217, 1980.
- [36] D.-M. Tsai and T.-Y. Huang, "Automated surface inspection for statistical textures," *Image and Vision computing*, vol. 21, pp. 307-323, 2003.
- [37] J. G. Daugman, "Two-dimensional spectral analysis of cortical receptive field profiles," *Vision research*, vol. 20, pp. 847-856, 1980.
- [38] K. L. Mak and P. Peng, "An automated inspection system for textile fabrics based on Gabor filters," *Robotics and Computer-Integrated Manufacturing*, vol. 24, pp. 359-369, 2008.
- [39] A. Bodnarova, M. Bennamoun, and S. Latham, "Optimal Gabor filters for textile flaw detection," *Pattern recognition*, vol. 35, pp. 2973-2991, 2002.
- [40] J. J. Liu and J. F. MacGregor, "Estimation and monitoring of product aesthetics: application to manufacturing of "engineered stone" countertops," *Machine Vision and Applications*, vol. 16, pp. 374-383, 2006.
- [41] S. G. Mallat, "A theory for multiresolution signal decomposition: the wavelet representation," *IEEE transactions on pattern analysis and machine intelligence*, vol. 11, pp. 674-693, 1989.
- [42] B. B. Mandelbrot and B. B. Mandelbrot, *The fractal geometry of nature* vol. 1: WH freeman New York, 1982.
- [43] R. M. Haralick, "Statistical and structural approaches to texture," *Proceedings of the IEEE*, vol. 67, pp. 786-804, 1979.
- [44] J. L. Marroquin, E. A. Santana, and S. Botello, "Hidden Markov measure field models for image segmentation," *IEEE Transactions on Pattern Analysis and Machine Intelligence*, vol. 25, pp. 1380-1387, 2003.
- [45] H. Deng and D. A. Clausi, "Gaussian MRF rotation-invariant features for image classification," *IEEE transactions on pattern analysis and machine intelligence*, vol. 26, pp. 951-955, 2004.
- [46] X.-c. Yuan, L.-s. Wu, and Q. Peng, "An improved Otsu method using the weighted object variance for defect detection," *Applied surface science*, vol. 349, pp. 472-484, 2015.
- [47] M. Aminzadeh and T. Kurfess, "Automatic thresholding for defect detection by background histogram mode extents," *Journal of Manufacturing Systems*, vol. 37, pp. 83-92, 2015.
- [48] X. Li, H. Jiang, and G. Yin, "Detection of surface crack defects on ferrite magnetic tile," *Ndt & E International*, vol. 62, pp. 6-13, 2014.
- [49] D. Zhu, R. Pan, W. Gao, and J. Zhang, "Yarn-dyed fabric defect detection based on autocorrelation function and GLCM," *Autex research journal*, vol. 15, pp. 226-232, 2015.
- [50] L. Zhang, J. Jing, and H. Zhang, "Fabric defect classification based on LBP and GLCM," *Journal of Fiber Bioengineering and Informatics*, vol. 8, pp. 81-89, 2015.
- [51] J. Wang, Q. Li, J. Gan, H. Yu, and X. Yang, "Surface defect detection via entity sparsity pursuit with intrinsic priors," *IEEE Transactions on Industrial Informatics*, vol. 16, pp. 141-150, 2019.
- [52] X. Kang, P. Yang, and J. Jing, "Defect detection on printed fabrics via gabor filter and regular band," *Journal of Fiber Bioengineering and Informatics*, vol. 8, pp. 195-206, 2015.
- [53] Y. Huang and K. L. Chan, "Texture decomposition by harmonics extraction from higher order statistics," *IEEE Transactions on Image Processing*, vol. 13, pp. 1-14, 2004.
- [54] C. E. Costa and M. Petrou, "Automatic registration of ceramic tiles for the purpose of fault detection," *Machine Vision and Applications*, vol. 11, pp. 225-230, 2000.
- [55] K. Y. Song, J. Kittler, and M. Petrou, "Defect detection in random colour textures," *Image and vision computing*, vol. 14, pp. 667-683, 1996.
- [56] W. Wen and A. Xia, "Verifying edges for visual inspection purposes," *Pattern recognition letters*, vol. 20, pp. 315-328, 1999.
- [57] A. Tolba and H. M. Raafat, "Multiscale image quality measures for defect detection in thin films," *The International Journal of Advanced Manufacturing Technology*, vol. 79, pp. 113-122, 2015.
- [58] J. Cao, J. Zhang, Z. Wen, N. Wang, and X. Liu, "Fabric defect inspection using prior knowledge guided least squares regression," *Multimedia Tools and Applications*, vol. 76, pp. 4141-4157, 2017.
- [59] J. P. Yun, S. J. Lee, G. Koo, C. Shin, and C. Park, "Automatic defect inspection system for steel products with exhaustive dynamic encoding algorithm for searches," *Optical Engineering*, vol. 58, pp. 023107-023107, 2019.

- [60] X. Zhou, Y. Wang, C. Xiao, Q. Zhu, X. Lu, H. Zhang, *et al.*, "Automated visual inspection of glass bottle bottom with saliency detection and template matching," *IEEE Transactions on Instrumentation and Measurement*, vol. 68, pp. 4253-4267, 2019.
- [61] C.-h. Chan and G. K. Pang, "Fabric defect detection by Fourier analysis," *IEEE transactions on Industry Applications*, vol. 36, pp. 1267-1276, 2000.
- [62] S. Gai, "New banknote defect detection algorithm using quaternion wavelet transform," *Neurocomputing*, vol. 196, pp. 133-139, 2016.
- [63] D.-M. Tsai, C.-P. Lin, and K.-T. Huang, "Defect detection in coloured texture surfaces using Gabor filters," *The Imaging Science Journal*, vol. 53, pp. 27-37, 2005.
- [64] Q. Zhu, M. Wu, J. Li, and D. Deng, "Fabric defect detection via small scale over-complete basis set," *Textile Research Journal*, vol. 84, pp. 1634-1649, 2014.
- [65] A. Conci and C. B. Proença, "A system for real-time fabric inspection and industrial decision," in *Proceedings of the 14th international conference on Software engineering and knowledge engineering*, 2002, pp. 707-714.
- [66] S. Moradi and T. Zayed, "Real-time defect detection in sewer closed circuit television inspection videos," in *Pipelines 2017*, ed, 2017, pp. 295-307.
- [67] X. Xie and M. Mirmehdi, "TEXEMS: Texture exemplars for defect detection on random textured surfaces," *IEEE transactions on pattern analysis and machine intelligence*, vol. 29, pp. 1454-1464, 2007.
- [68] H. Wang, J. Zhang, Y. Tian, H. Chen, H. Sun, and K. Liu, "A simple guidance template-based defect detection method for strip steel surfaces," *IEEE Transactions on Industrial Informatics*, vol. 15, pp. 2798-2809, 2018.
- [69] T. Czimmernann, G. Ciuti, M. Milazzo, M. Chiurazzi, S. Roccella, C. M. Oddo, *et al.*, "Visual-based defect detection and classification approaches for industrial applications—A survey," *Sensors*, vol. 20, p. 1459, 2020.
- [70] D.-T. Hoang and H.-J. Kang, "A survey on deep learning based bearing fault diagnosis," *Neurocomputing*, vol. 335, pp. 327-335, 2019.
- [71] X. Wei, Z. Yang, Y. Liu, D. Wei, L. Jia, and Y. Li, "Railway track fastener defect detection based on image processing and deep learning techniques: A comparative study," *Engineering Applications of Artificial Intelligence*, vol. 80, pp. 66-81, 2019.
- [72] J. Isavand, A. Kasaei, A. Peplow, X. Wang, and J. Yan, "A reduced-order machine-learning-based method for fault recognition in tool condition monitoring," *Measurement*, vol. 224, p. 113906, 2024.
- [73] L. Luo, W. Wang, S. Bao, X. Peng, and Y. Peng, "Robust and sparse canonical correlation analysis for fault detection and diagnosis using training data with outliers," *Expert Systems with Applications*, vol. 236, p. 121434, 2024.
- [74] L. Deng and D. Yu, "Deep learning: methods and applications," *Foundations and trends® in signal processing*, vol. 7, pp. 197-387, 2014.
- [75] P. Bergmann, S. Löwe, M. Fauser, D. Sattlegger, and C. Steger, "Improving unsupervised defect segmentation by applying structural similarity to autoencoders," *arXiv preprint arXiv:1807.02011*, 2018.
- [76] J. C. Cheng and M. Wang, "Automated detection of sewer pipe defects in closed-circuit television images using deep learning techniques," *Automation in Construction*, vol. 95, pp. 155-171, 2018.
- [77] J. Yang and G. Yang, "Modified convolutional neural network based on dropout and the stochastic gradient descent optimizer," *Algorithms*, vol. 11, p. 28, 2018.
- [78] K. Sun, J. Zhang, C. Zhang, and J. Hu, "Generalized extreme learning machine autoencoder and a new deep neural network," *Neurocomputing*, vol. 230, pp. 374-381, 2017.
- [79] L. Yu, H. Chen, Q. Dou, J. Qin, and P.-A. Heng, "Automated melanoma recognition in dermoscopy images via very deep residual networks," *IEEE transactions on medical imaging*, vol. 36, pp. 994-1004, 2016.
- [80] Y. Xue and Y. Li, "A fast detection method via region-based fully convolutional neural networks for shield tunnel lining defects," *Computer-Aided Civil and Infrastructure Engineering*, vol. 33, pp. 638-654, 2018.
- [81] J. Lei, X. Gao, Z. Feng, H. Qiu, and M. Song, "Scale insensitive and focus driven mobile screen defect detection in industry," *Neurocomputing*, vol. 294, pp. 72-81, 2018.
- [82] Z.-Q. Zhao, P. Zheng, S.-t. Xu, and X. Wu, "Object detection with deep learning: A review," *IEEE transactions on neural networks and learning systems*, vol. 30, pp. 3212-3232, 2019.
- [83] D. Tabernik, S. Šela, J. Skvarč, and D. Skočaj, "Segmentation-based deep-learning approach for surface-defect detection," *Journal of Intelligent Manufacturing*, vol. 31, pp. 759-776, 2020.
- [84] H. Lin, B. Li, X. Wang, Y. Shu, and S. Niu, "Automated defect inspection of LED chip using deep convolutional neural network," *Journal of Intelligent Manufacturing*, vol. 30, pp. 2525-2534, 2019.
- [85] S. Ren, K. He, R. Girshick, and J. Sun, "Faster r-cnn: Towards real-time object detection with region proposal networks," *Advances in neural information processing systems*, vol. 28, 2015.
- [86] Y. J. Cha, W. Choi, G. Suh, S. Mahmoudkhani, and O. Büyüköztürk, "Autonomous structural visual inspection using region-based deep learning for detecting multiple damage types," *Computer-Aided Civil and Infrastructure Engineering*, vol. 33, pp. 731-747, 2018.
- [87] Y. Wang, M. Liu, P. Zheng, H. Yang, and J. Zou, "A smart surface inspection system using faster R-CNN in cloud-edge computing environment," *Advanced Engineering Informatics*, vol. 43, p. 101037, 2020.
- [88] Y. Liu, Y. Yang, W. Chao, X. Xu, and T. Zhang, "Research on Surface Defect Detection Based on Semantic Segmentation," *DEStech Trans. Comput. Sci. Eng.*, 2019.

- [89] S. S. Kumar, D. M. Abraham, M. R. Jahanshahi, T. Iseley, and J. Starr, "Automated defect classification in sewer closed circuit television inspections using deep convolutional neural networks," *Automation in Construction*, vol. 91, pp. 273-283, 2018.
- [90] Y. Li and C. Zhang, "Automated vision system for fabric defect inspection using Gabor filters and PCNN," *SpringerPlus*, vol. 5, pp. 1-12, 2016.
- [91] H. Yang, T. Haist, M. Gronle, and W. Osten, "Realistic simulation of camera images of micro-scale defects for automated defect inspection," in *Forum Bildverarbeitung*, 2016.
- [92] A. Krizhevsky, I. Sutskever, and G. E. Hinton, "Imagenet classification with deep convolutional neural networks," *Advances in neural information processing systems*, vol. 25, 2012.
- [93] Y. He, K. Song, Q. Meng, and Y. Yan, "An end-to-end steel surface defect detection approach via fusing multiple hierarchical features," *IEEE transactions on instrumentation and measurement*, vol. 69, pp. 1493-1504, 2019.
- [94] J. Li, Z. Su, J. Geng, and Y. Yin, "Real-time detection of steel strip surface defects based on improved yolo detection network," *IFAC-PapersOnLine*, vol. 51, pp. 76-81, 2018.
- [95] S. Ozkan, B. Kaya, and G. B. Akar, "Endnet: Sparse autoencoder network for endmember extraction and hyperspectral unmixing," *IEEE Transactions on Geoscience and Remote Sensing*, vol. 57, pp. 482-496, 2018.
- [96] M. Toğaçar, B. Ergen, and Z. Cömert, "Waste classification using AutoEncoder network with integrated feature selection method in convolutional neural network models," *Measurement*, vol. 153, p. 107459, 2020.
- [97] J. Long, Z. Sun, C. Li, Y. Hong, Y. Bai, and S. Zhang, "A novel sparse echo autoencoder network for data-driven fault diagnosis of delta 3-D printers," *IEEE Transactions on Instrumentation and Measurement*, vol. 69, pp. 683-692, 2019.
- [98] K. Chen, K. Chen, Q. Wang, Z. He, J. Hu, and J. He, "Short-term load forecasting with deep residual networks," *IEEE Transactions on Smart Grid*, vol. 10, pp. 3943-3952, 2018.
- [99] A. Creswell, T. White, V. Dumoulin, K. Arulkumaran, B. Sengupta, and A. A. Bharath, "Generative adversarial networks: An overview," *IEEE signal processing magazine*, vol. 35, pp. 53-65, 2018.
- [100] J. Long, E. Shelhamer, and T. Darrell, "Fully convolutional networks for semantic segmentation," in *Proceedings of the IEEE conference on computer vision and pattern recognition*, 2015, pp. 3431-3440.
- [101] Y. Liu, K. Xu, Y. Xu, J. Liu, J. Wu, and Z. Zhang, "HTR: An ultra-high speed algorithm for cage recognition of clathrate hydrates," *Nanotechnology Reviews*, vol. 11, pp. 699-711, 2022.
- [102] N. Kheradmandi and V. Mehranfar, "A critical review and comparative study on image segmentation-based techniques for pavement crack detection," *Construction and Building Materials*, vol. 321, p. 126162, 2022.
- [103] K. E. Hazzan and M. Pacella, "Crack identification in tungsten carbide using image processing techniques," *Procedia Structural Integrity*, vol. 37, pp. 274-281, 2022.
- [104] R. Yadhunath, S. Srikanth, A. Sudheer, C. Jyotsna, and J. Amudha, "Detecting surface cracks on buildings using computer vision: an experimental comparison of digital image processing and deep learning," in *Soft Computing and Signal Processing: Proceedings of 3rd ICSCSP 2020, Volume 2*, 2022, pp. 197-210.
- [105] N. Aravind, S. Nagajothi, and S. Elavenil, "Machine learning model for predicting the crack detection and pattern recognition of geopolymer concrete beams," *Construction and Building Materials*, vol. 297, p. 123785, 2021.
- [106] H. S. Munawar, A. W. Hammad, A. Haddad, C. A. P. Soares, and S. T. Waller, "Image-based crack detection methods: A review," *Infrastructures*, vol. 6, p. 115, 2021.
- [107] N. Safaei, O. Smadi, B. Safaei, and A. Masoud, "Efficient road crack detection based on an adaptive pixel-level segmentation algorithm," *Transportation Research Record*, vol. 2675, pp. 370-381, 2021.
- [108] S. Kostić and D. Vasović, "Prediction model for compressive strength of basic concrete mixture using artificial neural networks," *Neural Computing and Applications*, vol. 26, pp. 1005-1024, 2015.
- [109] Y. Liu, B. He, F. Liu, S. Lu, and Y. Zhao, "Feature fusion using kernel joint approximate diagonalization of eigen-matrices for rolling bearing fault identification," *Journal of Sound and Vibration*, vol. 385, pp. 389-401, 2016.
- [110] Y. Meng, L. Lu, and J. Yan, "Shaft orbit feature based rotator early unbalance fault identification," *Procedia CIRP*, vol. 56, pp. 512-515, 2016.
- [111] K. Ščupáková, V. Terzopoulos, S. Jain, D. Smeets, and R. M. Heeren, "A patch-based super resolution algorithm for improving image resolution in clinical mass spectrometry," *Scientific reports*, vol. 9, p. 2915, 2019.
- [112] J. Zhang, P. Wang, R. X. Gao, and R. Yan, "An image processing approach to machine fault diagnosis based on visual words representation," *Procedia Manufacturing*, vol. 19, pp. 42-49, 2018.
- [113] K.-L. Hung and C. H. Tsai, "Image error detection and error concealment technique based on interleaving prediction and direction information hiding," in *2010 First International Conference on Pervasive Computing, Signal Processing and Applications*, 2010, pp. 371-376.
- [114] R. Lukac, K. Martin, and K. Platanoitis, "Digital camera zooming based on unified CFA image processing steps," *IEEE Transactions on Consumer Electronics*, vol. 50, pp. 15-24, 2004.
- [115] F. Wu, Z. Yang, X. Mo, Z. Wu, W. Tang, J. Duan, et al., "Detection and counting of banana bunches by integrating deep learning and classic image-processing algorithms," *Computers and Electronics in Agriculture*, vol. 209, p. 107827, 2023.
- [116] K. Adem, M. M. Ozguven, and Z. Altas, "A sugar beet leaf disease classification method based on image processing and deep learning," *Multimedia Tools and Applications*, vol. 82, pp. 12577-12594, 2023.
- [117] M. Rottmann and M. Reese, "Automated detection of label errors in semantic segmentation datasets via deep learning and uncertainty quantification," in *Proceedings of the IEEE/CVF Winter Conference on Applications of Computer Vision*, 2023, pp. 3214-3223.

- [118] S. Prabhakaran, R. A. Uthra, and J. Preetharoseyn, "Deep Learning-Based Model for Defect Detection and Localization on Photovoltaic Panels," *Computer Systems Science & Engineering*, vol. 44, 2023.
- [119] T.-Y. Lin, P. Dollár, R. Girshick, K. He, B. Hariharan, and S. Belongie, "Feature pyramid networks for object detection," in *Proceedings of the IEEE conference on computer vision and pattern recognition*, 2017, pp. 2117-2125.
- [120] C. Edwards, "Growing pains for deep learning," *Communications of the ACM*, vol. 58, pp. 14-16, 2015.

Table 4. Research Related Summary.

Author(s) /Year	Suggested method	Parameters and variables	Advantages / Result
[101] Liu et al. 2022	HTR algorithm efficiently and accurately recognizes cage structures.	Resources, gas storage, transport, separation, water desalination, refrigeration.	HTR algorithm efficiently identifies complete cages, hydrates in large-scale systems, and unique topological isomers of cages. Validated for clathrate hydrate identification under mechanical loads.
[102] Kheradmandi and Mehranfar 2022	Research analyses image segmentation algorithms for automated distress detection in pavement images under various conditions.	Image segmentation, irregular dark lines cracks	Research analyses image segmentation algorithms for automated distress detection in pavement images under various conditions.
[103] Hazzan and Pacella 2022	SEM images developed for crack identification method.	SEM images aid in crack identification and quantification.	Study uses MATLAB to identify and quantify cracks in SEM tungsten carbide microstructure, segmenting regions and extracting geometry information. SEM crack segmentation accuracy over 95% achieved using various laser processing parameters.
[104] Yadhunath et al. 2022	Computer vision techniques	Surface crack	The paper presents two approaches for surface crack inspection systems: digital image processing and deep learning.
[105] Aravind et al. 2021	Work uses image processing and machine learning algorithms to identify cracks and validate techniques.	Determine the confusion matrix, accuracy, precision, recall scores	Experimental images were processed and failure pattern recognition in Python using six machine learning classifiers. Support vector classifiers achieved 100% accuracy in identifying failure patterns, outperforming the other classifiers.
[106] Munawar et al. 2021	This paper provides a review of image-based crack detection techniques which implement image processing and/or machine learning	Crack detection, possible defects	Image processing and machine learning techniques analyze infrastructure parts for defects, improving performance and crack detection robustness. This paper provides a review of image-based crack detection techniques which implement image processing and/or machine learning. A total of 30 research articles have been collected for the review which is published in top tier journals and conferences in the past decade. A comprehensive analysis and comparison of these methods are performed to highlight the most promising automated approaches for crack detection.
[107] Safaei et al. 2021	New method detects cracks in 2-D pavement images using adapted weighted neighborhood pixels segmentation algorithm and Gaussian cumulative density function as adaptive threshold	Detect cracks	The proposed algorithm, tested on 300 images, is time and cost-efficient, taking less than 3.15 seconds per 320x480 pixels image. It is ideal for county-level pavement maintenance projects requiring cost-effective crack detection systems.
[108] Klára Ščupáková, et al.	Patch-based super-resolution (PBSR) enhances the spatial resolution of MSI by guiding high-resolution features from one	Linear interpolation (LI) image fusion (IF)	This study uses PBSR to improve MSI resolution, validated using phantom images and mouse cerebellum samples. PBSR outperformed linear interpolation and image fusion, showing advantages

Author(s) /Year	Suggested method	Parameters and variables	Advantages / Result
2019	modality to reconstruct low-resolution images.		in quantitative and qualitative assessments. It has potential clinical applicability in integrating structural and molecular information.
[109] Zhang et al. 2018	This paper presents an image-processing approach for extracting features from vibration signals using visual word representation. It uses PBSR to increase MSI resolution and validates its performance using phantom images and mouse cerebellum samples.	Machine fault diagnosis, remaining service life prognosis	This paper presents an image processing method for automatically extracting features from vibration signals using visual word representation. The method uses wavelet transform to recognize fault-related patterns and uses a sparse representation-based classifier for classification accuracy.
[110] Kuo-Lung Hung 2017	New image authentication technique embeds image block directions for verification.	Variability, error image transmission, detect transmission error	The image authentication technique addresses malicious image modification and error transmission issues. This paper proposes a new image authentication technique embedding image block directions for verification, extracting information to detect transmission errors, and incorporating an interleaving prediction method to repair erroneous regions, improving image quality post-transmission.
[111] Liu et al. 2016	Review of literature on component detection and defect detection, identifying challenges for future research.	Maintain the reliability, safety, and sustainability of power transmission	This paper summarizes literature techniques and methodologies, including data description and method performance. It reviews current works in component detection and defect detection diagnosis, identifying challenges for future research. Discusses deep-learning analysis methods for power lines inspection, identifies future research trends, and discusses data quality issues.
[112] Meng et al. 2016	Research develops webcam-based failure detection method for ME process.	Spaghetti-shape error, abnormal printing is detection	Webcam uses CNN for image classification and object recognition. The trained image model achieved 97% accuracy and was tested on a 3D printer monitoring system to detect "spaghetti-shape-error" and 96% abnormal deposition processes. The method analyses ME processes in real-time and informs users or halts them.
[113] Kosti and Vasovi 2015	Recent advancements in image processing systems reviewed and analyzed for future research.	Review Articles	Recent advancements in image processing systems reviewed and analyzed for future research. Advanced image processing systems developed; new techniques introduced for various applications.
[114] Lukac, Rastislav and Karl Martin 2014	Machine vision	Image enhancement, machine vision. Improving images	Image processing consists of two branches: image enhancement and machine vision. Enhancing images involves using blur filters and increasing contrast to enhance visual quality and display in the target environment. Machine vision focuses on understanding image meaning for tasks like robotics and image axis.
[115] Wu et al. 2023	Deep Learning	Bunch detection, target segmentation, accuracy rate	These algorithms combined to calculate the number of bunches in the two periods. The convolutional neural network Deeplab V3 + model and classic image-processing algorithm. The results indicated a target segmentation MIoU of 0.878 during the debudding period, a mean pixel precision of 0.936, and a final bunch detection accuracy rate of 86%. Bunch detection was highly challenging during the harvest period, with a detection accuracy rate of 76% and a final overall bunch counting accuracy rate of 93.2%.

Author(s) /Year	Suggested method	Parameters and variables	Advantages / Result
[116] Adem et al. 2023	Faster R-CNN, SSD, VGG16, Yolov4 deep learning models	Accuracy rate	Leaf spot disease appears as individual circular spots on the sugar beet leaves and over time spreads to the entire leaf, resulting in complete death of the leaf. Faster R-CNN, SSD, VGG16, Yolov4 deep learning models were used directly, and Yolov4 deep learning model with image processing was used in a hybrid way for automatic determination of leaf spot disease on sugar beet and classification of severity. The proposed hybrid method for the diagnosis of diseases and identifying the severity was trained and tested using 1040 images, and the classification accuracy rate of the most successful method was found to be 96.47%.
[117] Rottmann et al. 2023	deep neural networks (DNNs)	Accuracy rate	Annotation acquisition for semantic segmentation datasets is time-consuming and requires plenty of human labor. In particular, review processes are humans can easily overlook time consuming and label errors. The consequences are biased benchmarks and in extreme cases also performance degradation of deep neural networks (DNNs) trained on such datasets. DNNs for semantic segmentation yield pixel-wise predictions, which makes the detection of label errors via uncertainty quantification a complex task.
[118] Prabhakaran et al. 2023	Real-Time Multi Variant Deep Learning Model (RMVDM), Gray Scale Quantization Algorithm (GSQA), Multi Variant Deep learning	Accuracy rate	The method considers different defects like a spotlight, crack, dust, and micro-cracks to detect the defects as well as localizes the defects. The image data set given has been preprocessed by applying the Region-Based Histogram Approximation (RHA) algorithm. The preprocessed images are applied with Gray Scale Quantization Algorithm (GSQA) to extract the features. Extracted features are trained with a Multi Variant Deep learning model where the model trained with a number of layers belongs to different classes of neurons. Each class neuron has been designed to measure Defect Class Support (DCS). Further, the method uses the Higher- Order Texture Localization (HOTL) technique in localizing the defect. The proposed model produces efficient results with around 97% in defect detection and localization with higher accuracy and less time complexity.
[46] Hor et al. 2015	Combining color and texture features	High efficiency of the automatic method of recovery	Recovery systems aim to provide relevant information to users, with images being crucial for conveying significant information.

Fuzzy Logic Based Geographical Routing for Urban Vehicle Ad-Hoc Networks Based on Intersection Detection

Foruzan Samandari¹, Abdolnabi AnsariAsl¹ , Ali Barati¹

1- Department of Computer Engineering, Dezful Branch, Islamic Azad University, Dezful, Iran.
Email: samandari@iaud.ac.ir, ansariasl@iau.ac.ir (Corresponding author), abarati@iaud.ac.ir

ABSTRACT:

Vehicular ad-hoc networks are a type of ad-hoc network that lacks a fixed infrastructure. The network's nodes are vehicles that self-organize and perform various network operations, including packet routing and network management. These networks enable intelligent autonomous behavior in vehicles, particularly in situations such as accidents. Each vehicle in a vehicular ad-hoc network acts as a network node, and these nodes can collaborate to enhance network efficiency. Nowadays, technologies like vehicular ad-hoc networks are widely employed to enhance traffic flow and transportation in urban areas. Routing in vehicular ad-hoc networks remains a fundamental challenge in these networks. This article presents a routing method specifically designed for vehicular ad-hoc networks operating in urban environments. Given that urban environments consist of numerous roads and intersections, the proposed approach is divided into three phases. The first phase introduces an intersection detection method that does not require a city map. It classifies the network nodes into two categories: those located at intersections and those outside intersections. The second phase presents a routing method for nodes outside intersections, while the third phase outlines a method for determining routes for nodes within intersections. To evaluate the performance of the proposed method, key parameters such as packet delivery ratio, routing overhead, throughput, and end-to-end delay have been analyzed. The results indicate that the proposed method outperforms other existing methods.

KEYWORDS: Vehicular ad-hoc networks, Fuzzy logic, Routing, Intersection.

1- INTRODUCTION

Vehicular ad-hoc networks (VANETs) are a type of mobile ad hoc networks that enable communication between vehicles in close proximity and between vehicles and fixed equipment typically installed on the roadside [1]. The primary purpose of VANETs is to facilitate the establishment and maintenance of a communication network among vehicles in emergency situations, without relying on a central base station or controller [2]. The absence of infrastructure in VANETs places additional responsibilities on the network nodes, which are the vehicles themselves [3]. Each vehicle becomes an integral part of the network and assumes the responsibility of managing and controlling its communications within the network. Automotive ad hoc networks are responsible for facilitating communication between vehicles operating within a specific environment [4].

VANETs serve three main distinct purposes: safety, convenience, and commercial use. Vehicles can swiftly receive notifications about accidents within a few hundred meters and proactively adjust their routes [5]. They can also communicate with other vehicles to inquire about traffic conditions, obtain information about upcoming intersections or side streets, and share insights about the traffic situation [6]. By leveraging the information obtained from surrounding vehicles, drivers can make more informed decisions, resulting in safer, more comfortable, and enjoyable driving experiences [7].

Routing plays a crucial role in VANETs. Due to the high mobility nature of these networks, designing efficient routing protocols poses significant challenges [8]. The dynamic nature of VANETs creates obstacles in devising effective routing mechanisms [9]. Numerous routing protocols have been introduced in recent years to address these

Paper type: Research paper

<https://doi.org/>

Received: 28 April 2024; revised: 18 May 2024; accepted: 29 June 2024; published: 1 September 2024

How to cite this paper: F. Samandari, A. AnsariAsl, A. Barati, “**Fuzzy Logic Based Geographical Routing for Urban Vehicle Ad-Hoc Networks Based on Intersection Detection**”, *Majlesi Journal of Telecommunication Devices*, Vol. 13, No. 3, pp. 137-149, 2024.

challenges. These protocols enable data exchange between separate nodes through intermediate network nodes [10]. Sending real-time and timely messages in VANETs is particularly challenging, as prompt message delivery is crucial in critical scenarios such as accidents. Delays in delivering warning messages can lead to irreversible consequences [11]. The unique characteristics of these networks, including drivers' decision-making processes, high speeds, and continuous vehicle movements, necessitate robust routing mechanisms for efficient data dissemination [12]. Due to the high mobility nature of VANETs, designing efficient routing protocols is an arduous task [13].

The research motive of the proposed method presented in this article is:

- Geographical routing in VANETs has significant potential for optimizing network resource utilization and reducing communication overhead. By taking into account the geographical location and movement patterns of vehicles, intelligent routing decisions can be made to establish efficient and direct communication paths. This approach reduces latency, mitigates packet loss, and improves overall network throughput, enabling real-time data exchange such as traffic updates, emergency notifications, and route recommendations among vehicles.

- Geographical routing offers resilience against network disruptions, including node failures, limited connectivity, and high congestion. By utilizing spatial information, routing protocols can dynamically select alternate routes based on real-time traffic conditions, ensuring reliable end-to-end communication. This resilience is crucial for critical applications such as collision avoidance systems, emergency services coordination, and cooperative driving, where even a momentary communication breakdown can have severe consequences.

- Geographical routing algorithms are specifically designed to handle the challenges posed by high vehicle density, complex road networks, and heterogeneous mobility patterns in urban areas. They take into account the unique characteristics of urban environments, adapting to dynamic vehicular traffic, accommodating frequent changes in network topology, and addressing obstacles such as buildings and urban infrastructure. By incorporating contextual information such as road conditions, traffic congestion, and vehicle density, geographical routing enables efficient and context-aware data dissemination, facilitating intelligent traffic management and urban planning.

To achieve these goals, we propose a routing method for vehicular ad-hoc networks in urban environments. Given the complex nature of urban areas with multiple roads and intersections, our approach consists of three steps. In the first step, we introduce an intersection detection method that operates without relying on a city map. This method categorizes the vehicles in the network into two groups: those located within intersections and those outside of intersections. In the second step, we present a routing method specifically designed for vehicles outside of intersections. This routing method aims to efficiently direct the traffic flow and optimize communication paths between these vehicles. In the third step, we propose a method for determining the routes of vehicles within intersections. This method takes into account various factors, such as traffic conditions and priority rules, to ensure safe and efficient movement of vehicles within these complex road junctions. The main contributions and innovations of our proposed method include:

- Intersection detection method without the need for an urban map: One of the key innovations of this paper is the introduction of an intersection detection method for VANET networks in urban environments that does not rely on an urban map. This method accurately detects intersections without requiring detailed or up-to-date city maps. This capability is particularly valuable in situations where precise city maps are unavailable or outdated.

- State-based intersection routing method: The paper presents a routing method for vehicles both inside and outside intersections in VANET networks. This method performs routing separately based on the status of vehicles at intersections and those outside of them. This innovation improves routing performance in VANET networks in urban environments.

- Comprehensive evaluation of the proposed method's performance: The paper conducts a thorough evaluation of the proposed routing method, considering metrics such as packet delivery ratio, routing overhead, throughput, and end-to-end latency. The results demonstrate that the proposed method outperforms other methods, affirming its effectiveness and efficiency in VANET routing in urban environments.

The remaining sections of the paper are organized as follows: Section 2 provides an overview of the related work. Section 3 presents the details of the proposed method. The simulation and analysis of the proposed method are presented in Section 4. Finally, Section 5 concludes the paper.

2- RELATED WORKS

In [14], a routing protocol called Rectangle-Aided LAR (RALAR) is proposed for Vehicular Ad-Hoc Networks (VANETs). The protocol incorporates a heuristic approach to differentiate accurate GPS location data from weaker ones, thereby improving data reliability. RALAR utilizes a moving rectangular zone based on node mobility models to optimize routing decisions. Furthermore, a Genetic Algorithm (GA) is employed to optimize the selection of a time-out variable, further enhancing the protocol's performance. The performance of RALAR is compared to that of LAR and KALAR protocols, using metrics such as Packet Delivery Ratio (PDR), average End-to-End Delay (E2E Delay), routing

overhead, and energy consumption.

In [15], a routing protocol called TAD-HOC (TROPHY-based Ad Hoc) is proposed for VANET networks with the aim of enhancing efficiency and resource utilization. The TAD-HOC protocol combines the ad hoc network with the TROPHY protocol to enable data transmission based on time demand while ensuring desired authentication. Experimental results demonstrate improved performance in terms of packet delay, transmission range, and end-to-end delay when compared to I-AODV, AODV-R, and AODV-L protocols. The integration of ad hoc principles with secure routing capabilities in the TAD-HOC protocol provides an effective solution for VANET networks, surpassing other protocols in terms of network performance measures.

In [16], a hybrid routing algorithm called GAACO (Genetic Algorithm and Ant Colony Optimization) is proposed for optimizing VANET routing in realistic traffic scenarios. GAACO combines genetic algorithm (GA) and ant colony optimization (ACO) techniques to enhance routing efficiency. The algorithm is compared to traditional VANET routing approaches and metaheuristic methods using traffic scenarios from Dehradun City. The implementation is tested using SUMO and NS3.2 simulation tools. Performance evaluation encompasses metrics such as average throughput, packet delivery ratio, end-to-end delay, and packet loss. Experimental results demonstrate that GAACO outperforms other protocols, including PSO, ACO, and AODV across all scenarios.

In [17], the authors introduce DyTE, a novel routing protocol for VANETs that dynamically selects a trilateral zone based on node coordinates to enhance Packet Delivery Ratio (PDR) and throughput. DyTE restricts participation to only relevant nodes, thereby reducing the network routing load. Comparative analysis with existing protocols demonstrates that DyTE significantly improves PDR and throughput while maintaining reliability. By dynamically adjusting the communication zone, DyTE optimizes routing and promotes efficient data transmission in VANETs. The protocol's ability to selectively involve relevant nodes contributes to improved network performance, making it a promising solution for enhancing routing efficiency in VANETs.

In [18], the authors propose ECRDP, an Efficient Clustering Routing approach for vehicular networks. ECRDP utilizes a clustering algorithm that combines Density Peaks Clustering (DPC) and Particle Swarm Optimization (PSO). The approach involves using PSO or a new fitness function based on DPC to determine cluster heads. Clustering is performed based on the link reliability between vehicles. Additionally, a maintenance phase is introduced to update cluster heads and redistribute vehicles as needed. The ECRDP approach aims to optimize cluster formation and routing efficiency in vehicular networks by selecting appropriate cluster heads and adapting to network changes. By combining DPC and PSO, the method improves network performance and adaptability, leading to enhanced efficiency in vehicular network routing.

In [19], a Hybrid Genetic Firefly Algorithm-based Routing Protocol (HGFA) is proposed for Vehicular Ad-Hoc Networks (VANETs) with the objective of enhancing communication speed. The protocol integrates the Genetic Algorithm (GA) with the Firefly algorithm to achieve faster and more reliable routing in both sparse and dense network scenarios. By combining the adaptive mutation capability of GA with the efficient routing properties of the Firefly algorithm, the HGFA protocol enables dynamic adjustment and optimization of routing strategies based on VANET requirements. This hybrid approach significantly improves VANET routing performance, enhancing communication speed and reliability.

In [20], the authors present TGRV, a trust-based geographic routing protocol designed for VANETs (Vehicular Ad-Hoc Networks). TGRV aims to mitigate the involvement of malicious vehicles by considering both direct and recommendation trust when selecting the next-hop for packet forwarding. A monitoring system is employed to enable vehicles to assess the packet forwarding rate of their next-hop and update trust values accordingly. Push-based notifications facilitate the sharing of observations among vehicles and the update of recommendation trust with neighboring vehicles. The monitoring system utilizes distance prediction and a modified promiscuous mode to accurately estimate the packet forwarding capability of vehicles. Trust values decay over time, enhancing the accuracy of trust management. Additionally, TGRV incorporates the number and trust levels of two-hop neighbors to select a more trusted next-hop for routing.

In [21], the authors propose DARVAN, a fully decentralized infrastructure aimed at addressing location privacy and reliability issues in VANET routing protocols. DARVAN utilizes a distributed database and collective consensus mechanisms to minimize the exposure of data typically stored in centralized units. The I2P (Invisible Internet Project) protocol is modified to enhance routing reliability and resilience against various adversary activities in VANETs. Notably, DARVAN provides an effective and efficient network-level mitigation for Sybil attacks in VANETs. By adopting a decentralized approach, DARVAN offers anonymous and reliable routing while ensuring location privacy. The protocol's emphasis on decentralization and security makes it a promising solution for improving the performance and security of VANET routing protocols.

In [22], the authors propose RTRV, an RSU-assisted trust-based routing protocol for VANETs (Vehicular Ad-Hoc Networks). RTRV incorporates trust criteria to ensure secure routing in the network. The protocol includes a reliable

monitoring process where two vehicles observe the behavior of the next-hop in forwarding packets, updating the direct trust value. These observations are reported to RSUs (Roadside Units), which update the indirect trust and provide recommendations to nearby vehicles. RSUs also actively participate in data packet routing, contributing to improved performance. RTRV aims to identify and limit the influence of malicious nodes, thereby increasing resistance to trust-based attacks. By integrating trust management and leveraging the capabilities of RSUs, RTRV enhances routing security and efficiency in VANETs.

In [23], the authors propose TT-SHO, a novel secured protocol for VANETs. TT-SHO combines Tent Tuned Spotted Hyena Optimization (TT-SHO) for routing and Hybrid Chaotic Encryption for data transmission security. The TT-SHO algorithm optimizes the shortest path for routing while ensuring the transmission of chaotic encrypted data with a focus on maintaining Quality of Service (QoS). Experimental results demonstrate low latency, high Packet Delivery Ratio (PDR), and reliable throughput when compared to existing frameworks. The proposed protocol outperforms other approaches, providing safe, reliable, and robust data transmission in VANETs. The integration of TT-SHO and Hybrid Chaotic Encryption enhances security and maintains QoS, making it a promising solution for secure and efficient communication in VANET environments.

3- PROPOSED METHOD

The proposed approach is divided into three phases. In the first phase, an intersection detection method is presented that does not require a city map. The status of the Duran network vehicles is categorized into two groups: those located within the intersection and those outside the intersection. In the second phase, a routing method is introduced for the nodes outside the intersection. In the third phase, a method is provided for determining the route for the nodes within the intersection. In the proposed method, each node periodically sends a packet containing its ID, location, direction, speed, and sending time at specific intervals. This packet is broadcasted to all neighboring nodes. The structure of this message is illustrated in Figure (1).

ID	Location	Direction	Speed	Time
----	----------	-----------	-------	------

Fig. 1. INF packet structure

Each node maintains a neighbors table to store information about its neighboring vehicles. The structure of this table is depicted in Table (1).

ID	Location	Direction	Speed	Time
----	----------	-----------	-------	------

After receiving the INF packet from its neighbors, the vehicle performs the following actions based on the neighbor vehicle ID:

- If the vehicle ID exists in the table and the packet time is older than the recorded time in the neighbor table, the packet is discarded.
- If the vehicle ID exists in the table and the received packet time is newer than the recorded time in the neighbor table, the corresponding row in the table is updated.
- If the vehicle ID of the received packet is not found in the table, a new row is created to register the new vehicle in the table.

Considering the dynamic nature of the network topology in vehicular environments, if a packet from a vehicle is not received and the corresponding row in the neighbor table is not updated for a period exceeding $2t$, it is assumed that the vehicle has left the neighborhood. Consequently, the corresponding row is removed from the table. Here, t represents the time interval for sending the INF packet to the neighbors. The steps of the proposed method are described below.

8. 3-1- First phase: Intersection detection

The intersection detection method is performed individually by each node in the proposed approach. In this method, an intersection is defined as a location where a moving vehicle can establish communication not only in the direct direction (front and rear) but also with vehicles in other directions. The different types of intersections that are possible

are illustrated in Figure (2).

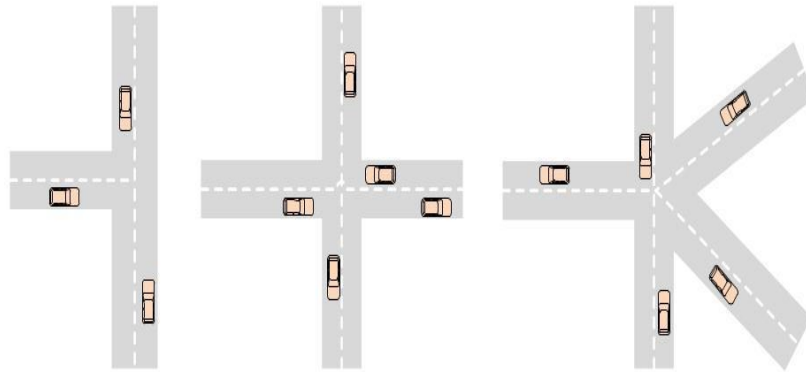


Fig. 2. Types of intersections

Considering that routing in the proposed method is based on the positioning of nodes within the intersection, the status of each node in the network is categorized into two states: being in the intersection and being outside the intersection. Consequently, each node in the network determines its status by examining the packets received and stored in the neighbor table. The following steps outline the process of determining the node's status.

Step 1: Each node defines a circular wireless communication space around itself with a radius of r (communication range). This communication space is divided into eight equal and non-overlapping slices using four diameters, as depicted in Figure (3).

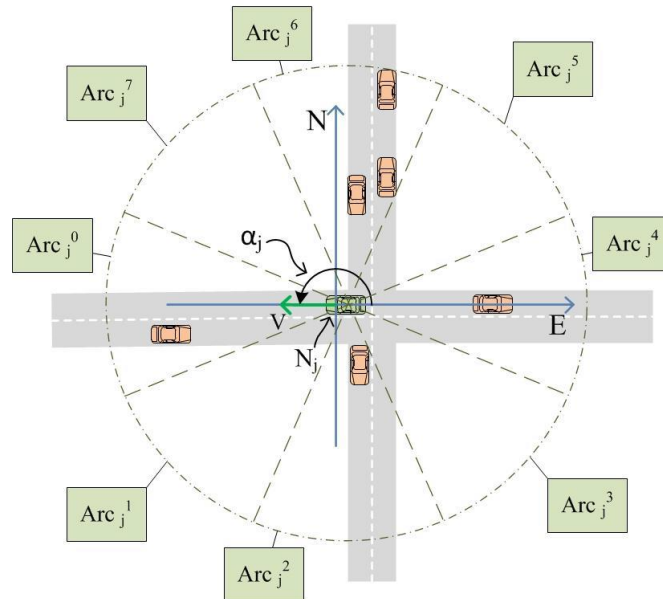


Fig. 3. Intersection division

Step 2: The starting and ending angles of each arc are calculated using Equation (1).

$$Arc_i^j = \begin{cases} start : \alpha_j + \frac{i\pi}{4} - \frac{\pi}{8} \\ End : \alpha_j + \frac{i\pi}{4} + \frac{\pi}{8} \end{cases} \quad (1)$$

Where $i=0,1,2,\dots,7$ and α_j is the angle of the speed vector of node j with respect to the horizontal coordinate axis.

Step 3: Each vehicle sends an ARCINFO packet to its neighbors. Based on the information in the neighbor table, the vehicle calculates the difference in direction with the neighboring node using Equation (2).

$$Direction_{ij} = |Direction_i - Direction_j| \quad (2)$$

Where $Direction_{ij}$ indicates the difference in the direction of the source vehicle i and the source vehicle j . $Direction_i$ is the direction of the source node and $Direction_j$ is the direction of the neighboring node j .

Step 4: Based on the calculated direction difference, the arc representing the location of each neighboring node is determined and recorded in the neighbor table.

Step 5: If all the neighboring nodes in the neighbor table are positioned within the arcs in front of and behind the node, it indicates that the node is not within the intersection.

Step 6: If half of the neighboring nodes of the current node are located within arcs other than the arc in front of and behind the node, it indicates that the node is within the intersection.

9. 3-2- Second phase: Routing outside the intersection

Routing is conducted outside the intersection among vehicles traveling in the same direction on a road. In this phase of the proposed method, each node follows the following steps to determine its next move, utilizing the information stored in the neighbor table.

Step 1: Initially, the source vehicle compares the direction of the destination with the direction of its neighboring vehicles (as indicated by the Direction field in the neighbor table). Vehicles that are moving in the opposite direction of the destination are excluded from the routing process. Nodes that are traveling in the same direction as the destination vehicle are added to set D, utilizing Equation (3).

$$D = \{N_i | N \in \text{Neighbors Table. } Direction_i - Direction_d < 90 \quad (3)$$

Where $Direction_d$ is the direction of the destination node and $Direction_i$ is the direction of the neighboring node.

Step 2: The source vehicle calculates the distance to the destination for the nodes in set D using Equation (4) and determines the speed difference between itself and each node using Equation (5).

$$Distance_{id} = \sqrt{(x_i - x_d)^2 + (y_i - y_d)^2} \quad (4)$$

Where (x_i, y_i) are the coordinates of the neighboring node and (x_d, y_d) are the coordinates of the destination node.

$$DiffSpeed_{si} = Speed_s - Speed_i \quad (5)$$

Where $Speed_s$ is the speed of the origin node and $Speed_i$ is the speed of the neighboring node.

Step 3: the source vehicle evaluates the member nodes of set D using equation (6).

$$Fit_i = \left(1 - \frac{Distance_{id}}{Distance_{sd}}\right) + \left(1 - \frac{DiffSpeed_{si}}{\max(diffspeed)}\right) \quad (6)$$

Where $Distance_{id}$ is the distance of the neighboring node to the destination node and is calculated based on equation (4), $Distance_{sd}$ is the distance of the origin node to the destination node and is calculated based on equation (7). $DiffSpeed_{si}$ is the speed difference of the neighboring node with the original node, which is calculated based on the equation (3-5), and $\max(diffspeed)$ is the maximum speed difference calculated with the neighbors in set D.

$$Distance_{sd} = \sqrt{(x_s - x_d)^2 + (y_s - y_d)^2} \quad (7)$$

Where (x_s, y_s) are the coordinates of the origin node and (x_d, y_d) are the coordinates of the destination node.

Step 4: The source vehicle evaluates the scores of the nodes in set D, and selects the nodes whose score is greater than or equal to half of the highest score. These selected nodes are then included in set C, determined using Equation (8).

$$C = \{N_i | N \in D. Fit_i \geq \frac{\max(Fit_i)}{2}\} \quad (8)$$

Step 5: The source vehicle sends the data packet to the neighboring vehicle in set C that has the shortest distance to the destination.

10. 3-3- Third phase: Routing at the intersection

If the node detects that it is in an intersection, the next step is chosen by taking into account the relevant factors and employing fuzzy logic. The following steps outline this phase of the proposed method.

11. Step 1: Fuzzy inputs

The inputs of the fuzzy system at this stage are density and distance to the destination.

- Density or the number of neighbors: This parameter is significant and influential in selecting the next step, as it affects the network's connectivity and potential delays. A high density of nodes can lead to increased connections and network congestion, while a low number of neighbors can result in a higher likelihood of failure and weaker links between nodes. To determine the density of neighboring nodes, the source node sends a REQ packet to its neighbors. In response, the neighboring nodes send the count of their neighbors, based on the neighbor table, to the source node in the form of a REP message. The structure of the REP message is illustrated in Figure (4).

ID	Density
----	---------

Fig. 4. REP packet structure

The membership diagram for neighbor density is depicted in Figure (5).

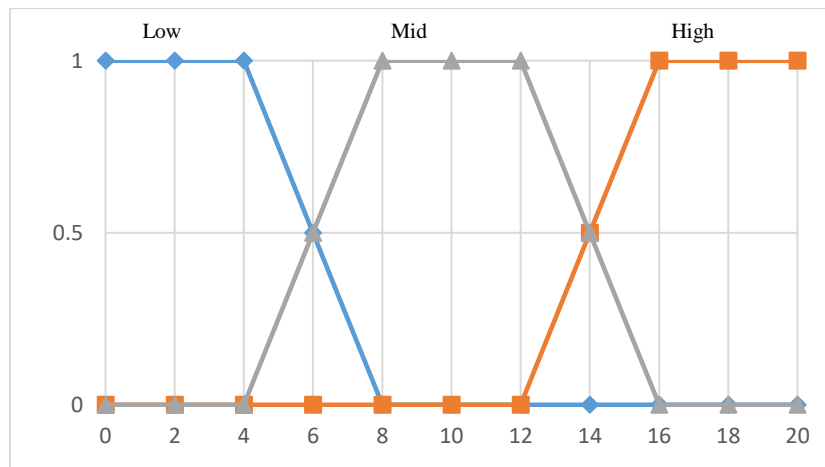


Fig. 5. Density membership chart

- Distance to the destination: Each node computes the distance of its neighboring nodes to the destination using Equation (9) based on the information available in the neighbor table.

$$Distance_{id} = \sqrt{(x_i - x_d)^2 + (y_i - y_d)^2} \tag{9}$$

Where (x_i, y_i) is the coordinates of the neighboring node and (x_d, y_d) is the coordinates of the destination node. The membership chart of the distance to the destination is shown in Figure (6).

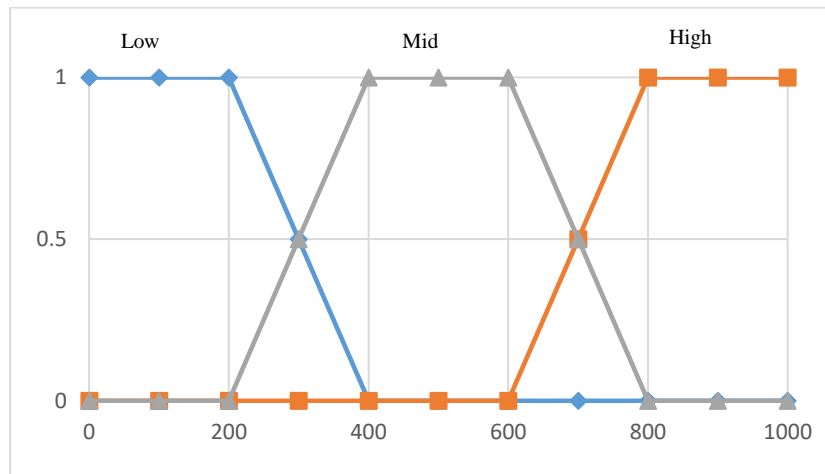


Fig. 6. Distance density membership chart

12. Step 2: Fuzzy rule

A fuzzy if-then rule follows the structure "if fuzzy statement, then fuzzy statement." By employing fuzzy if-then rules, the necessary rules for decision-making can be formulated. The interpretation of these rules is a crucial aspect. In two-valued logic, when considering the rule $P \Rightarrow Q$, its value can be easily determined since the final interpretation is based on the true and false states. The truth table of a regular conditional statement illustrates the relationship between the antecedent and the consequent. In essence, the conditional statement is false when the antecedent is true and the consequent is false. In the proposed method, each input possesses three states: low, medium, and high. The fuzzy system consists of two inputs. The number of fuzzy rules in the proposed method amounts to 9, as exhibited in Table (2).

Table 2. Fuzzy rules

No	IF		Then
	Distance	Density	Cost
1	Low	Low	Medium
2	Low	Mid	Very High
3	Low	High	High
4	Mid	Low	Low
5	Mid	Mid	High
6	Mid	High	Medium
7	High	Low	Very Low
8	High	Mid	Medium
9	High	High	Low

13. Step 3: Fuzzy output

The output function in the proposed method is responsible for determining the probability of selecting a node as the next step in the routing process. The value of the output membership function is obtained using the output weighted average method. In the proposed method, five outputs are considered for the fuzzy system, as illustrated in Figure (7).

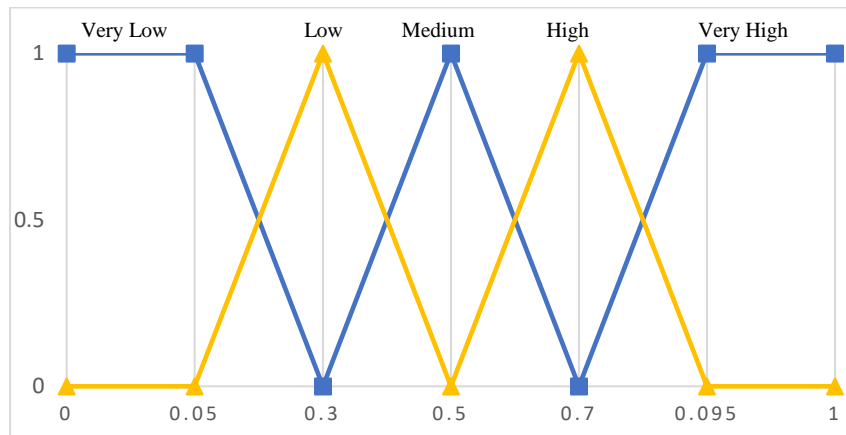


Fig. 7. Fuzzy output.

4- SIMULATION AND RESULTS

The effectiveness of the proposed approach is demonstrated using MATLAB simulation software. The proposed method is compared with DBAFS [24] and EGSR [25] methods. The simulation parameters are provided in Table (3).

Table 3. Simulation parameters.

Parameter	Value
Network size	5000 m^2
Number of nodes	0-500
Velocity	0-42 $\frac{m}{s}$
Communication range	150 m
Source/destination	Random
Simulation time	300 s
Channel type	Wireless channel
MAC type	IEEE 802.11

To assess the performance of the proposed method, various parameters including packet delivery ratio, routing overhead, throughput, and end-to-end delay have been analyzed.

The packet delivery ratio represents the ratio of successfully delivered data packets to the destination compared to the total number of packets sent in the network. The comparison of the packet delivery ratio between the proposed method, DBAFS, and EGSR methods is illustrated in Figure (8), while Figure (9) displays the variation of the packet delivery ratio with respect to different vehicle speeds.

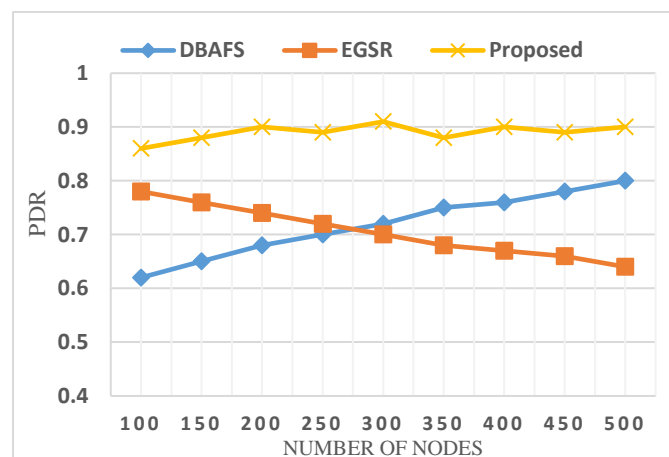


Fig. 8. Packet delivery rate in different number of nodes.

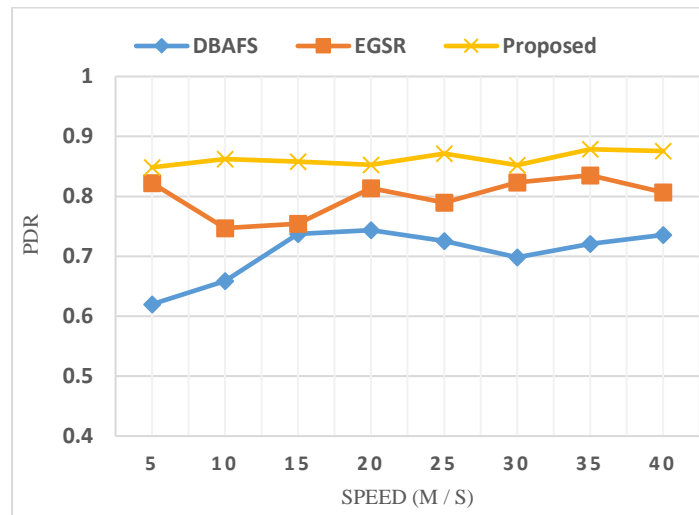


Fig. 9. Packet delivery rate at different speeds of nodes.

In the proposed method, vehicles exchange their information with neighboring nodes at predefined time intervals. If a neighboring node fails to provide its location information within the designated time interval, it is removed from the routing table. This prevents the transmission of packets to neighboring vehicles that are outside the communication range of the source, thus reducing packet loss. Additionally, the proposed method employs two different routing approaches: inside and outside the intersection. In routing outside the intersection, the parameters considered for selecting the next step are the distance to the destination and the speed difference with the neighboring vehicle. In routing within the intersection, the parameters of distance to the destination and density are taken into account, and the best next step is determined using fuzzy logic. Considering these parameters helps establish more stable routes for packet transmission. Consequently, the strategies employed in the proposed method enhance the packet delivery ratio compared to other methods.

The time required for a data packet to travel from the source to the destination is referred to as the end-to-end delay. It encompasses delays stemming from packet buffering, route discovery process, retransmission process, and propagation time. Communication link losses often contribute to delays in many instances. In a vehicular ad-hoc networks, increasing the speed and density of the network raises the likelihood of communication link losses and subsequently increases the end-to-end delay. In the proposed method, selecting more stable routes and considering the parameters of speed and density in both the routing process outside and inside intersections minimize the occurrence of broken links during data transmission, thereby reducing the average end-to-end delay. Hence, as demonstrated in Figure (10) and Figure (11), the proposed method outperforms other methods in various density and speed scenarios within the vehicle network.

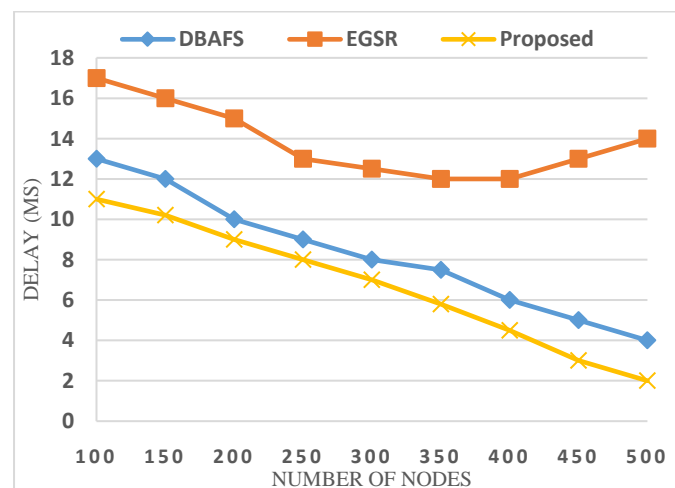


Fig. 10. Average end-to-end delay in different number of nodes.

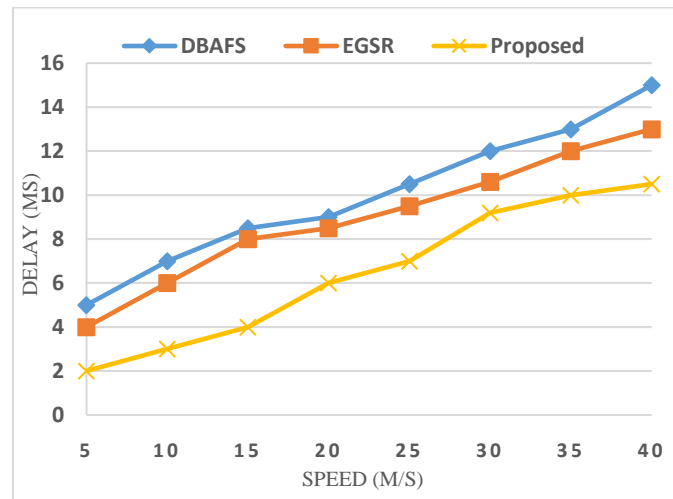


Fig. 11. Average end-to-end delay at different vehicle speeds.

Control messages, such as INFO messages and route discovery messages, serve as control signals and contribute to network overhead, known as control overhead. In the proposed method, control messages are utilized for neighbor table registration and route discovery between vehicles. Additionally, at intersections, control messages are employed for route discovery purposes. As the proposed method is a reactive protocol, it incurs higher control overhead compared to DBAFS methods. Figure (12) illustrates the comparison of control overhead between the proposed method and other methods. It is evident that control overhead increases with a higher number of nodes in the network.

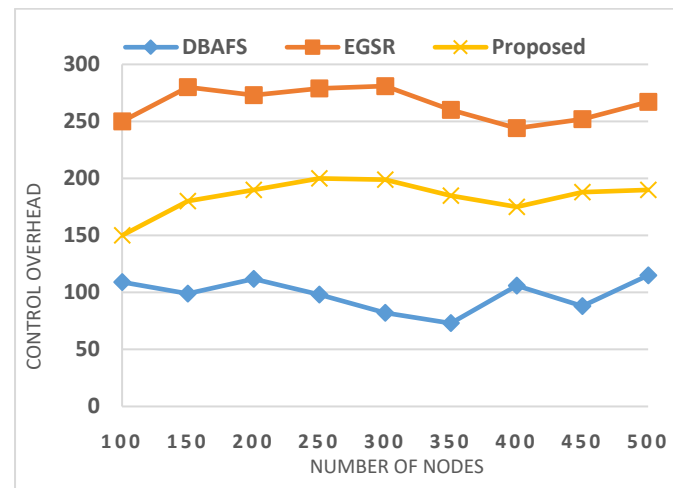


Fig. 12. Control overhead in different number of nodes.

5- CONCLUSION

The primary objective of vehicular ad-hoc networks is to establish communication between vehicles, both within and between road units. Several routing protocols have been proposed for these networks, but they often fail to address all the challenges specific to such environments. This paper presents a routing method for vehicular ad-hoc networks in urban environments. Given the complex nature of urban settings, the proposed approach is divided into three phases. In the first phase, an intersection detection method is introduced eliminating the need for a city map. The vehicles in the network are categorized into two groups: those located within intersections and those outside intersections. The intersection detection mechanism is performed independently by each node. Since the routing method in the proposed approach is chosen based on the vehicle's location in the intersection, each node in the network is assigned one of two states: within the intersection or outside the intersection. In the second phase, a routing method is devised for nodes outside the intersection, while in the third phase, a method is presented for determining the route for nodes within the intersection. In the third phase, the selection of the next step is made by considering relevant parameters and employing fuzzy logic. MATLAB simulation software is employed to validate the effectiveness of the proposed approach. A

comparison is made between the proposed method and the DBAFS and EGSR methods. The simulation results demonstrate that the proposed method achieves satisfactory outcomes in terms of packet delivery ratio, routing overhead, throughput, and end-to-end delay.

REFERENCES

- [1] M.Lee,., and T. Atkison.. (2021), “**VANET applications: Past, present, and future**”, *Vehicular Communications*, 28, 100310.
- [2] M.J.N. Mahi,S. Chaki,., S.Ahmed, , M.Biswas, M.S.Kaiser, M.S.Islam,.,and M. Whaiduzzaman, (2022). “**A review on VANET research: Perspective of recent emerging technologies**”, *IEEE Access*, 10, pp.65760-65783.
- [3] A.Katiyar, D.Singh, and R.S. Yadav. (2020). State-of-the-art approach to clustering protocols in VANET: a survey. *Wireless Networks*, 26, pp.5307-5336.
- [4] M.A.Al-shareeda, M.A.Alazzawi, M.Anbar.S. Manickam, and a.k. Al-Ani. (2021, July), “**A comprehensive survey on vehicular ad hoc networks (vanets)**”, *presented at 2021 Int. Conf. Advanced Computer Applications (ACA)* ,pp. 156-160,IEEE.
- [5] O.Senouci, ,S. Harous, and Z Aliouat, . (2020), “**Survey on vehicular ad hoc networks clustering algorithms: Overview, taxonomy, challenges, and open research issues**”, *Int. Journal of Communication Systems*, 33(11), e4402.
- [6] Z.Xia, ,J. Wu, L. Wu, Y.Chen, J.Yang, and P.S. Yu. (2021), “**A comprehensive survey of the key technologies and challenges surrounding vehicular ad hoc networks**”, *ACM Transactions on Intelligent Systems and Technology (TIST)*, 12(4), 1-30.
- [7] T.K.Bhatia, R.K.Ramachandran, R.Doss and L.Pan.. (2020, June), “**A comprehensive review on the vehicular ad-hoc networks**, *presented at 2020 8th Int. Conf. on Reliability, Infocom Technologies and Optimization (Trends and Future Directions)(ICRITO)* (pp. 515-520). IEEE.
- [8] M.S.Azhdari, A.Barati, and H. Barati,., (2022). “**A cluster-based routing method with authentication capability in Vehicular Ad hoc Networks (VANETs)**”, *Journal of Parallel and Distributed Computing*, 169, pp.1-23.
- [9] E.Moridi, and H. Barati, (2023). “**Increase efficiency and reliability in multicasting geographical routing based on Fuzzy Logic in VANETs**”, *Journal of Soft Computing and Information Technology*, 12(1), pp.11-19.
- [10] P.K.Shrivastava, and L.K Vishwamitra. (2021). “**Comparative analysis of proactive and reactive routing protocols in VANET environment**”, *Measurement: Sensors*, 16, 100051.
- [11] L.Hota, B.P.Nayak, A.Kumar, B.Sahoo, and G.M.N. Ali. (2022), “**A performance analysis of VANETs propagation models and routing protocols**”, *Sustainability*, 14(3), 1379.
- [12] E.Moridi, and H. Barati. (2017), “**RMRPTS: a reliable multi-level routing protocol with tabu search in VANET**”, *Telecommunication Systems*, 65(1), pp.127-137.
- [13] E. Bozorgzadeh, H. Barati, , and A. Barati. (2020), “**3DEOR: an opportunity routing protocol using evidence theory appropriate for 3D urban environments in VANETs**”, *IET Communications*, 14(22), pp.4022-4028.
- [14] R C. Muniyandi, ,F. Qamar, and A.N. Jasim. (2020), “**Genetic optimized location aided routing protocol for VANET based on rectangular estimation of position**”, *Applied Sciences*, 10(17), 5759.
- [15] R. Sadakale, N. K. Ramesh, and R. Patil. (2020), “**TAD-HOC routing protocol for efficient VANET and infrastructure-oriented communication network**”, *Journal of Engineering*, 2020, pp.1-12.
- [16] G.D. Singh, S. Kumar, H. Alshazly, S.A. Idris, M. Verma and S.M. Mostafa. (2021), “**A novel routing protocol for realistic traffic network scenarios in VANET**”, *Wireless Communications and Mobile Computing*, 2021, pp.1-12.
- [17] A. K. Kazi, and S.M. Khan. (2021), “**DyTE: an effective routing protocol for VANET in urban scenarios**”, *Engineering, Technology & Applied Science Research*, 11(2), pp.6979-6985.
- [18] K. Kandali, L. El Bennis, O. Bannay, and H. Bennis. (2022), “**An intelligent machine learning based routing scheme for VANET**”, *IEEE Access*, 10, pp.74318-74333.
- [19] G. D. Singh, M. Prateek, S. Kumar, M. Verma, D.Singh, and H. N. Lee. (2022), “**Hybrid genetic firefly algorithm-based routing protocol for VANETs**”, *IEEE Access*, 10, pp.9142-9151.
- [20] S. Shokrollahi, and M. Dehghan. (2023), “**TGRV: A trust-based geographic routing protocol for VANETs**”, *Ad Hoc Networks*, 140, 103062.

- [21] S. K. Monfared, and S. Shokrollahi. (2023), “**DARVAN: A fully decentralized anonymous and reliable routing for VANets**”, *Computer Networks*, 223, 109561.
- [22] M. Azizi, and S. Shokrollahi. (2024), “**RTRV: An RSU-assisted trust-based routing protocol for VANETs**”, *Ad Hoc Networks*, 154, 103387.
- [23] M. Abul Hassan, A.A.Al-Awady, A.Ali, M. Sifatullah, Akram, M.M. Iqbal, M. M and Y.A. Abdelrahman Ali. (2024), “**ANN-Based Intelligent Secure Routing Protocol in Vehicular Ad Hoc Networks (VANETs) Using Enhanced AODV**”, *Sensors*, 24(3), 818.
- [24] S. Haider, G. Abbas, Z. H. Abbas, and T. Baker. (2019), “**DABFS: a robust routing protocol for warning messages dissemination in VANETs**”, *Computer Communications*, 147, pp.21-34.
- [25] F. Goudarzi, H.Asgari, and H. S. Al-Raweshidy, (2018), “**Traffic-aware VANET routing for city environments—A protocol based on ant colony optimization**”, *IEEE Systems Journal*, 13(1), pp.571-581.

Design of Current Starved Voltage Controlled Oscillator with Phase Locked Loop to Estimate the Process Corner Analysis

K. Annamma¹ , Sohbit Saxena², Govin Singh Patel³

1- Research scholar, School of Electronics & Electrical Engineering, Lovely Professional University, Punjab, India.

Email: anusasmi@gmail.com (Corresponding author)

2- School of Electronics & Electrical Engineering, Lovely Professional University, Punjab, India.

Email : sobhit.23364@lpu.co.in

3- School of Electronics & Electrical Eng. ECE Dept, SITCOE, Yadrav, Kolhapur, Greater Noida, India.

Email: govindpatel1104@gmail.com

ABSTRACT:

This paper consists of a performance comparison of Current Starved Voltage Controlled Oscillator (CSVCO) for Phase Locked Loop (PLL). The design of Current Starved VCO is implemented using sleepy stack low power leakage technique. This has been implemented in 45nm CMOS Technology with a supply voltage of 0.45V in Cadence Software. The parameters such as average power, oscillation frequency, and delay are calculated in different process corners showing the performance of improvement results of cadence simulation. After comparison of the various parameters of PLL implemented with Sleep Stack CSVCO and Basic CSVCO, the sleepy stack approach is particularly useful in low power applications, The recommended PLL has a much smaller chip than previous designs, much lower power consumption and significantly higher efficiency. The proposed design of the PLL with Sleep Stack Technique makes the circuit efficiently to reduce sub-threshold leakage current, and achieves Frequency of 2.759 GHz, Power 2.559 μ w, phase noise -63.8(dBc/Hz) and Delay(μ s) 0.0006544, respectively.

KEYWORDS: VCO, PLL, Gain, Gain-or, Lector, Control Voltage, Current starved VCO, Oscillation Frequency, Sleepy Stack, Tuning Range.

14. INTRODUCTION

The Phase Locked Loop (PLL) is a control system used to generate the phase of output signal which is related to the phase of the input signal. The major blocks present in the PLL are Voltage controlled Oscillator and phase detector in a feedback loop. This paper depicts one of the major blocks called VCO. The main functionality of the VCOs is in the communication systems. Among the multiple types of VCOs, the ring oscillators and LC oscillators plays a major role in terms of high frequency, less noise, wide tuning range [1], and the area occupancy. The LC VCO which consists of an inductor and capacitor occupies more area. The ring oscillators consist of the delay cells which have the same functionality similar to the buffer and these cells would occupy more area. In a ring oscillator, the last delay cell output is connected to the first delay cells input [2], which is called feedback. The delay cells can be either single ended or differential accordingly [4]. The increase in the number of delay cells give rise to consumption of area [6]. Because of the differences in the driving capability, the characteristics of the VCO become nonlinear which can be avoided by adding feedback circuit. By adding this feedback circuit, it further leads to the increase in cost of the circuit [7]. The current starved VCO technique was designed in order to overcome the disadvantages caused by the previous VCO's [7].

Paper type: Research paper

<https://doi.org/>

Received: 12 May 2024; revised: 7 June 2024; accepted: 3 July 2024; published: 1 September 2024

How to cite this paper: K. Annamma, S. Saxena, G. Singh Patel, "Design of Current Starved Voltage Controlled Oscillator with Phase Locked Loop to Estimate the Process Corner Analysis", *Majlesi Journal of Telecommunication Devices*, Vol. 13, No. 3, pp. 151-158 2024.

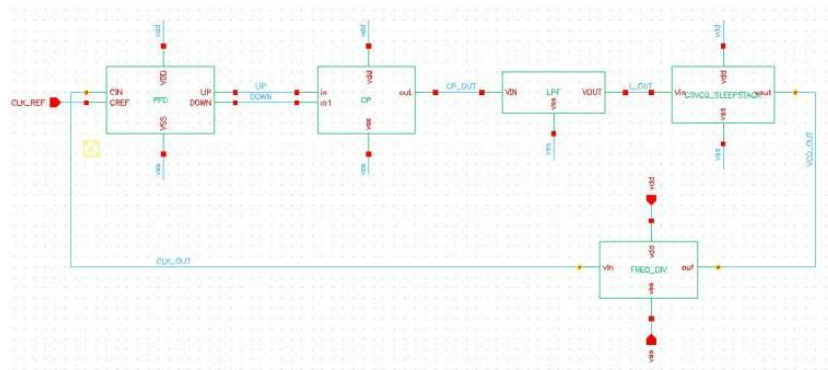


Fig. 1. Schematic diagram for PLL with Sleep Stack Current Starved VCO.

This paper is organized as follows. Section 2 explains basic Current Starved VCO. Section 3 describes different leakage power reduction techniques in CMOS circuits. Section 4 defines simulation results and design comparisons. Finally, section 5 concludes this paper.

2. CURRENT STARVED RING VCO WITH SLEEPY STACK & KEEPER TECHNIQUE

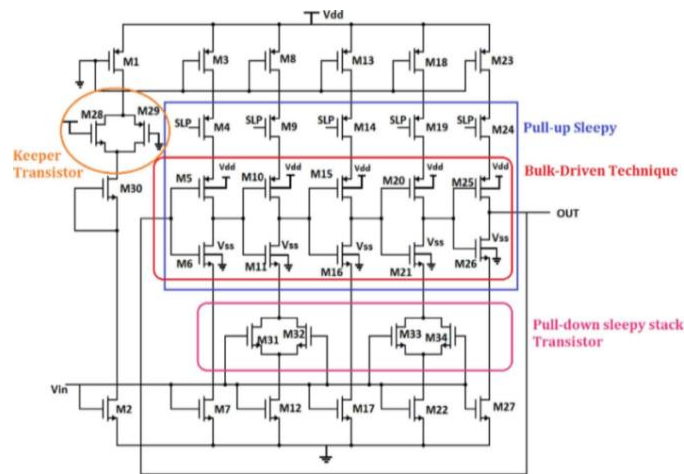


Fig. 2. Current Starved Ring VCO with Sleepy Stack & Keeper Technique Circuit.

The sleepy stack approach is particularly useful in low-power applications or when power efficiency is a critical design consideration. It helps to reduce power consumption without sacrificing the speed or performance of the circuit. The purpose of the alternative arrangement in the proposed circuit is to reduce the number of transistors and the area utilization. The alternative arrangement of the proposed design itself makes the circuit works efficiently to reduce sub-threshold leakage current, which in turn reduces power consumption. Therefore, not all the delay cells in the proposed design need to be connected with the sleepy stack approach.

3. CURRENT STARVED VCO PLL ARCHITECTURE WITH SLEEPY STACK TECHNIQUE

Among the different types of VCO's, ring oscillator is the efficient in terms of frequency and driving capabilities. The ring VCO has been designed with delay stage. When these delay stages increased, lead to the non-linearity of the circuit. This non-linearity can be overcome by increasing the number of delay cells which has increased the complexity of the circuit and also increasing the power consumption [8]. The output frequencies of a basic VCO are controlled by the control voltage whereas the current is controlled by the current starved VCO [9]-[10]. The circuit consists of delay cells along with the current mirror which is used to limit the current to all the delay cells. The current starved VCO alone has also increased the leakages and power consumption [1]. These leakages can be further reduced by applying the low leakage techniques to the delay cells and by varying the aspect ratio of transistors which reduces the threshold voltage of basic current starved VCO [11].

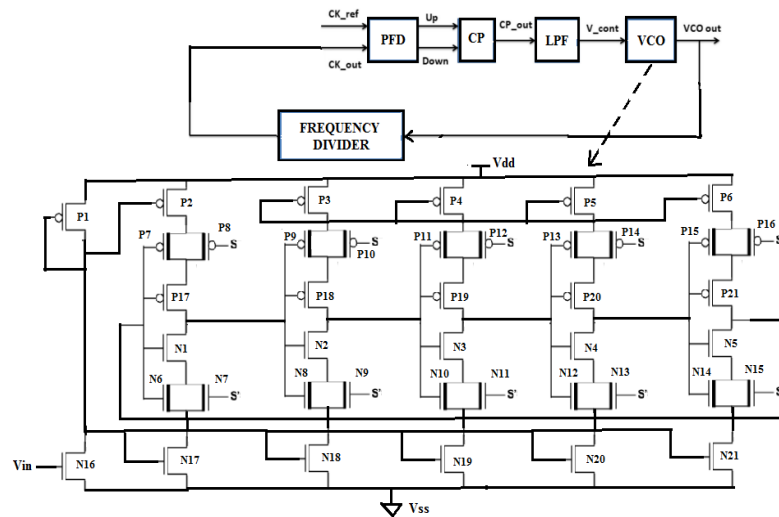


Fig.3. PLL Architecture with current starved VCO.

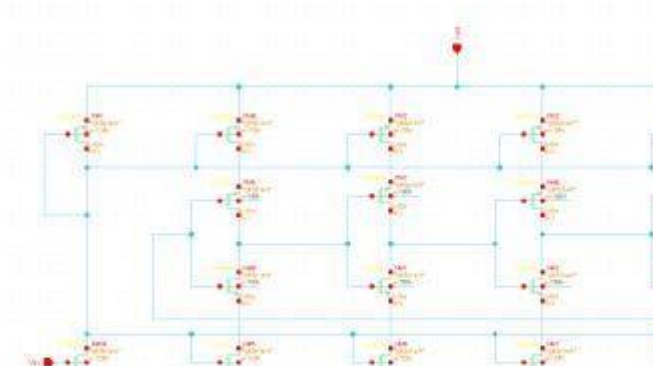


Fig. 3.1. Schematic diagram for Current Starved VCO.

In order to avoid this power consumption, a VCO named current starved was designed. The output frequencies of a basic VCO are controlled by the control voltage whereas the current is controlled by the current starved VCO [9]-[10]. The circuit consists of delay cells along with the current mirror which is used to limit the current to all the delay cells. The current starved VCO alone together has also increased the leakages and power consumption [1]. These leakages can be further reduced by applying the low leakage techniques to the delay cells and by varying the aspect ratio of transistors which reduces the threshold voltage [11].

4. LEAKAGE REDUCTION TECHNIQUES IMPLEMENTED IN VCO

The basic CSVCO, Current Starved Voltage Controlled Oscillator, is operated with the input voltage namely control voltage (V_{ctrl}). As the V_{ctrl} decreases, the current that is to be mirrored from the transistor M1 reduces when it is passed through the different PMOS in the delay stages. Because of the active mode of transistors in the CSVCO, the leakage power has been increased [1]. In this paper, the current starved VCO has been implemented with different low power leakage techniques like Gale-or, Lector, Sleepy Keeper, Sleep Stack, and Sleepy Stack to observe the better performance of the circuit [12]. Performance analysis can be observed in terms of different parameters like frequency, delay, and average power is calculated in different process corners showing the improved performance Phase Locked Loop, For different applications

4.1. Current Starved VCO with Sleep Stack Technique

The CSVCO circuit is implemented with Stack technique as shown in Figure 6, in which both the stack and sleep techniques are implemented above and below the pull-up and pull-down network, respectively. In normal mode, the sleep transistor would go to sleep mode, then the stack transistors reduce the leakages [24]-[26]. In case of the active mode, the sleep transistor becomes ON and stack transistors are OFF, reducing the leakages in CSVCO circuit.

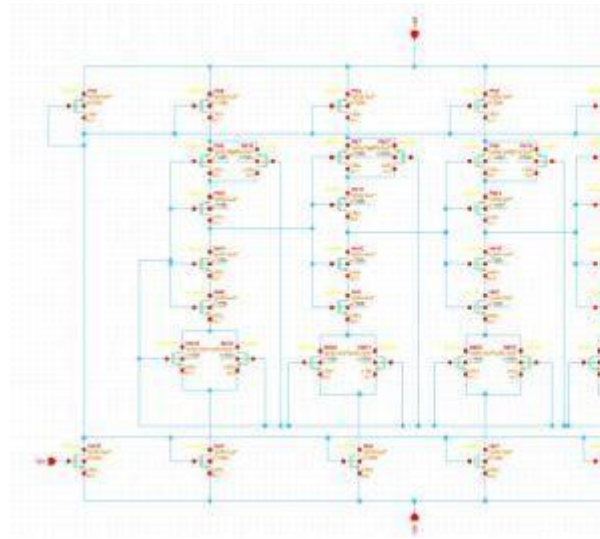


Fig. 4. CSVCO using Sleepy Stack Technique.

5. PROCESS CORNER ANALYSIS

Corner analysis provides a convenient way to measure circuit performance while simulating a circuit with sets of parameter values that represent the most extreme variations in a manufacturing process. All the proposed circuits with different low leakage techniques have their average power, oscillating frequency, and tuning range calculated in process corners like nominal, slow-fast, fast-slow, fast-fast and slow-slow conditions.

The mobility and the threshold voltage which in turn effect the device performance. If the threshold voltage is lowered, then there is more current and effectively the device is faster, however, if the threshold voltage is increased there is less current and the device could be slower. A lower supply voltage causes slower switching of the gates and results into an overall slower circuit, a high supply voltage drives faster switching of the larger gates which makes the circuits faster.

In addition to temperature and voltage analysis, the process corner analysis is carried out with the Cadence Virtuoso tool using the 45 NM generic process design kit (GPDK) technology file at 27°C (fig.5).

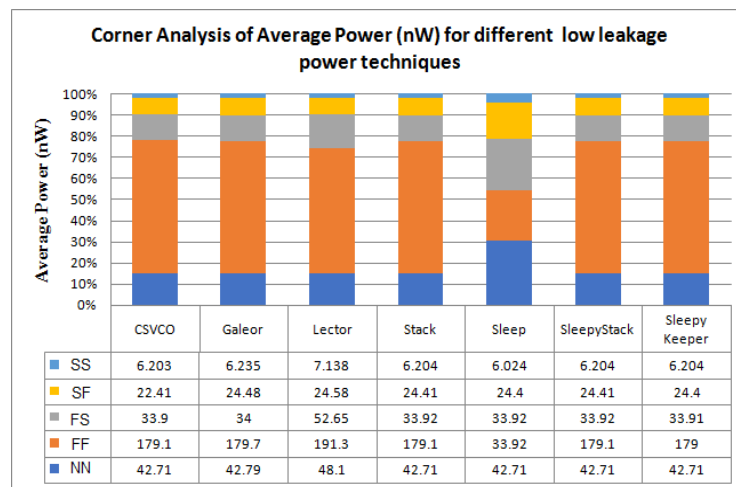


Fig. 5. Corner Analysis of P_{avg} for CSVCO applied with different low leakage techniques.

From the above plotted graph, it is observed that the average power in all the corners remained almost constant and in the Sleep Technique is always low in all the corners.

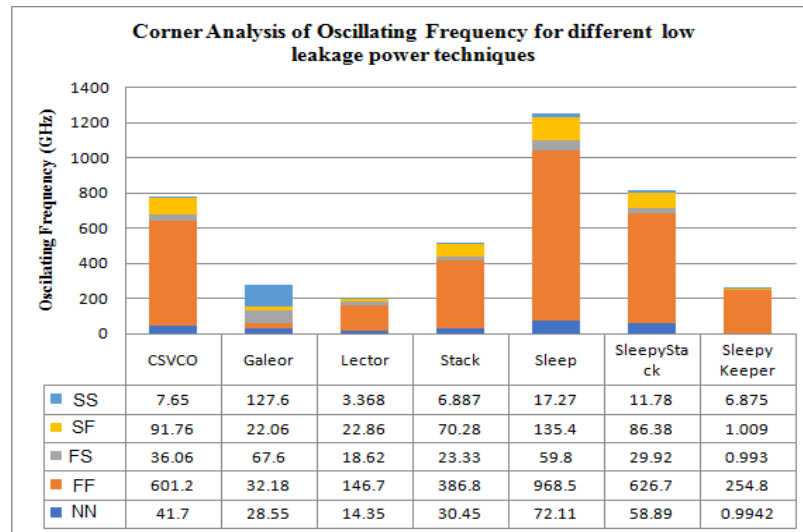


Fig. 5.1. Corner Analysis of Oscillating Frequency (GHz) for CSVCO applied with different low leakage techniques.

From the above plotted graph, it is observed that the oscillation frequency in all the corners remained low and, in the Gale,-or Technique is significantly reduced in all the corners.

From the below plotted graph, it is observed that the frequency tuning range calculated in percentage for all the corners in case of Sleep technique remained high and in the Lector Technique it is significantly reduced in all the corners.

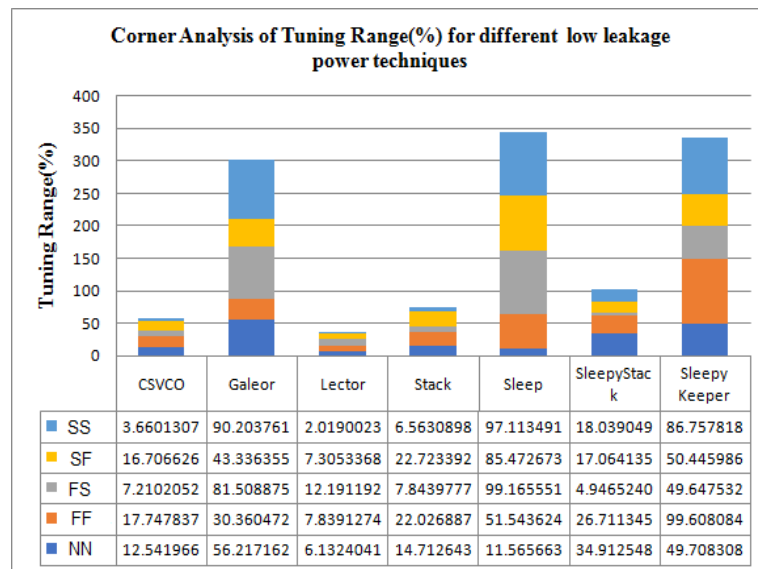


Fig.5.2. Corner analysis plot of Frequency Tuning Range (%) for CSVCO applied with different low leakage techniques.

6. SIMULATION AND RESULT ANALYSIS

To analyze the circuit and to perform the simulation results of the CSVCO implemented different low leakage techniques, the circuits has been implemented in virtuoso tool in Cadence Software in 45nm technology with a supply voltage of 0.45V. The simulated output of the oscillator is obtained by initializing setting the output node to either 1 or 0 to get the proper oscillations. The parameters like average power (P_{avg}), delay, Oscillation frequency and gain are calculated at a room temperature of 27°C and with a control voltage of 0.45V.

Table 1. Simulation results for parameters with different low leakage power techniques in CSVCO.

S. No.	Low Leakage Power Techniques	Average Power (W)	Area (μm^2)	Delay (μs)	Frequency (GHz)	Gain (Ghz/V)	Tuning Range (%)
1	Gale-or	48.20 e-9	37.5769	19.56	13.81	3.07	56.21
2	Lector	49.77 e-9	35.58125	32.25	14.34	3.19	6.07
3	Sleep	40.45 e-12	26.3169	327.8	72.11	16.02	98.76
4	Stack	49.56 e-9	56.4001	19.03	30.45	6.76	14.71
5	Sleep Stack	58.32 e-9	37.5769	0.4896	58.89	13.87	34.86

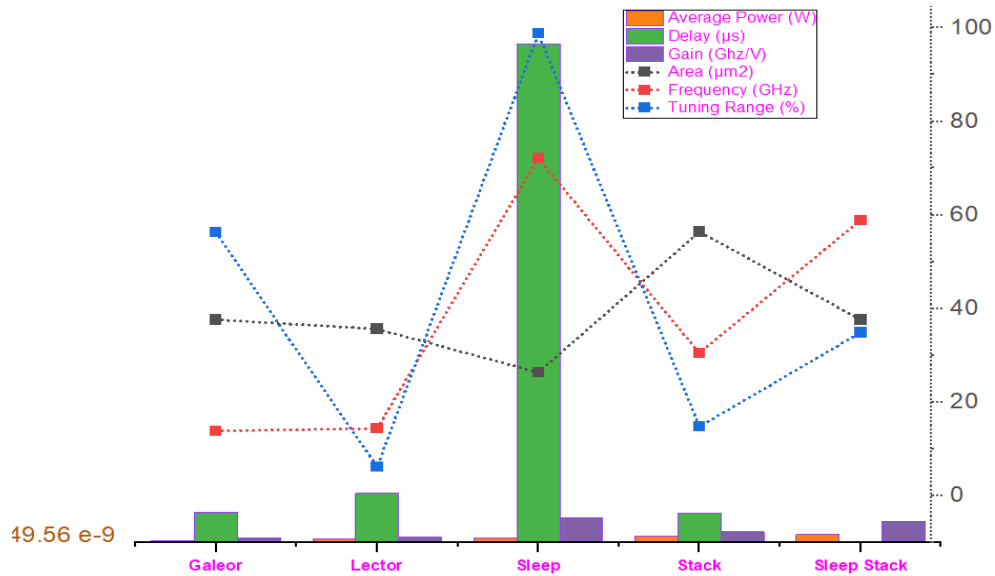
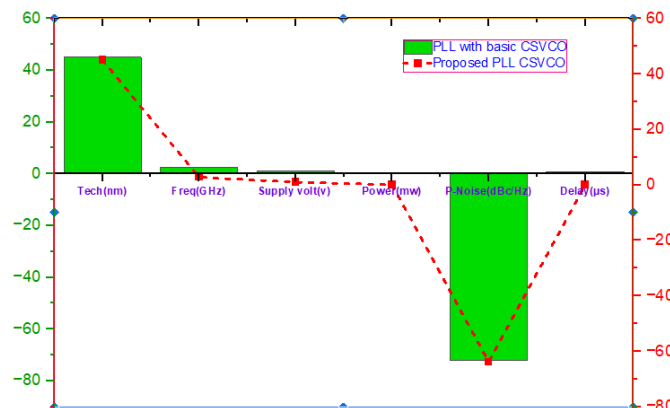


Fig. 6. Parameter analysis of CSVCO with different low leakage power techniques.

Table 2. Comparison analysis of PLL CSVCO VS sleep stack PLL CSVCO.

Parameters	PLL with basic CSVCO	Proposed work-PLL with SLEEP STACK CSVCO
VCO type	Ring	Ring
Tech (NM)	45	45
Freq (GHz)	2.592	2.759
Supply volt(v)	1	1
Power (MW)	0.002686	0.002559
P-Noise(dBc/Hz)	-72.2	-63.8
Delay(μ s)	0.866	0.0006544

From the above table and simulation result of parameter analysis with low leakage power techniques, the current starved VCO with sleep stack and keeper technique overcome the challenges present in the existing VCO in wide tuning, high frequency applications. Also, these challenges include leakage power, phase noise and limited frequency range. To ensure its robustness, extensive simulations are performed under extreme conditions such as different process corners, varying control voltage, and at extreme temperatures. The proposed CSVCO PLL circuit consumes less power. It achieves 20 % improvement in oscillation frequency because of the pull-up sleepy and pull-down sleepy stack transistor arrangement. The frequency tuning range of the proposed circuit also exhibits 27 % improvement. It also achieves less delay with the phase noise and FOM improvement of 17.29 % and 10.74 % ,respectively.

**Fig. 7.** Comparison analysis of PLL CSVCO & Sleep Stack PLL CSVCO.

The above figure confirms the robustness of the proposed design, making it a promising solution for high-frequency applications. These improvements are achieved at a supply voltage of 1 V. To ensure the stability of the circuit, Monte-Carlo analysis also conducted for various parameters. From the obtained results, it is concluded that the proposed design outperforms existing works in various performance parameters and it is highly suitable for PLL applications including wireless communication and radio frequency.

7.CONCLUSIONS AND FUTURE SCOPE

From the above tabular column and the graphs plotted it is observed that all the low leakage power techniques applied to the existing CSVCO are better in one or the other parameter like average power, oscillation frequency, delay and the gain. It is also observed that as the temperature is increased from corner analysis 27°C to 80°C then the power and delay are increased and they are decreased when the temperature is decreased to -40°C.

After comparing the various parameters of PLL implemented with Sleep Stack CSVCO and Basic CSVCO, it is observed that Sleep Stack has better performance. To achieve further, higher frequencies vary the supply voltage and the number of stages in the CSVCO from 5 stages to 7,9,11 and so on, but with increase in other parameters like area and power.

REFERENCES

- [1] M.Sivasakthi, P. Radhika, "Design and analysis of PVT tolerant hybrid current starved ring VCO with bulk driven keeper technique at 45 NM CMOS technology for the PLL application," *j.aeue*.2023.154987, 2023.
- [2] C.K. Pothina, N. P. Singh, J. L. Prasanna, C.Santhosh, M.R Kumar, "Design of Efficient Phase Locked Loop For Low Power Applications", doi.org/10.3390/2023.
- [3] B. Singh, S. Kumar, R. K. Chauhan, "Design of energy efficient VCO PLL Application Analog Integrated Circuits & Signal Processing", 2023.
- [4] K.B.Meena Kumari, G. Kavya, "Implementation of Digital Phase Locked loop", *Int. Journal of Egg. Technology and Management Sciences*, 2023.
- [5] D.M.Ellaithy, "Voltage-controlled oscillator-based analog-to-digital converter in 130-nm CMOS for biomedical applications" *Journal of Electrical Systems and Information Technology*, volume 10, 2023.
- [6] kumar P. Chavan, R. Aradhya, "Design of 5.1GHz ultra low power and wide Tuning range Hybrid oscillator," doi.org/10.11591/ijece. v13i4.pp:3778, 2023.
- [7] R Gurjar, DK Mishra, "Design and performance analysis of low phase noise LC-voltage controlled oscillator", doi.org/10.12928/telkomnika. v21i4.22341, 2023.
- [8] D. Ellaithy, "Voltage-controlled oscillator-based analog-to-digital converter in 130-nm CMOS for biomedical Applications" DOI:10.1186/s43067-023-00109-x, 2023.
- [9] P.Thool, J.D. Dhande, Y. A. Sadawarte, "A Review on Design and Analysis of Low Power PLL for Digital Applications and Multiple Clocking Circuits" ISSN: 2321-9653, 2022.
- [10] K. Kasilingam, P. Balaiyah, P. Kumar Shukla, "Design of a high-performance advanced phase locked loop with high stability external loop filter" doi.org/10.1049/cds2.12130, 2022.
- [11] T .Nirmalraj, S .Radha krishnan, R. K .Karn, "Design of low power, high speed PLL frequency synthesizer using dynamic CMOS VLSI technology". *IEEE*, 2022.
- [12] T. Bao Phuc Ton, C. Thinh Dang, "A Design of 45nm Low Jitter Charge Pump Phase-Locked Loop Architecture for VHF and UHF Fields" DOI: 10.21203/rs.3.rs-1804148/v1[4].B , 2022.
- [13] S. Dhanush, T.N.Vaishnavi S. Parashar, "Design and Implementation of High Frequency and Low-Power Phase-locked Loop, U.Porto" *Journal of Engineering* DOI:10.24840/2183-6493_007.004_0006, 2021.
- [14] P. Srivastava, R. Chandra Si. Chauhan, "Design of Power Efficient Phase Frequency Detector and Voltage Controlled Oscillator for PLL Applications in 45nm CMOS Technology", 2021.
- [15] V. Kumar Sharma, "A survey of leakage reduction techniques in CMOS digital circuits for nano scale regime", *Australian Journal of Electrical & Electronics Engineering*, DOI: 10.1080/1448837X.2021.1966957, 2021.
- [16] B. Dharani, U. Nanda, "Impact of Sleepy Stack MOSFETs in CS-VCO on Phase Noise and Lock Performance of PLL", DOI:10.1007/s633-021-01446-0, 2021.
- [17] Kumar Tiwari, "Leakage Power Reduction in CMOS VLSI Circuits using Advance Leakage Reduction Method", (*IJRASET*) , 2021.
- [18] R.Prithiviraj, J.Selva kumar , "Design and Analysis of Low power and High Frequency Current Starved Sleep voltage Controlled Oscillator for Phase Locked Loop Applications", DOI:10.1007/s020-00619-7, 2021.
- [19] S. Rani, M. Vinothkumar, K. Krishnamoorthy, "Design of low power VCO using FinFET technology for biomedical applications. *Materials Today*": Proceedings, 45, pp.2145–2151. 10.1016/j, 2021.
- [20] M. Maiti, S. Kumar Saw, A. J. Mondal, A. Majumder, "A hybrid design approach of PVT tolerant, power efficient ring VCO" doi. org /10. 1016/ j.asej. 2019. 10.009, 2020.
- [21] U.Nanda, D.P.Acharya, and D. Nayak,. "Process Variation Tolerant Wide-band Fast PLL with Reduced Phase Noise using Adaptive Duty Cycle Control Strategy". *International Journal of Electronics*.2020
- [22] Sh.Askari, M.Saneei, "Design and analysis of differential ring voltage controlled oscillator for wide tuning range and low power applications", doi.org/10.1002/cta.2582, 2018.
- [23] B.S.Choudhury, S.Maity "A low phase noise cmos ring vco for short range device application. In: Conf. proceedings", *EESCO-IEEE*, 2015.
- [24] N. Pathak, R. Mohan, "Phase Locked Loop Design and Implementation using Current Starved Voltage Controlled Oscillator " *IJERTV3IS2074*, 2014.
- [25] H .Malviya, S. Nayar C. Roy "A New Approach FOR Leakage Power Reduction Techniques in Deep Sub micron Technologies in CMOS Circuit for VLSI Applications" *Computer Sci Software Eng*. 25, 2013.
- [26] PK. Pal, R.S. Rathore AK. , Rana, G. Saini, "New low power techniques: Leakage feedback with stack & sleep stack with the keeper". In: *ICCCT-2010. IEEE*. pp.296–301.2010.
- [27] J. C. Park and V. J. M. III, "Sleepy stack leakage reduction," *IEEE Trans. Very Large Scale Integrate. (VLSI) Syst.*, vol. 14, pp. 1250- 1263, 2006.
- [28] J. Ch. Park, "Sleepy stack: a new approach to low power VLSI logic and memory", *School of electrical and computer engineering*, Georgia institute of technology, 2005.

Classification of Brain Tumors based on Coherence-based Atoms Correction in Overcomplete Models Learning

Samira Mavaddati¹ , Hamidreza Koohi², Ziad Kobti³

1- Department of Engineering and Technology, University of Mazandaran, Babolsar, Iran.

Email: s.mavaddati@umz.ac.ir (Corresponding author)

2,3- School of Computer Science, University of Windsor, Ontario, Canada.

Email: koohi@uwindsor.ca, kobti@uwindsor.ca

ABSTRACT:

Brain tumor detection using MRI imaging has the potential to be greatly improved through the integration of medical knowledge. Solving the problem of brain tumor classification is highly important in the field of medicine as it can greatly impact the effectiveness of treatment options. However, the classification of tumors into Benign or Malignant categories remains a challenging task due to the need for detailed texture analysis and the possibility of errors. Image processing techniques such as dictionary learning-based classifiers can play a critical role in this field. This paper proposes a method that combines textural-statistical features to categorize brain tumors based on employing sparse non-negative matrix factorization (SNMF) and a dictionary learning-based model using a sparse representation technique. In the next step, the extracted features from the sparse coefficient matrix were fed into a ResNet10 model for the classification of the input image. The experimental results emphasize that the proposed method, which trains the dictionary atom based on the combinational features vector, can accurately distinguish different types of brain tumors with high precision. This is a significant method as it can improve the effectiveness of brain tumor classification, leading to more accurate treatment decisions for patients.

KEYWORDS: Brain Tumor Classification, Dictionary Learning, Sparse Representation, ResNet Deep Model, Sparse Non-negative Matrix Factorization.

1. INTRODUCTION

The investigation of magnetic resonance images (MRI) by a doctor plays an essential role in determining the type of tumor. Brain tumor diagnosis involves distinguishing the brain texture from the tumor and classifying it as Benign and Malignant. The classification is performed based on the comparison of healthy and diseased hemispheres, taking into account that the tumor is not located in symmetrical hemispheres. Signal processing techniques play a key role in brain tumor classification, especially when applied in combination with machine learning algorithms [1]-[3]. In [4], an algorithm for the classification of Benign, Malignant, and normal tumors was developed using texture features and a probabilistic neural network (PNN). The coefficients of wavelet transform in different frequency bands are used in this algorithm. The classification of four types of tumors, Astrocytoma, Meningioma, Carcinoma, and Sarcoma using gray-level co-occurrence matrix-based (GLCM) features, a neural network, and a non-linear optimization algorithm Levenberg Marquart was investigated in [5]. In [6], the classification of brain and bone tumors was done using features extracted from the GLCM and a back-propagation neural network. The results were reported for four levels of tumors. In [7], the classification of brain tumors was proposed using features extracted from the GLCM and fast discrete curvelet transform (FDCT) and PNN with radial basis functions (RBF). The classification was done for Benign, Malignant, and normal types of tumors. In [8], the coefficients extracted from GLCM and K-nearest neighbor (K-NN) classification were used

Paper type: Research paper

<https://doi.org/>

Received: 29 May 2024; revised: 23 June 2024; accepted: 16 July 2024; published: 1 September 2024

How to cite this paper: S. Mavaddati¹, H. Koohi, and Z. Kobti, "Classification of Brain Tumors based on Coherence-based Atoms Correction in Overcomplete Models Learning", *Majlesi Journal of Telecommunication Devices*, Vol. 13, No. 3, pp. 159-169, 2024.

to classify normal and abnormal tumor data. In [9], the coefficients extracted from the GLCM and spatial K-means clustering were used to detect abnormal brain tumors. The classification procedure with the mentioned feature vectors was performed using neural network in [10]. In [11], the GLCM feature matrix extracted from MRI and tomography images and RBF neural network categories and support vector machine (SVM) are used to detect normal and abnormal brain tumors. In [12], the combination of features extracted from histogram, GLCM, gray level repetition length matrix, and SVM are used to identify Benign and Malignant tumors. In [13], the authors presented a classification algorithm for brain tumors based on PNN trained with the help of GLCM feature matrix and morphological operators obtained from discrete wavelet transform (DCT) coefficients. In [14], the authors compared the different algorithms presented for classifying brain tumors based on different characteristics and categories and evaluated their effectiveness in the diagnosis. In [15], the authors presented a method for identifying Malignant and normal brain tumors based on features obtained from the GLCM matrix and shape-based features extracted from the connected areas of the image. In [16], a sparse representation-based approach was presented to classify brain MR images that consists of least square regularized minimization technique to solve the problem of multiclass classification of tumors in brain MRI by exploring the discriminating properties of sparse representation. A brain tumor MR image classification method using convolutional dictionary learning with local constraint was introduced in [17]. The method integrates the multi-layer dictionary learning process into a convolutional neural network (CNN) structure to explore the discriminatory information present in the data. In [18], the authors propose a novel approach for multi-class brain tumor classification based on sparse coding and dictionary learning that uses K-singular value decomposition (K-SVD) algorithm. The authors propose that this approach combines topological and texture features to learn a dictionary. Although in the researches of recent years, methods based on deep learning have been used with good accuracy, but methods based on model learning include many advantages for the reasons that are mentioned below. A dictionary-based learning algorithm can be beneficial for solving brain tumor classification than deep learning-based classifiers because of its efficiency, robustness, flexibility, and simplicity. These algorithms are typically faster than deep learning-based methods, which can be advantageous when working with large medical image datasets. Also, the performance of dictionary-based learning algorithms is less dependent on the quality and quantity of the training data and more adaptable to different datasets and application scenarios. than deep learning-based methods. The dictionary learning-based algorithms are generally simpler and less computationally expensive than deep learning-based methods. This can make them more accessible to researchers and practitioners without specialized knowledge in deep learning. Also, dictionary-based learning algorithms are often more interpretable than deep learning-based methods, which can make them easier to understand and diagnose [19]-[20].

The proposed approach integrates various statistical and texture features to train comprehensive models representing the attributes of each recognized brain tumor category using dictionary-learning technique, sparse representation concepts, and SNMF dictionary learning algorithm. Careful consideration of the consistency parameter ensures appropriate classification results. The features extracted from the sparse coefficient matrix in the previous step were subsequently fed into a deep learning model, namely, the ResNet10 model, to classify the input image. The purpose of this classification process is to analyze the features and determine the probability of the input image belonging to a certain category. The ResNet10 model is designed to handle images with high spatial dimensionality, which makes it an ideal candidate for this classification task. The extracted features are used as the input to the ResNet10 model, which applies multiple layers of convolutional neural networks to process the features and generate a final classification decision. The entire process is automated and the results can be obtained rapidly, making it a convenient solution for image classification tasks. The proposed method has several significant contributions to the field of medical, including:

- Introducing a new method for brain tumor classification that can mitigate the imbalances in the data.
- Addressing challenges in brain tumor classification, such as data representation, and model complexity.
- Developing and optimizing a dictionary learning-based model with the multi-attention mechanism to enhance the performance of classifiers.
- Employing the statistical-textural feature vector to capture low-level and high-level structures and learn complex relations between the captured features.
- Utilizing the benefits of employing coherence parameters to design a comprehensive overcomplete dictionary.
- Demonstrating the dictionary's ability to accurately classify brain tumor types under multiple scenarios, showing its efficiency and adaptability to varying situations.
- Offering an effective and scalable solution for enhancing the performance of this classification task based on ResNet deep model, with potential applications in the medical and treatment of patients.

Section 2 covers the dictionary learning and sparse representation algorithms. The texture and statistical features involved in categorization are thoroughly examined in Section 3. The proposed brain tumor categorization algorithm is provided in Section 4. In Section 5, the outcomes from applying the proposed method are evaluated and compared with others. A conclusion concerning the research findings is drawn in the final Section.

2. DICTIONARY LEARNING AND SPARSE REPRESENTATION TECHNIQUES

Brain tumors are a serious medical condition that can lead to severe health problems and even death if left untreated and their classification is a critical step in the diagnosis and treatment of this condition. Concepts of dictionary learning and sparse representation techniques can be helpful in this diagnostic step. In these techniques, the digital image I can be modeled as $I_m = DX$ [21]. I_m is a data matrix consisting of different pieces of the input image I divided into blocks of 8×8 dimensions, where index m refers to the coordinates of the pieces. The sparse representation technique is used to code the data matrix I_m as a linear combination of atoms in an overcomplete dictionary D where $D \in \mathbb{R}^{N \times L}$, $L > N$. An overcomplete dictionary is a matrix where the number of columns or atoms is multiple times the number of rows or the dimension of the feature space of the problem. The matrix D contains L columns or atoms with unit norm that each input data vector can be coded as a linear combination of K trained atoms, and usually, K is a small number [22]. Therefore, the sparse representation problem is expressed as follows based on the approximation or reconstruction error parts as

$$X^* = \arg \min_x \|I_m - DX\|_r \text{ s.t. } \|X\|_0 \leq K \quad (1)$$

The technique of learning an over-complete dictionary and sparse representation was proposed for the first time to remove noise from the image data [21]-[22]. This was followed by the development of the K -SVD algorithm, which led to the favorable results. The dictionary learning process includes two stages: sparse coding and updating atoms. The sparse coding procedure can be performed with any desired algorithm, and the sparse representation step used in the K -SVD algorithm is the orthogonal matching pursuit (OMP) method [23]. It is important to adjust the sparsity or cardinality rate carefully so that the approximation error does not increase beyond an optimal level.

3. THE COMBINATIONAL STATISTICAL-TEXTURAL FEATURE VECTOR

The first step in the proposed algorithm is the preprocessing step. This includes converting the MRI images to gray levels and then reducing the dimensions of the images. This step is necessary to prepare the images for feature extraction. After that, feature extraction should be performed which is divided into two parts, texture-based and statistical-based feature vectors. local binary pattern (LBP) is a robust feature extraction method that is widely used in texture processing of image parts, particularly in analyzing gray spectrum images. This method is suitable for texture analysis in MRI images, as it can handle rotations of neighboring textures. Also, histogram of oriented gradients (HOG) is another popular feature extraction method that is efficient in target recognition. This method uses the gradient information of the local parts of the image to calculate the features. This technique is very sensitive to rotations and brightness variations. Also, the GLCM feature matrix is widely used in the field of image processing and can provide information about the texture of an image. The resulting statistical parameters are used to determine the content of the image texture. In the field of image processing, Moment parameters extracted from the image have gained importance due to their resistance to rotation. This feature set includes seven coefficients of the first to seventh Moments and has the beneficial feature that its values do not change when the image is rotated in the desired direction [5]- [7]- [15]- [22].

4. CLASSIFICATION OF BRAIN TUMORS IN THE PROPOSED METHOD

The proposed method classifies the MRI images into three categories: Meningioma, Glioma, and Pituitary brain tumors which are more common brain tumors types [17]- [22]. Feature extraction is performed for each data class, including a set of images related to a specific type of tumor. The extracted features are used as inputs to the classification model for recognition of tumor type. The recognition of brain tumors in this paper was performed in the different scenarios based on various feature vectors and two spars-based dictionary, KSVD/OMP, and SNMF dictionary learning method [24]-[25]. The first of these feature vectors is LBP widely used in the field of texture processing of image parts and is known to be robust. It is used to extract the features of adjacent textures in the analysis of gray scale images. This feature makes changing the position of the tumor in the image less unfavorable. Different patterns can be used to calculate the coefficients of LBP codes, including circular and diagonal neighborhoods. In the proposed method, a cell size of 8×8 and a block size of 2×2 is used. The second texture-based method is HOG that is efficient in target recognition and can handle rotations and brightness variations well. It uses the gradient information of the local parts of the image to calculate the features. The third method is GLCM used commonly to extract the texture of an image and is used in the analysis of gray level images. Other statistical characteristics that can be considered important in the field of image processing and are rotation-insensitive include the Moment parameters extracted from the image [22]- [26]. These parameters include the first to seventh Moments of the image and do not change when the image is rotated in the desired directions. Therefore, they can be valuable in the discussion of identifying targets in which rotation is one of the basic challenges, as well as in the analysis of texture information.

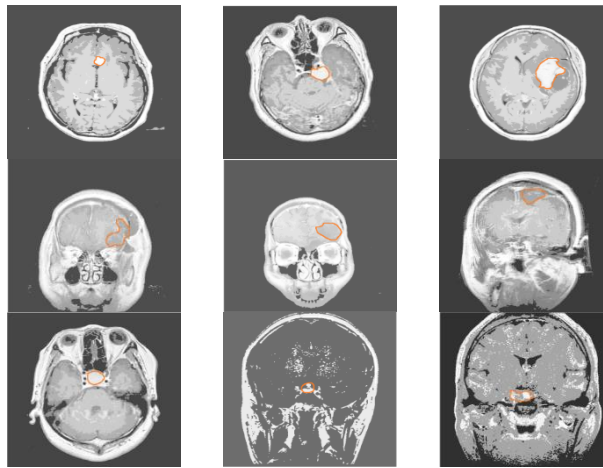


Fig. 1: Examples of MRI images related to tumors: first row: Meningioma. Second row: Glioma. Third row: Pituitary gland. The boundaries of tumors are marked with red color.

In the proposed method, feature extraction is performed for each data set, including a set of images related to a type of tumor, and examples of these images are shown in Figure 1. In the following section, we will explain and examine in detail the different parts of the proposed method for detecting tumors from MRI images. The first step in dictionary training is to represent each piece of input image data using a small number of atoms, known as the dictionary. This is achieved by applying a sparse representation to the data, where each piece is represented as a linear combination of a smaller number of atoms than the total number of pixels in the image. The number of atoms used to represent the data is determined by a parameter called the cardinality rate, which is set by the user or learned from the data. The next step in dictionary training is to update the dictionary atoms based on the input data pieces. This is done by iteratively adjusting the coefficients of each atom to minimize a cost function, which measures the similarity between the image data and the linearly combined atoms. This process is called dictionary optimization, and there are many different algorithms that can be used to perform this optimization. One of the algorithms used in the proposed brain tumor classification algorithm is the least angle regression with coherence criterion (LARC) sparse representation method, which is a generalization of the least-angle regression (LARS) algorithm [27]. In this method, the sparseness of the representation is achieved by calculating the coefficients that represent the linear combination of atoms. The stopping condition for calculating the sparseness coefficients is based on the fact that the atoms must be consistent with the data pieces to represent the content of the training set more appropriately. This consistency is measured by a parameter called residual coherence. If this parameter is less than a predetermined threshold, then the atoms are considered to be consistent with the data and can be used to represent the input images. By reducing the dimensionality of the data using a small number of atoms, and then adjusting the atom coefficients to optimize the similarity between the data and the representation, the dictionary training process transforms the input images into a set of coefficients that can be used to represent the content of the training set more compactly. The LARC algorithm is known for its use of a variable sparsening rate rather than a fixed rate used by most representation methods. This means that the upper limit for the sparseness parameter K is determined and each piece of data can be represented by a maximum of K atoms. This representation method was initially presented to represent the sparseness of speech signals. The sparse representation based on this technique can be expressed as:

$$X^* = \text{LRAC}(D, X, K, \text{Coh}) \quad (2)$$

where K represents the sparsening rate or the variable cardinality, and the Coh parameter expresses the degree of remaining coherence. When setting the cardinality rate, it is important to note that an incorrect setting does not lead to source disturbance or source distortion. The Coh parameter represents the coherence between the atom and the data. It is important to note that setting the value of this parameter too high can cause only the atoms that have coherence higher than this value to be included in the dictionary, and their number is small and may cause a problem in designing a complete dictionary with the desired redundancy rate. Conversely, if the value of this parameter is chosen low, then the data consistency parameter and the atom selection method will not have much effect in designing dictionary atoms compatible with the data.

In this study, a novel brain tumor classification method was presented using a combination of coherence-based learning and dictionary learning techniques. The goal of the proposed method is to extract the key features from the

MRI images of brain tumors that can be used to construct the classification model. The dictionary learning algorithm based on K-SVD is a suitable procedure for training atoms based on a set of training data. Regarding the consistency between the dictionary atoms, it is crucial to note that there is minimal consistency between the dictionary atoms so that the spatial bases are as independent as possible from each other and the representation is done to show the content of the data pieces in the best way. The significance of addressing these parameters increases when the training data belonging to different classes are structurally very similar. In this case, the higher consistency between the dictionary atoms belonging to each class and the lower mutual consistency between the atoms of different dictionaries will result in a lower approximation error, and the data classification model of every class will be done with higher accuracy. The mutual coherence parameter between the atoms of a dictionary is defined as the maximal value obtained by multiplying different atoms by two:

$$\mu(D) = \max_{1 \leq i, j \leq L, i \neq j} |d_i \cdot d_j| \quad (3)$$

where d stands for the dictionary atoms. To minimize the approximation error in the sparse representation, it is crucial to optimize the consistency parameters and ensure minimal consistency between the dictionary atoms. The proposed brain tumor classification method involves training a neural network model to recognize the type of brain tumor present in MRI images [27]. The model is trained using a dictionary learning algorithm based on K-SVD, which is a suitable procedure for training atoms based on a set of training data. Each input image is represented with a sparse linear combination of K atom coefficients that are learned by considering the two data consistency factors. The first factor measures the degree of consistency between the input data and the dictionary atoms, while the second factor measures the consistency between the dictionary atoms. The goal is to reduce the approximation error in the sparse representation of the input data as much as possible, which can be done by optimizing the consistency parameters and ensuring minimal consistency between dictionary atoms. In [28], a novel method called Iterative Rotation and Representation (IPR) is introduced to obtain the Gram matrix as unitary as possible for each dictionary. The first step of IPR involves thresholding the non-diagonal coefficients of the Gram matrix based on a set of rules. These rules, referred to as structural constraints, limit the number of nonzero eigenvalues. The thresholding process sets the off-diagonal coefficients that should be zero in the ideal state of the Gram matrix to a very small determined coherence value to reduce the Frobenius norm of the error between the Gram matrix and the unit matrix. Next, the eigenvalues of the Gram matrix are limited by keeping only the N largest eigenvalues. The second step of IPR involves rotating the dictionary atoms using an orthogonal matrix W so that the approximation error does not increase due to the thresholding done in the first step. This technique was initially presented to improve music signal reconstruction [28] that applied to improve the training procedure of the dictionaries used in brain tumor classification. In this problem, the learned dictionaries for each data class should not be similar as much as possible and the distinction between different categories should be well established. Therefore, it will be important that the atoms of the dictionaries associated with each of the classes have the least degree of coherence with the atoms of the dictionaries of other classes. So what matters is whether there are atoms with the same structure in the dictionary associated with each data class. If there is similarity between the trained atoms, then a procedure should be adopted to reduce this dependence. In the proposed method, in order to correct this problem and reduce the coherence between the dictionary atoms of a class, first a compound dictionary $D = [D_M D_G D_P]$ consisting of dictionaries related to the tumor data of Meningioma D_M , Glioma D_G , and Pituitary D_P is made. Then, the coding of the data volume related to each type of tumor is done on this compound dictionary as

$$\begin{aligned} X_M^*, X_G^*, X_P^* &= \text{LARC}(I, [D_M D_G D_P], \text{coh}) \\ &\rightarrow \arg \min_{X_M, X_G, X_P} \|I - [D_M D_G D_P] \begin{bmatrix} X_M \\ X_G \\ X_P \end{bmatrix}\|_F \end{aligned} \quad (4)$$

In order to evaluate the effectiveness of the proposed, the extracted features from the sparse coefficient matrix were then introduced into the ResNet10 model, which is a deep learning model designed to classify images. The purpose of this process is to analyze the features and determine the probability of the input image belonging to a particular category. The ResNet10 model is designed to handle images with high spatial dimensionality, which makes it an ideal candidate for this task. The extracted features serve as the input to the ResNet10 model, which applies multiple layers of convolutional neural networks to process the features and generate a final classification decision. The entire process is automated, and the results can be obtained quickly, making it a convenient solution for image classification tasks. Overall, the goal is to minimize the degree of coherence between the dictionary atoms of different dictionaries to enhance the distinction between different classes. By performing this process, the proposed solution addresses the issue of similarity among dictionary atoms belonging to different classes, ensuring appropriate representation of the data for classification purposes. The proposed category classification method, which leverages dictionary-based sparse

representation, is shown in Figure 2. The input data is first processed using the combined dictionary D to obtain its sparse representation. Then, the ResNet10 deep model was employed to classify the input image based on the sparse representation feature vectors. The sparse representation-based classification technique has been used in many applications so far [18]-[19]-[31]-[32]. By using a sparse representation-based method, the proposed solution does not require additional categories and can classify inputs solely by analyzing their sparse representation on each dictionary. This paper addresses the problem of representing brain tumor data using a set of incoherent dictionaries to improve the classification accuracy. The resulting classification method is efficient and reliable, avoiding the need to rely on other classifiers such as neural networks or SVM.

5. THE PROPOSED BRAIN TUMOR CLASSIFICATION METHOD

To simulate the results of the proposed method, two-dimensional MRI images were used [29]. These images were the result of T1-weighted CE-MRI imaging collected from 233 patients between 2005 and 2010. This collection included 3064 images of three types of brain tumors, including 708 images of Meningioma, 1426 images of Glioma, and 930 images of the Pituitary gland. The dimensions of these images were 512×512 , and the size of the pixels was 0.49×0.49 mm square.

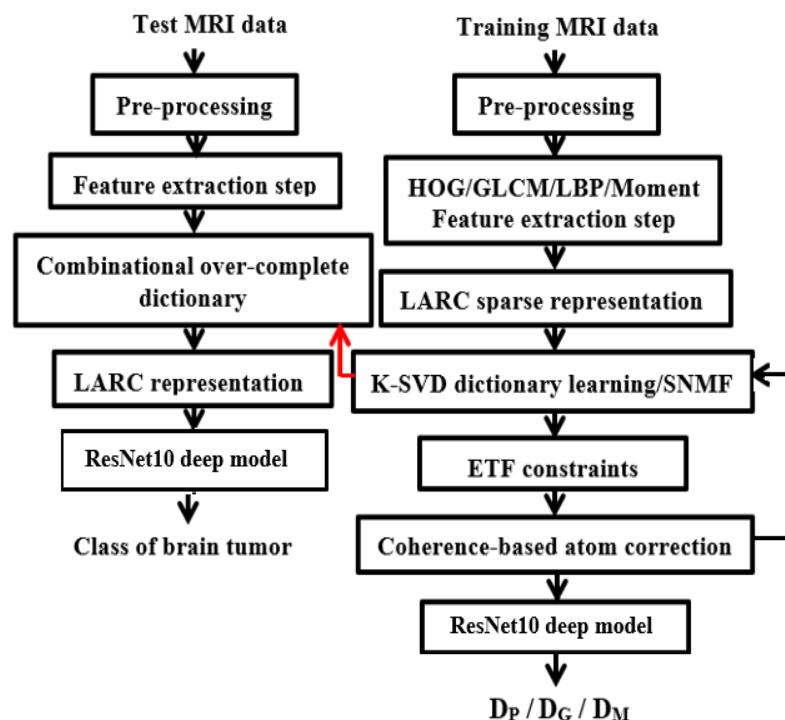


Fig. 2: Block diagram of the dictionary learning-based method for brain tumor classification.

5.1. Simulation Details

In the proposed method, dictionary training is used to classify brain tumor types. In the simulations, various features introduced in Section 3 were used as training data extracted from images. The sparsity rate required in sparse coding using the LARC algorithm depends on the dimension of the training data and is different for each feature extraction procedure. The Coh coherence parameter used in Equation 4 was set to 0.15 in all simulations. Also, according to the results of the simulations, the lower limit value of atom-data coherence used in the LARC algorithm was considered to 0.45. The redundancy rate for overcomplete dictionaries of all brain tumor classes was adjusted depending on the type of features, which states with what redundancy rate each dictionary will be super complete. To learn the dictionary in the training step, 70% of the data from each class was used, and the rest was used in the test step and for evaluation. The performance of the algorithm was evaluated based on its classification accuracy rate, which was calculated as the percentage of correctly classified data to the total test data. Feature extraction in the experiments of this section was done with the help of the HOG directional gradient histogram descriptor with a cell size of 8×8 with 50% overlap and a block size of 2×2 . The adaptive moment estimation (Adam) optimizer that computes adaptive learning rates for each

parameter is selected for the designed ResNet10 model. This optimizer is employed in stochastic gradient descent (SGD) to train deep-learning model layers. Using this optimizer an initial learning rate of 0.001 is used which is multiplied by 0.1 at epochs 10 and 20. Also, the learning rate is decreased every 10 epochs by 50% and the batch size is set to 32. For more efficiency, the number of iterations is set to 15 and the ResNet10 is learned for 50 epochs at each iteration.

6. Results and Discussions

As mentioned, feature extraction was performed using the invariant LBP coefficients with rotation and non-overlapping 2×2 cells, resulting in 10 features per image. The important parameters obtained from the GLCM matrix were also investigated, including nine characteristics of average, variance, energy, range of changes in relative abundance values, contrast, homogeneity, maximum relative abundance value, correlation, and entropy. The co-occurrence matrix coefficients of the gray level were calculated in four directions 0° , 45° , 90° , and 135° , resulting in a feature vector with 36 coefficients for each input image. In this paper, three scenarios are considered to compare the effect of each statistical or textural feature and the classifier. The feature vector in the first scenario (Scenario I) is based on a combinational vector that includes HOG and GLCM. After conducting several simulations for each feature vector independently, the results were found to be inadequate and omitted from the report. In the second Scenario (Scenario II), the feature vector in Scenario I is concatenated with the LBP features. Also, in the third scenario (Scenario III), all mentioned statistical-textural feature vectors consisting of HOG, GLCM, LBP, and Moments are employed to learn dictionary atoms using sparsity and coherence constraints. The results of the proposed brain tumor classifier are compared to a multi-layer perceptron (MLP) neural network with 5 hidden layers [30], a SVM classifier [31], and SNMF [32]. The results of the sparsity and redundancy rates for these features are set to 100 and 2, respectively. The results for Scenario I, Scenario II, and Scenario III are demonstrated in Tables 1-3.

The obtained results show that the use of statistical features such as parameters extracted from GLCM coefficients and Moments, along with other texture-based features such as LBP and HOG, leads to favorable results in the field of brain tumor data classification based on dictionary model learning, and also SNMF. In order to check the performance of the atom correction step proposed in the previous section, the results of the proposed category based on learning the model without the atom correction step are reported in Table 4.

Table 1. Accuracy of classification of brain tumors based on MLP neural network, SVM, NMF and the proposed dictionary-based method in the Scenario I.

	MLP [30]	SVM [31]	SNMF [32]	Proposed
Meningioma	80.36	84.38	89.08	92.22
glioma	81.71	83.56	88.33	93.67
Pituitary	85.49	82.52	88.14	92.61

Table 2. Accuracy of classification of brain tumors based on MLP neural network, SVM, NMF and the proposed dictionary-based method in the Scenario II.

	MLP [30]	SVM [31]	SNMF [32]	Proposed
Meningioma	86.25	86.26	91.24	94.22
glioma	87.41	87.33	91.48	94.61
Pituitary	88.52	87.47	90.51	95.27

Table 3. Accuracy of classification of brain tumors based on MLP neural network, SVM, NMF and the proposed dictionary-based method in the Scenario III.

	MLP [30]	SVM [31]	SNMF [32]	Proposed
Meningioma	88.63	87.59	93.56	96.22
glioma	89.93	88.48	92.96	96.67

Pituitary	90.05	89.61	93.22	97.31
-----------	-------	-------	-------	--------------

These results clearly demonstrate the positive impact of the atom correction step by removing atoms with similar performance in representing input data, which ultimately increased the classification accuracy. In the third scenario, which produced the best results according to Table 3, it was shown that the effectiveness of the atom correction step in dictionary training has a significant impact on the accuracy of the proposed method. If this step is not performed, the results of the simulation are nearly identical to those obtained using the non-negative method. Therefore, it is evident that the proposed method, with the atom correction step applied, is the more effective approach. Table 5 assesses the impact of three key blocks, including LARC sparse representation steps, ETF dictionary correction, and atom correction of different dictionaries, on the mutual coherence of atom-data, within coherence between atoms of the same dictionary, and the coherence between atoms of a dictionary with the dictionaries of other classes. The results of the coherence value based on the trained dictionary with the help of the LARC sparse representation method, which has no coherence constraint, are consistently lower than other scenarios. When applying the LARC algorithm with an increased atom-data coherence constraint, which selects only atoms with high atom-data coherence and ignores those with low coherence, the coherence values increase. This improvement has a positive impact on signal reconstruction, as it increases the extracted feature of the correct sparse representation and helps to classify the test data more accurately using ResNet10 deep model.

Table 4. Accuracy of brain tumors classification based on the combined feature vectors in Scenario III of the proposed method with and without atom correction step.

	SNMF	Proposed without atom correction step	Proposed
Meningioma	93.56	93.68	95.22
glioma	92.96	93.05	94.67
Pituitary	93.22	93.14	95.31

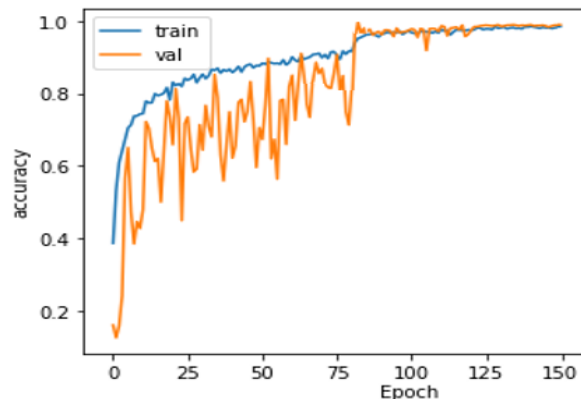


Fig. 3. The traing progress plot of the accuracy the proposed ResNet10-based brain tumor classifier based on model learning procedure in the training step.

Table 5. Coherence value between atoms and data, coherence value within dictionary atoms of each class, and coherence value between dictionary atoms of different classes in the proposed method.

	Atom-data Coherence			Whitin class coherence			Between class coherence		
	Meningioma	Glioma	Pituitary	Meningioma	Glioma	Pituitary	Meningioma/ Glioma	Glioma/ Pituitary	Pituitary/ Meningioma
OMP sparse representation	0.42	0.49	0.45	0.77	0.72	0.74	0.62	0.46	0.73

LARC sparse representation	0.75	0.80	0.74	0.73	0.68	0.66	0.70	0.75	0.79
LARC sparse representation /ETF post processing	0.76	0.82	0.76	0.41	0.45	0.44	0.69	0.73	0.71
LARC sparse representation /ETF post-processing /Atom correction (Proposed)	0.75	0.85	0.79	0.36	0.45	0.43	0.56	0.48	0.54

Additionally, after applying a dictionary editing step to achieve an ETF dictionary, which ensures that the dictionary's Gram matrix is as close to a unitary matrix as possible, the coherence parameter of dictionary atoms decreases as much as possible. Last but not least, in the proposed method, a step has been applied to correct the coherence of atoms related to other classes by removing the atoms of a dictionary that have a large representation energy in coding the data of the adjacent class. Overall, the proposed method, which includes all three steps, has been able to achieve the desired coherence values. The results indicate that the proposed approach results in improved coherence values, which ultimately enhances the accuracy of the classification process. Also, the training progress plot of the accuracy and loss function in the train and test steps for the employed ResNet10 model can be seen in Figure 3 which emphasizes the proper convergence in this classification task.

7.CONCLUSION

The development of effective tools for medical image processing is a critical field due to the vital role they play in improving treatment outcomes. To address this, a solution has been proposed in this paper to classify brain tumors using sparse representation and dictionary learning techniques. Features obtained from these concepts are employed to design an over-complete model. The proposed approach, which integrates the sparse representation and dictionary learning steps, yields over-complete models that exhibit maximum consistency between atoms and data and minimum consistency between atoms within their dictionary and atoms across different dictionaries. Then, a ResNet10 deep model was employed to classify the input image based on the sparse representation coefficients in model learning of the combinational feature vector. Furthermore, this paper compares different feature extraction methods, including texture-based and statistical techniques. It reveals that the combined feature category of GLCM/MOM/LBP/HOG leads to more favorable results for tumor classification in MRI images in comparison to other approaches such as neural networks, SNMF, and SVM classifiers. Therefore, using this combined feature category as the optimal feature set for brain tumor classification in medical image processing is recommended.

REFERENCES

- [1] H. Kibriya, R. Amin, J. Kim, M. Nawaz, and R. Gantassi, "A novel approach for brain tumor classification using an ensemble of deep and hand-crafted features," *Sensors*, vol. 23, 2023.
- [2] J. Amin, M. Sharif, A. Haldorai, and et al. "Brain tumor detection and classification using machine learning: a comprehensive survey," *Complex Intell. Syst.* 8,p. 316183, 2022. <https://doi.org/10.1007/s40747-021-00563-y>.
- [3] E. U. Haq, H. Jianjun, X. Huarong, K. Li, and L. Weng, "A hybrid approach based on deep CNN and machine learning classifiers for the tumor segmentation and classification in brain MRI," *Computational and mathematical methods in medicine*, vol. 2022, Article ID 6446680, 2022. <https://doi.org/10.1155/2022/6446680>.
- [4] J. Pauline, "Brain tumor classification using wavelet and texture based neural network," *International Journal of Scientific & Engineering Research*, vol. 3, no. 10, 2012.
- [5] N. Zulpe, and V. Pawar, "GLCM textural features for brain tumor classification," *IJCSI International Journal of Computer Science Issues*, vol. 9, pp. 3549, 2012.
- [6] S. Jain, "Brain cancer classification using GLCM based feature extraction in artificial neural network," *International Journal of Computer Science & Engineering Technology*, vol. 4, no. 7, pp. 966-970, 2013.

- [7] G. Preethi, and V. Sornagopal, "MRI image classification using GLCM texture features," *International Conference on Green Computing Communication and Electrical Engineering (ICGCCEE)*, Coimbatore, pp. 1-6, 2014.
- [8] N.V. Chavan, B.D. Jadhav, and P.M. Patil, "Detection and classification of brain tumors," *International Journal of Computer Applications*, vol. 112, no. 8, 2015.
- [9] P. Udayabhanu, V. Anjaly, and S. Padmarajan, "MRI brain image classification using GLCM feature extraction and probabilistic neural networks," *IOSR Journal of Electronics and Communication Engineering*, pp. 4-15, 2016.
- [10] S. Lekshmi, and I. Ratheesh, "Classification of brain tumor using neural network," *International Journal for Research in Applied Science & Engineering Technology (IJRASET)*, vol. 4, no. 8, pp. 93-97, 2016.
- [11] B. Thamarachelvi, and G. Yamuna, "Gray level co- occurrence matrix features based classification of tumor in medical images," *ARPJ Journal of Engineering and Applied Sciences*, vol. 11, no. 19, pp. 11403-11414, 2016.
- [12] A. Harshavardha, S. Babu, and T. Venugopal, "Analysis of feature extraction methods for the classification of brain tumor detection," *International Journal of Pure and Applied Mathematics*, vol. 117, no. 7, pp. 147-155.
- [13] N. Varuna, and T.N.R. Kumar, "Identification and classification of brain tumor MRI images with feature extraction using DWT and probabilistic neural network," *Brain Informatics*, pp. 23-30, 2017.
- [14] L. Kapoor, "A survey on brain tumor detection using image processing techniques," *7th International Conference on Cloud Computing, Data Science & Engineering*, pp. 582-585, 2017.
- [15] S. Kumar, and V.S. Dharun, "Extraction of texture features using GLCM and shape features using connected regions," *International Journal of Engineering and Technology (IJET)*, pp. 2926-2930, 2017.
- [16] M. Nasir, A. Baig, and A. Khanum, "Brain tumor classification in MRI scans using sparse representation," In: Elmoataz, A., Lezoray, O., Nouboud, F., Mammass, D. (eds) *Image and Signal Processing. ICISP. Lecture Notes in Computer Science*, vol.8509. Springer, Cham, 2014. <https://doi.org/10.1007/978-3-319-07998-1-72>
- [17] X. Gu, Z. Shen, J. Xue, Y. Fan and T. Ni "Brain Tumor MR image classification using convolutional dictionary learning with local constraint," *Front. Neurosci.* 15:679847,2021.doi: 10.3389/fnins.2021.679847.
- [18] S. D. S. Al-Shaikhli, M. Y. Yang and B. Rosenhahn, "Brain tumor classification using sparse coding and dictionary learning," *IEEE International Conference on Image Processing (ICIP)*, Paris, France, pp. 2774-2778, 2014. doi: 10.1109/ICIP.2014.7025561.
- [19] G. Sandhya, A. Srinag, G.B. Pantangi, J.A., Kanaparthi, "Sparse coding for brain tumor segmentation based on the non-linear features," *JBBBE49*, pp.63-73, 2021.<https://doi.org/10.4028/www.scientific.net/jbbbe.49.63>.
- [20] G. S. Gopika, J. Shanthini, Muthu Subash Kavitha, and R. Sabitha "Brain tumor detection with biologically inspired watershed segmentation and classification based on feed-forward neural network," (FNN). *J. Medical Imaging Health Informatics* 11(12): 3181-3190, 2021.
- [21] S. Al-Shaikhli, S. Dawood, M.Ying and R., Bodo. "Brain tumor classification and segmentation using sparse coding and dictionary learning," *Biomedical Engineering / Biomedizinische Technik*, vol. 61, no. 4, 2016, pp. 413-429. <https://doi.org/10.1515/bmt-2015-0071>.
- [22] S. Mavaddati, "Classification of brain tumor using model learning based on statistical and texture features," *Journal of Iranian Association of Electrical and Electronics Engineers*, vol. 19, no. 2, pp.177-188, 2022.
- [23] M. Ghasemi, M. Kelarestaghi, F. Eshghi, and A. Sharifi, "T2-FDL: A robust sparse representation method using adaptive type-2 fuzzy dictionary learning for medical image classification," *Expert Systems with App.*, vol. 158, 2020.
- [24] A. Bougacha, I. Njeh, J. Boughariou, O. Kammoun, B. Mahfoudh, M. Dammak, C. Mhiri, and B. A. Hamida "Rank-Two NMF clustering for glioblastoma characterization," *J Health Eng.* 2018 Oct 23; 2018:1048164. doi: 10.1155/2018/1048164. PMID: 30425818; PMCID: PMC6218733.
- [25] S. Ortega-Martorell, P.J. Lisboa, and A. Vellido, "Non-negative matrix factorization methods for the spectral decomposition of MRS data from human brain tumors," *BMC Bioinformatics*, vol. 13, no. 38, 2012. <https://doi.org/10.1186/1471-2105-13-38>.
- [26] S.Z. Kurdi, M.H. Ali, M.M. Jaber, T. Saba, A. Rehman, R. Damaševičius, "Brain tumor classification using meta-heuristic optimized convolutional neural networks," *J Pers Med.*, vol. 13, no. 2, 2023. doi: 10.3390/jpm13020181. PMID: 36836415; PMCID: PMC9965936.

- [27] C.D. Sigg, T. Dikk, J. M., Buhmann, “**Speech enhancement using generative dictionary learning**,” *IEEE Transactions on Audio, Speech and Language Processing*, vol. 20, no. 6, pp.1698-1712, 2012.
- [28] D. Barchiesi, M. D. Plumbley, “**Learning incoherent dictionaries for sparse approximation using iterative projections and rotations**,” *IEEE Transactions on Signal Processing*, vol. 61, no. 8, pp. 205565, 2013.
- [29] https://figshare.com/articles/brain_tumor_dataset/1512427.
- [30] R. Achkar, M. Owayjan, B. Harajli, D. Khazaal, M. Dbouk and G. Magnifico, “**Brain Tumor Classification Using Back Propagation Algorithm in MLP**,” 2019 *Fourth International Conference on Advances in Computational Tools for Engineering Applications (ACTEA)*, Beirut, Lebanon, 2019, pp. 1-5, doi: 10.1109/ACTEA.2019.8851109.
- [31] A. B. Malarvizhi, A. Mofika, M. Monapreetha, and A. M. Arunnagiri, “**Brain tumour classification using machine learning algorithm**,” *J Phys Conf Ser*, vol. 2318, no. 1, p. 012042, Aug. 2022, doi: 10.1088/1742-6596/2318/1/012042.
- [32] S. Mavaddati, S. Mavaddati, “**Rice classification and quality detection based on sparse non-negative matrix factorization**,” *Journal of Iranian Association of Electrical and Electronics Engineers*, vol. 17, no. 1, pp. 11-21, 2020.

Adaptive Sliding Mode Control Design based on Disturbance Compensator for Controlling Multi-Agent Robots

Samira Zalaghi¹ , Amir Hossein Zaeri²

1- Department of Electrical and Electronic Engineering, Islamic Azad University, Tehran, North Branch, Iran.
Email: Zalaghi.matpa@gmail.com (Corresponding author)

2- Department of Electrical and Electronic Engineering, Shahinshahr Branch, Islamic Azad University, Shahinshahr, Isfahan, Iran.
Email: amzaeri@gmail.com

ABSTRACT:

In this research, the goal is to develop a sliding mode control strategy based on the disturbance compensator to control the arrangement of a multi-agent system. For this purpose, the exponential access law is used to derive chattering-independent sliding mode control laws. In this design method, the sliding level information and its sign are used simultaneously, and by properly adjusting the sliding gain so that it is relatively larger than the switching gain, chattering effects can be removed significantly. On the other hand, since the adjustment of the switching gain is closely related to the changes of uncertainty and external disturbances, an adaptive approach is used to determine it. This is done using the Lyapunov stability theory and it is expected that the switching gain matching law is directly dependent on the instantaneous information of the sliding surface. In addition, to improve the consistency of the closed loop and adaptability to the environmental conditions and parameter changes of the system, a perturbation observer such as the developed mode observer is used.

KEYWORDS: Multi-agent System, Arrangement Control, Sliding Mode Control, Adaptive Disturbance Observer.

15. INTRODUCTION

The problem of controlling the arrangement of multi-agent systems has attracted a lot of attention due to its wide applications in many fields such as unmanned vehicles and so on. The purpose of arrangement control is to design control rules to move the agents towards their desired state and thus achieve the target arrangement. Arrangement approaches can be divided into leaderless, single-leader and multi-leader. In the multi-leadership challenge, the goal is to direct followers to some desired space surrounded by leaders. This improves flexibility and maneuverability; Because the configuration can be easily controlled by controlling a small part of it. To realize the arrangement problem in multi-agent systems, the dynamics of the agents and the leader must be determined first. In these models, state variables, control signals and their descriptive parameters such as dynamic coupling coefficients between factors should be specified.

In addition, various performance objectives can be explored in this field, among which can be mentioned the arrangement in the presence of model uncertainties, external disturbances, fault of stimuli and delay in received data. In addition, another important issue is to avoid the collision of agents in different operating environments, which, of course, is related to the nature of the arrangement control algorithm. In other words, the control method should be able to properly by designing a suitable guidance and tracking program for the followers so that the agents always have a suitable relative distance from their neighbors. Therefore, the structure of a control algorithm in this field depends on

Paper type: Research paper

<https://doi.org/>

Received: 14 June 2024; revised: 26 July 2024; accepted: 11 August 2024; published: 1 September 2024

How to cite this paper: S. Zalaghi, A. H. Zaeri, "Adaptive Sliding Mode Control Design based on Disturbance Compensator for Controlling Multi-Agent Robots", *Majlesi Journal of Telecommunication Devices*, Vol. 13, No. 3, pp. 171-182, 2024.

the nature of predetermined performance goals, the type of agents and leaders used, and the conditions of the agents' functional environment.

In practical applications, individual equipment cannot achieve high efficiency and low cost target control. To improve efficiency, increase execution accuracy, reduce costs and reduce maintenance cost, several small devices with low cost, simple structure and easy assembly and maintenance are employed to work together to achieve the desired goals. The control objective is to replace a single-factor complex agent. Compared to single-agent systems, multi-agent systems have advantages:

- 1) Cooperation between agents can greatly increase the ability to perform the work of the automation device. Based on the extension of task performance capability, multi-agent systems can perform many complex tasks that are difficult to achieve by a single agent.
- 2) Multi-agent systems have lower energy costs and are easier to construct and maintain, which lead to better economic returns.
- 3) Multi-agent systems have better performance and higher efficiency.

A multi-agent system is a system that consists of a group of agents and can solve problems that are difficult for an individual agent through communication, consultation and cooperation between agents and the environment. Multiple agents cooperating with each other can complete work beyond the capacity range of an individual agent and manage the capacity of the entire system better than a single agent. Applications of multi-agent systems have increased in recent years, and control models and theories related to multi-agent systems have been used in engineering fields day by day. In aerospace technology, spacecraft can be considered as an agent. Tasks such as system cost reduction, system stability improvement, and performance scalability can be achieved by developing coordinated attitude control and multiple spacecraft formation control [1]–[2]. Using multi-agent technologies, multiple spacecraft systems, where spacecraft have simple structures and processes, can deal with collective targets that are difficult for a single spacecraft to process[3]. In the application of military technology, the use of multiple unmanned aerial vehicles (UAVs) [4]– [5] to perform reconnaissance and combat, the use of multiple robots for search, rescue, patrolling, mine clearance, etc., or the use of autonomous underwater vehicles to cruise under the sea can greatly improve overall combat capability, increase task completion and accuracy, and reduce casualties [6]–[7]. In industrial manufacturing processes, using multiple robotic arms to perform complex tasks on a production line can often improve assembly accuracy and production efficiency [8]–[9]. Research on multi-agent systems, as a new and comprehensive topic, has a wide range of applications and enormous potential value, attracting researchers in various fields and promoting the rapid development of related theories[10]–[11].

16. DYNAMICS OF THE SECOND ORDER MULTI AGENT SYSTEM

In general, graph theory is used as an effective mathematical tool to describe coordinates and relationships between agents in a multi-agent system. Suppose $\Omega = \{\phi, \psi\}$ that represents a directed graph where $\phi = \{0, 1, 2, \dots, n\}$, represents the set of nodes, node i for the i -th agent, and represents the set of edges. An edge in the Ω set is an ordered pair (i, j) , which means that agent i can transmit information directly to agent j , but not necessarily the other way around. In contrast to the direct graph, the pairs of nodes in an indirect graph are not ordered, which means that the edge (i, j) describes the paired information transfer between agent i and agent j . Hence, an undirected graph can be considered as a special case of a directed graph[6]. The matrix $A = (a_{i,j}) \in R^{(n+1) \times (n+1)}$ is a weighted adjacency matrix of the set with non-negative elements. Based on this, if there is an edge between the i -th factor and the j -th factor, $a_{i,j} = 1$ and otherwise $a_{i,j} = 0$. in other words:

$$a_{ij} = \begin{cases} 1 & , \text{ if } (i, j) \in \Omega \\ 0 & \text{ otherwise} \end{cases} \quad (1)$$

The weight of communication between the i -th agent and the leader is denoted by b_i . If here is an edge between the i -th agent and the leader, $b_i = 1$ and zero otherwise. in other words:

$$b_i = \begin{cases} 1 & , \text{ if agent } i \text{ is connected to leader} \\ 0 & \text{ otherwise} \end{cases} \quad (2)$$

The adjacency matrix can be rewritten as follows:

$$A = \begin{bmatrix} 0 & 0 & \dots & 0 \\ a_{10} & a_{11} & \dots & a_{1n} \\ \vdots & \vdots & \ddots & \vdots \\ a_{n0} & a_{n1} & \dots & a_{nn} \end{bmatrix}_{(n+1)(n+1)} \quad (3)$$

Based on the direct topology, the following points should be considered:

- Only some factors are directly related to the leader.
- Some agents must be coordinated with the leader's behavior only by following the behavior of other agents.
- Finally, all agents must be able to follow the leader's direction.

The communication between the agents or the agent with the leader is considered one-way.

The general multi-agent system used in this article includes the dynamic equation of the active leader as follows:

$$\begin{cases} \dot{x}_0 = v_0 \\ M_0 \dot{v}_0 = u_0 \end{cases} \quad (4)$$

in which, $x_0 \in \mathbb{R}$ and $v_0 \in \mathbb{R}$ represent the momentary position and speed of the leader, respectively. $u_0 \in \mathbb{R}$ is a time-varying control input with condition $\|u_u\| \leq \bar{u}_0, u_0 > 0$ and $M_0 \in \mathbb{R}$ inertial leader. The point that should be remembered is that in the general dynamic state of the leader, it keeps its changes in the whole movement process and its behavior is independent of the followers. The dynamic equation of forces is described as follows:

$$\begin{cases} \dot{x}_i = v_i \\ m_i \dot{v}_i = u_i + f_i \end{cases}, \quad i = 1, 2, \dots, N \quad (5)$$

Where $x_i \in \mathbb{R}$ and $v_i \in \mathbb{R}$ represent the instantaneous position and speed of follower i , respectively. $u_i \in \mathbb{R}$ represents the time-varying control input and $m_i \in \mathbb{R}$ is the follower's inertia. Also, $f_i \in \mathbb{R}$ represents the uncertainty of the system caused by modeling errors and represents external disturbances, so that the condition $|f_i| \leq F, F > 0$ is always assumed. This means that the instantaneous value of the uncertainty is not known, but the maximum range of its changes must be predetermined. N also represents the number of followers. Therefore, in the general state, the second-order general multifactorial system has $N+1$ state variables, and the dynamic behavior of the leader is somehow considered as a reference model, and the control rules of the followers are calculated from the momentary difference between the leader and the followers at the position level.

17. ADAPTIVE SLIDING MODE CONTROL BASED ON DISTURBANCE COMPENSATOR

In this section, the following exponential access condition is used to define the control rules [12]:

$$\dot{s}_i = -\eta_{1i} \operatorname{sgn}(s_i) - \eta_{2i} s_i, \quad i = 1, 2, \dots, N \quad (6)$$

In fact, considering relation (6) for each follower, the control system is designed with two parameters. By considering the parameters, a stable dynamic can be achieved for the slip surface derivative. This problem means that the derivative of the slip surface becomes zero with the passage of time. Similarly, with high-order sliding mode controllers, in this situation, we can expect to reduce or eliminate chattering in the control signal by increasing the sliding mode gain. In other words, the section containing the slip surface has a great influence in dealing with the switching effects caused by the section containing the sign of the slip surface. As we know, the principles of sliding mode control are based on establishing the sliding condition. In the following, we show that using the above condition, Lyapunov stability is also established. For this purpose, we consider the Lyapunov function similar to the first design equal to the square of the slip surface:

$$V_i = \frac{1}{2} s_i^2, \quad i = 1, 2, \dots, N \quad (7)$$

By deriving it, we can write:

$$\begin{aligned}
\dot{V}_i &= s_i \dot{s}_i \\
&= s_i (-\eta_{1i} \operatorname{sgn}(s_i) - \eta_{2i} s_i) \\
&= -\eta_{1i} s_i \operatorname{sgn}(s_i) - \eta_{2i} s_i^2
\end{aligned} \tag{8}$$

We know that:

$$\begin{cases} s_i \geq 0 \rightarrow \operatorname{sign}(s_i) = 1 \rightarrow s_i \operatorname{sign}(s_i) > 0 \\ s_i < 0 \rightarrow \operatorname{sign}(s_i) = -1 \rightarrow s_i \operatorname{sign}(s_i) > 0 \end{cases} \tag{9}$$

Therefore, the derivative of the Lyapunov function in relation (8) is negative and the slip condition is established. The defined slip surface guarantees that in addition to the slip surface, its derivative also converges to zero. As a result, the exponential access condition can be expressed as follows:

$$\begin{aligned}
\ddot{e}_i &= \lambda_{1i} \dot{e}_i + \lambda_{2i} e_i = -\eta_{1i} \operatorname{sgn}(s_i) - \eta_{2i} s_i, \quad (10) \\
i &= 1, 2, \dots, N
\end{aligned}$$

By inserting the second derivative, we have the convergence error in the above relation:

$$\begin{aligned}
\sum_{j=1}^N a_{ij} \left(\frac{u_i}{m_i} + \frac{f_i}{m_i} - \frac{u_j}{m_j} - \frac{f_j}{m_i} \right) + b_i \left(\frac{u_i}{m_i} + \right. \\
\left. \frac{f_i}{m_i} - \frac{u_0}{M_0} \right) + \lambda_{1i} \dot{e}_i + \lambda_{2i} e_i = -\eta_{1i} \operatorname{sgn}(s_i) - \\
\eta_{2i} s_i
\end{aligned} \tag{11}$$

Therefore, the sliding mode control law is derived as follows:

$$U = B^{-1} (-F - K_1 \operatorname{sgn}(S) - K_2 S) \tag{12}$$

where in:

$$F = \begin{bmatrix} -\frac{b_1}{M_0} u_0 + \frac{f_1}{M_1} + \lambda_{11} \dot{e}_1 + \lambda_{21} e_1 \\ -\frac{b_2}{M_0} u_0 + \frac{f_2}{M_1} + \lambda_{12} \dot{e}_2 + \lambda_{22} e_2 \\ \vdots \\ -\frac{b_N}{M_0} u_0 + \frac{f_N}{M_1} + \lambda_{1N} \dot{e}_N + \lambda_{2N} e_N \end{bmatrix} \tag{13}$$

18. DISTURBANCE COMPENSATOR DESIGN

As can be seen in relation (12), the vector function F includes nonlinear functions and the effects of external disturbances of follower dynamics. In this paper, a disturbance compensator is used to estimate these nonlinear effects including uncertainties and external disturbances. For this purpose, first consider the dynamics of the second-order multi agent system as follows:

$$\begin{cases} \dot{x}_1 = x_2 \\ \dot{x}_2 = \frac{f_1}{M_1} + \frac{u_1}{M_1} \end{cases}, \begin{cases} \dot{x}_3 = x_4 \\ \dot{x}_4 = \frac{f_2}{M_2} + \frac{u_2}{M_2} \end{cases}, \dots, \begin{cases} \dot{x}_{N-1} = x_N \\ \dot{x}_N = \frac{f_N}{M_N} + \frac{u_N}{M_N} \end{cases} \tag{14}$$

Now, the nonlinear part including the uncertainty and the effects of external disturbances in the dynamics of each follower is considered as a state variable. In this case, the relation (14) can be rewritten as follows:

$$\begin{cases} \dot{x}_1 = x_2 \\ \dot{x}_2 = z_1 + \frac{u_1}{M_1} \\ \dot{z}_1 = h_1 \end{cases}, \begin{cases} \dot{x}_3 = x_4 \\ \dot{x}_4 = z_2 + \frac{u_2}{M_2} \\ \dot{z}_2 = h_2 \end{cases}, \dots, \begin{cases} \dot{x}_{N-1} = x_N \\ \dot{x}_N = z_N + \frac{u_N}{M_N} \\ \dot{z}_N = h_N \end{cases} \quad (15)$$

where in:

$$\begin{cases} z_1 = \frac{f_1}{M_1} \\ h_1 = \frac{d}{dt} \left(\frac{f_1}{M_1} \right) \end{cases}, \begin{cases} z_2 = \frac{f_2}{M_2} \\ h_2 = \frac{d}{dt} \left(\frac{f_2}{M_2} \right) \end{cases}, \dots, \begin{cases} z_N = \frac{f_N}{M_N} \\ h_N = \frac{d}{dt} \left(\frac{f_N}{M_N} \right) \end{cases} \quad (16)$$

In this case, the dynamic equations of the disturbance estimator for the first follower are described as follows[13]:

$$\begin{aligned} \hat{x}_1(t) &= \hat{x}_2(t) + \frac{\alpha_1}{\beta^3} [\beta^5 (x_1(t) - \hat{x}_1(t))]^\eta \\ \hat{x}_2(t) &= \hat{z}_1(x) + \frac{u_1}{M_1} + \frac{\alpha_2}{\beta} [\beta^5 (x_1(t) - \hat{x}_1(t))]^\eta \\ \hat{z}_1(t) &= \alpha_3 \beta [\beta^5 (x_1(t) - \hat{x}_1(t))]^\eta \end{aligned} \quad (17)$$

And for the second follower, we can write:

$$\begin{aligned} \hat{x}_3(t) &= \hat{x}_4(t) + \frac{\alpha_1}{\beta^3} [\beta^5 (x_3(t) - \hat{x}_3(t))]^\eta \\ \hat{x}_4(t) &= \hat{z}_2(x) + \frac{u_2}{M_2} + \frac{\alpha_2}{\beta} [\beta^5 (x_3(t) - \hat{x}_3(t))]^\eta \\ \hat{z}_2(t) &= \alpha_3 \beta [\beta^5 (x_3(t) - \hat{x}_3(t))]^\eta \end{aligned} \quad (18)$$

And for follower N we will have:

$$\begin{aligned} \hat{x}_{N-1}(t) &= \hat{x}_N(t) + \frac{\alpha_1}{\beta^3} [\beta^5 (x_{N-1}(t) - \hat{x}_{N-1}(t))]^\eta \\ \hat{x}_N(t) &= \hat{z}_N(x) + \frac{u_N}{M_N} + \frac{\alpha_2}{\beta} [\beta^5 (x_{N-1}(t) - \hat{x}_{N-1}(t))]^\eta \\ \hat{z}_N(t) &= \alpha_3 \beta [\beta^5 (x_{N-1}(t) - \hat{x}_{N-1}(t))]^\eta \end{aligned} \quad (19)$$

In the above relationships, β and η are positive design parameters. Furthermore, the relationship is $[\square]^r = |\square|^r \text{sgn}(\square)$. The components of $\alpha_{1,2,3}$ are positive and must be determined in such a way that the matrix $\begin{bmatrix} -\alpha_1 & 1 & 0 \\ -\alpha_2 & 0 & 1 \\ -\alpha_3 & 0 & 0 \end{bmatrix}$ is stable. In this case, the vector function F is rewritten as below:

$$F = \begin{bmatrix} -\frac{b_1}{M_0} u_0 + \hat{z}_1 + \lambda_{11} \dot{e}_1 + \lambda_{21} e_1 \\ -\frac{b_2}{M_0} u_0 + \hat{z}_2 + \lambda_{12} \dot{e}_2 + \lambda_{22} e_2 \\ \vdots \\ -\frac{b_N}{M_0} u_0 + \hat{z}_N + \lambda_{1N} \dot{e}_N + \lambda_{2N} e_N \end{bmatrix} \quad (20)$$

19. EVALUATION OF AMBIGOBOT MULTI-ROBOT ARRANGEMENT CONTROL USING THE PROPOSED METHOD

In the rest of this section, a multi-agent system including a number of mobile robots is explained. As seen in Figure 1, each robot is an AmbigoBots type, the actual view of which is presented in Figure.2[14].

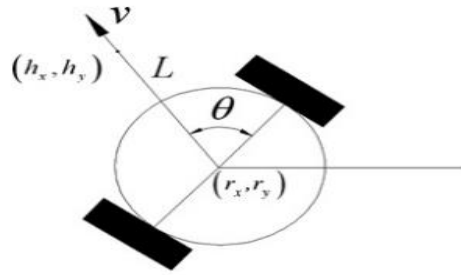


Fig. 1. Schematic view of AmbigoBots non-holonomic differential mobile robot[14].

According to Fig.1, the kinematic equations of each moving robot can be expressed as follows:

$$\begin{aligned} \dot{r}_{xi} &= v_i \cos(\theta_i), \\ \dot{r}_{yi} &= v_i \sin(\theta_i) \\ \dot{\theta}_i &= w_i, \quad i = 1, 2, \dots, N \end{aligned} \tag{21}$$



Fig. 2. A view of AmbigoBots mobile robot multimedia system.

In which, r_{xi} and r_{yi} represent the position of the center of mass of the mobile robot i and θ_i represent its momentary orientation. On the other hand, the position of each follower will be equal to:

$$\begin{bmatrix} h_{xi} \\ h_{yi} \end{bmatrix} = \begin{bmatrix} r_{xi} \\ y_{yi} \end{bmatrix} + L_i \begin{bmatrix} \cos(\theta_i) \\ \sin(\theta_i) \end{bmatrix}, \quad i = 1, 2, \dots, N \tag{22}$$

By deriving equation (22) once, we can write:

$$\begin{bmatrix} \dot{h}_{xi} \\ \dot{h}_{yi} \end{bmatrix} = \begin{bmatrix} v_i \cos(\theta_i) \\ v_i \sin(\theta_i) \end{bmatrix} + L_i w_i \begin{bmatrix} -\sin(\theta_i) \\ \cos(\theta_i) \end{bmatrix}, \quad i = 1, 2, \dots, N \tag{23}$$

In simple terms:

$$\begin{bmatrix} \dot{h}_{xi} \\ \dot{h}_{yi} \end{bmatrix} = \begin{bmatrix} \cos(\theta_i) & -L_i \sin(\theta_i) \\ \sin(\theta_i) & L_i \cos(\theta_i) \end{bmatrix} \begin{bmatrix} v_i \\ w_i \end{bmatrix}, \quad i = 1, 2, \dots, N \tag{24}$$

$$\begin{bmatrix} \dot{h}_{xi} \\ \dot{h}_{yi} \end{bmatrix} = \begin{bmatrix} -w_i \sin(\theta_i) & -L_i w_i \cos(\theta_i) \\ w_i \cos(\theta_i) & -L_i w_i \sin(\theta_i) \end{bmatrix} \begin{bmatrix} v_i \\ w_i \end{bmatrix} + \begin{bmatrix} \cos(\theta_i) & -L_i \sin(\theta_i) \\ \sin(\theta_i) & L_i \cos(\theta_i) \end{bmatrix} \begin{bmatrix} \dot{v}_i \\ \dot{w}_i \end{bmatrix} \tag{25}$$

By deriving the equation (24), we have:

The relation (25) can be written as the following general relation:

$$\begin{bmatrix} \ddot{h}_{xi} \\ \ddot{h}_{yi} \end{bmatrix} = \begin{bmatrix} u_{xi} \\ u_{yi} \end{bmatrix} + \begin{bmatrix} g_{xi} \\ g_{yi} \end{bmatrix}, \quad i = 1, 2, \dots, N \quad (26)$$

where in:

$$\begin{aligned} \begin{bmatrix} u_{xi} \\ u_{yi} \end{bmatrix} &= \begin{bmatrix} \cos(\theta_i) & -L_i \sin(\theta_i) \\ \sin(\theta_i) & L_i \cos(\theta_i) \end{bmatrix} \begin{bmatrix} \dot{v}_i \\ \dot{w}_i \end{bmatrix}, \\ \begin{bmatrix} g_{xi} \\ g_{yi} \end{bmatrix} &= \begin{bmatrix} -w_i \sin(\theta_i) & -L_i w_i \cos(\theta_i) \\ w_i \cos(\theta_i) & -L_i w_i \sin(\theta_i) \end{bmatrix} \begin{bmatrix} v_i \\ w_i \end{bmatrix} \end{aligned} \quad (27)$$

The control rules for solving the problem of the formation of the robotic multi-agent system are briefly mentioned below:

$$\begin{aligned} e_{xi} &= \sum_{j=1}^N a_{ij} (h_{xi} + \Delta_{xi} - h_{xj} - \Delta_{xj}) + b_i (h_{xi} + \Delta_{xi} - h_{x0} - \Delta_{x0}) \\ e_{yi} &= \sum_{j=1}^N a_{ij} (h_{yi} + \Delta_{yi} - h_{yj} - \Delta_{yj}) + b_i (h_{yi} + \Delta_{yi} - h_{y0} - \Delta_{y0}) \end{aligned} \quad (28)$$

$i=1, 2, \dots, N$

By deriving the equation (28), we can write:

$$\begin{cases} \dot{e}_{xi} = \sum_{j=1}^N a_{ij} (\dot{h}_{xi} - \dot{h}_{xj}) + b_i (\dot{h}_{xi} - \dot{h}_{x0}) \\ \dot{e}_{yi} = \sum_{j=1}^N a_{ij} (\dot{h}_{yi} - \dot{h}_{yj}) + b_i (\dot{h}_{yi} - \dot{h}_{y0}) \end{cases} \quad (29)$$

where in:

$$\begin{cases} \dot{h}_{xi} = v_i \cos(\theta_i) - L_i w_i \sin(\theta_i) \\ \dot{h}_{x0} = v_0 \cos(\theta_0) - L_0 w_0 \sin(\theta_0) \\ \dot{h}_{yi} = v_i \sin(\theta_i) + L_i w_i \cos(\theta_i) \\ \dot{h}_{y0} = v_0 \sin(\theta_0) + L_0 w_0 \cos(\theta_0) \end{cases} \quad (30)$$

By re-derivation from the error signals, we have:

$$\begin{cases} \ddot{e}_{xi} = \sum_{j=1}^N a_{ij} (\ddot{h}_{xi} - \ddot{h}_{xj}) + b_i (\ddot{h}_{xi} - \ddot{h}_{x0}) \\ \ddot{e}_{yi} = \sum_{j=1}^N a_{ij} (\ddot{h}_{yi} - \ddot{h}_{yj}) + b_i (\ddot{h}_{yi} - \ddot{h}_{y0}) \end{cases} \quad (31)$$

On the other hand, for the dynamics of follower robots, we can write:

$$\begin{bmatrix} \ddot{h}_{xi} \\ \ddot{h}_{yi} \end{bmatrix} = \begin{bmatrix} u_{xi} \\ u_{yi} \end{bmatrix} + \begin{bmatrix} f_{xi} \\ f_{yi} \end{bmatrix} \quad (32)$$

where in:

$$\begin{bmatrix} f_{xi} \\ f_{yi} \end{bmatrix} = \begin{bmatrix} -v_i w_i \sin(\theta_i) - L_i w_i^2 \cos(\theta_i) \\ v_i w_i \cos(\theta_i) - L_i w_i^2 \sin(\theta_i) \end{bmatrix} \quad (33)$$

Also, for the leader robot, we can write:

$$\begin{bmatrix} \ddot{h}_{x0} \\ \ddot{h}_{y0} \end{bmatrix} = \begin{bmatrix} f_{x0} \\ f_{y0} \end{bmatrix} \quad (34)$$

$$\begin{cases} f_{x0} = u_{x0} - v_0 w_0 \sin(\theta_0) - L_0 w_0^2 \cos(\theta_0) \\ f_{y0} = u_{y0} - v_0 w_0 \cos(\theta_0) - L_0 w_0^2 \sin(\theta_0) \end{cases}$$

Therefore, the second-order dynamics of tracking error signals can be expressed as follows:

$$\begin{aligned} \ddot{e}_{xi} &= \sum_{j=1}^N a_{ij} (u_{xi} + f_{xi} - u_{xj} - f_{xj}) + b_i (u_{xi} + f_{xi} - f_{x0}) \\ \ddot{e}_{yi} &= \sum_{j=1}^N a_{ij} (u_{yi} + f_{yi} - u_{yj} - f_{yj}) + b_i (u_{yi} + f_{yi} - f_{y0}) \end{aligned} \quad (35)$$

The relative degree of error dynamics compared to the control signals is of the first order, so the slip levels are defined as follows:

$$\begin{bmatrix} \dot{s}_{xi} \\ \dot{s}_{yi} \end{bmatrix} = \begin{bmatrix} \ddot{e}_{xi} + \lambda_{1i} \dot{e}_{xi} + \lambda_{2i} e_{xi} \\ \ddot{e}_{yi} + \lambda_{1i} \dot{e}_{yi} + \lambda_{2i} e_{yi} \end{bmatrix} \quad (36)$$

Based on the access condition, we can write:

$$\begin{aligned} \sum_{j=1}^N a_{ij} (u_{xi} + f_{xi} - u_{xj} - f_{xj}) + b_i (u_{xi} + f_{xi} - f_{x0}) + \lambda_{1i} \dot{e}_{xi} + \lambda_{2i} e_{xi} &\leq -\eta_i \operatorname{sgn}(s_{xi}) \\ \sum_{j=1}^N a_{ij} (u_{yi} + f_{yi} - u_{yj} - f_{yj}) + b_i (u_{yi} + f_{yi} - f_{y0}) + \lambda_{1i} \dot{e}_{yi} + \lambda_{2i} e_{yi} &\leq -\eta_i \operatorname{sgn}(s_{yi}) \end{aligned} \quad (37)$$

In the matrix form, the relation $BU + F \leq -\Gamma \operatorname{sgn}(S)$ is obtained in which:

$$F = \begin{bmatrix} -b_1 f_{x0} + (a_{12} + a_{13} + \dots + a_{1N} + b_1) f_{x1} - a_{12} f_{x2} - \dots - a_{1N} f_{xN} + \lambda_{11} \dot{e}_{x1} + \lambda_{21} e_{x1} \\ -b_1 f_{y0} + (a_{12} + a_{13} + \dots + a_{1N} + b_1) f_{y1} - a_{12} f_{y2} - \dots - a_{1N} f_{yN} + \lambda_{11} \dot{e}_{y1} + \lambda_{21} e_{y1} \\ -b_2 f_{x0} + (a_{21} + a_{23} + \dots + a_{2N} + b_2) f_{x1} - a_{21} f_{x2} - \dots - a_{2N} f_{xN} + \lambda_{12} \dot{e}_{x2} + \lambda_{22} e_{x2} \\ -b_2 f_{y0} + (a_{21} + a_{23} + \dots + a_{2N} + b_2) f_{y1} - a_{21} f_{y2} - \dots - a_{2N} f_{yN} + \lambda_{12} \dot{e}_{y2} + \lambda_{22} e_{y2} \\ \vdots \\ f_{x0} + (a_{N1} + a_{N2} + \dots + a_{NN-1} + b_N) f_{x1} - a_{N2} f_{x2} - \dots - a_{NN-1} f_{xN-1} + \lambda_{1N} \dot{e}_{xN} + \lambda_{2N} e_{xN} \\ f_{y0} + (a_{N1} + a_{N2} + \dots + a_{NN-1} + b_N) f_{y1} - a_{N2} f_{y2} - \dots - a_{NN-1} f_{yN-1} + \lambda_{1N} \dot{e}_{yN} + \lambda_{2N} e_{yN} \end{bmatrix} \quad (38)$$

$$U = \begin{bmatrix} u_{x1} \\ u_{y1} \\ \vdots \\ u_{xN} \\ u_{yN} \end{bmatrix}, S = \begin{bmatrix} s_{x1} \\ s_{y1} \\ \vdots \\ s_{xN} \\ s_{yN} \end{bmatrix}, \Gamma = \operatorname{diag}(\eta_{x1}, \eta_{y1}, \eta_{x2}, \eta_{y2}, \dots, \eta_{xN}, \eta_{yN}) \quad (39)$$

$B =$

$$\begin{bmatrix} \alpha_1 & 0 & -a_{12} & 0 & -a_{13} & 0 & \dots & -a_{1N} & 0 \\ 0 & \alpha_1 & 0 & -a_{12} & 0 & -a_{13} & \dots & 0 & -a_{1N} \\ -a_{21} & 0 & \alpha_2 & 0 & -a_{23} & 0 & \dots & -a_{2N} & 0 \\ 0 & -a_{21} & 0 & \alpha_2 & 0 & -a_{23} & \dots & 0 & -a_{2N} \\ \vdots & \vdots & \vdots & \ddots & \vdots & \vdots & \dots & \vdots & \vdots \\ -a_{N1} & 0 & -a_{N2} & 0 & -a_{N3} & 0 & \dots & \alpha_N & 0 \\ 0 & -a_{N1} & 0 & -a_{N2} & 0 & -a_{N3} & \dots & 0 & \alpha_N \end{bmatrix}$$

As a result, the control rules for each follower are obtained as follows:

$$U = B^{-1}(-F - K \operatorname{sgn}(S)) \quad (40)$$

For the robotic system including one leader and four followers, the control parameters are considered as follows:

$$\lambda_1 = 8, \lambda_2 = 16, \eta_1 = 0.01, \eta_2 = 1.5, \alpha_1 = 15, \alpha_2 = 75, \alpha_3 = 125, \beta = 2, \eta = 0.8, \mu = 0.002$$

The same communication topology as the second-order multi agent system is considered. As seen in Fig. 3 and Fig. 4, the follower robots are located at a certain relative distance from the leader robot and follow the leader's dynamic behavior with high performance accuracy. This problem can be better understood especially in the formation presented in two-dimensional space. The control signals in Figure 6 have a large amplitude in the start-up conditions and no chattering effect is observed in them. Figure 7 and Figure 8 show that the disturbance compensator is well able to estimate the nonlinear effects of follower dynamics. The course of the switching gain changes is also presented in Figure 9, which is their time-varying nature due to their dependence on the slip surfaces.

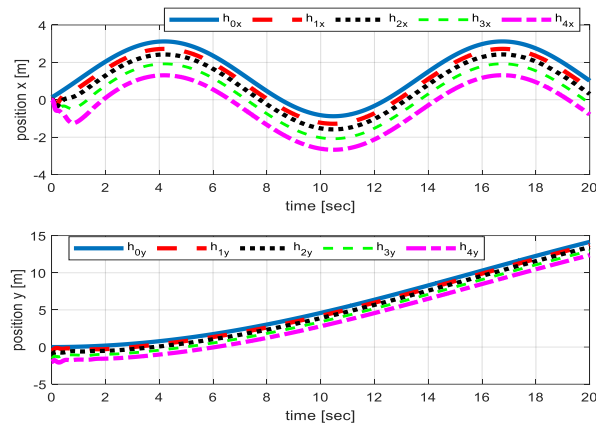


Fig. 3. Robotic system arrangement control using adaptive sliding mode control based on disturbance compensator.

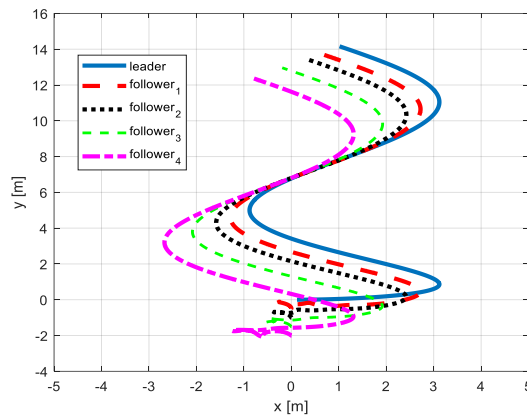


Fig.4. Robotic system arrangement control in two-dimensional space using adaptive sliding mode control based on disturbance compensator.

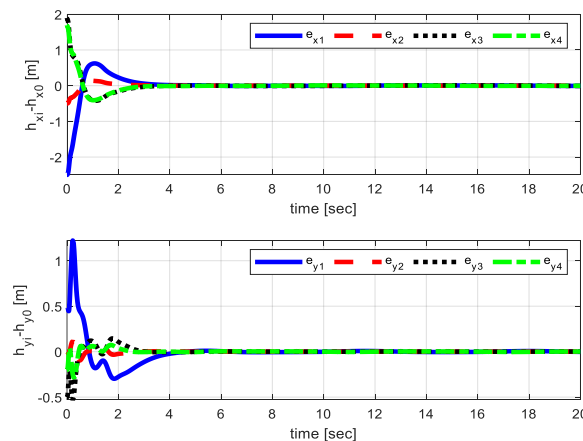


Fig.5. Robotic system alignment error using adaptive sliding mode control based on disturbance compensator.

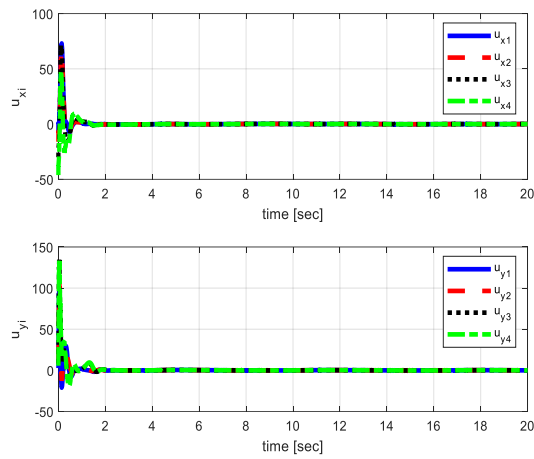


Fig. 6. Control signals for starting robotic system using adaptive sliding mode control based on disturbance compensator.

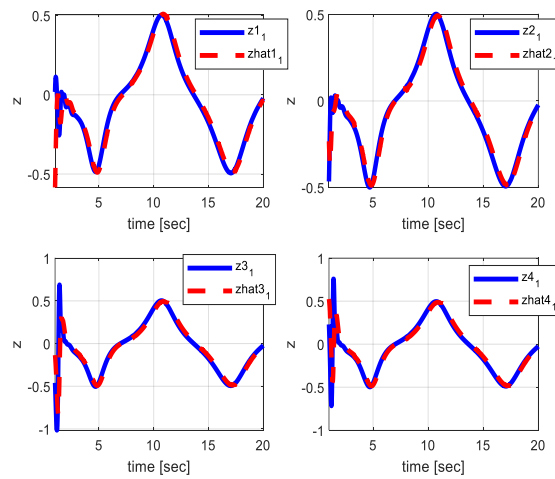


Fig. 7. Estimation of the first component of the nonlinear part of robot dynamics using the disturbance compensator.

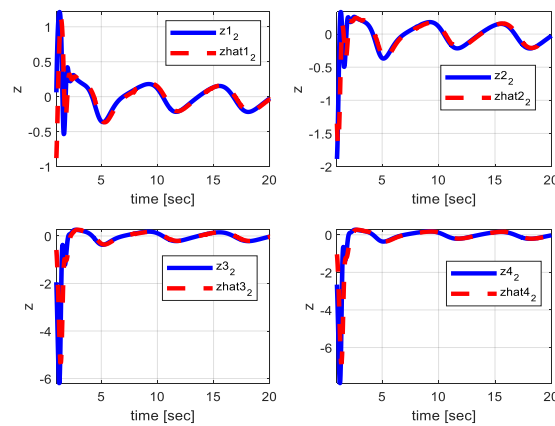


Fig.8. Estimation of the second component of the non-linear part of robot dynamics using the disturbance compensator.

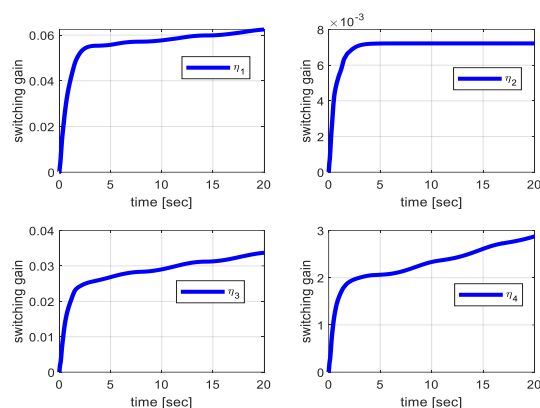


Fig. 9. The course of control gains changes with the help of switching gain adaptive algorithm.

20. COMPARISON OF RESULTS WITH REFERENCE PAPER

In this section, a comparison has been made according to the proposed method and the reference article [13], and the following results have been obtained:

In the proposed method, the movement path of the robots is much more complicated than Zhang's method, and also four robot followers are considered, while in Zhang's method, there are two followers. Observer error is much less in the proposed method. To estimate the path of the followers, the error of the proposed method is less, while in Zhang's method, the path reaches the correct value by spending a lot of time and energy.

21. CONCLUSION

In this paper, the main goal was to realize the control of the arrangement of multi-agent robots with the help of the adaptive sliding mode control approach based on the disturbance compensator. Based on this, first, the dynamic equations of the leader-follower of the robotic multi-agent system were presented. Then, considering the direct topology and a communication graph between the agents with each other and the agents with the leader, the way to formulate the classical sliding mode control rules for robots was stated. To solve the chattering problem, the sliding mode control strategy based on the exponential access condition was used. In addition, the structure of disturbance compensator for instantaneous estimation of nonlinear effects including uncertainty and external disturbances was explained analytically. Also, an adaptive algorithm was derived for instantaneous estimation of switching gain in control rules. In evaluating the performance of the proposed algorithm, it can be stated that the control approach presented in this research is able to realize the multi-agent arrangement in the presence of uncertainty by eliminating the chattering phenomenon. In this paper, sliding mode control method based on adaptive viewer was used to remove chattering and disturbances. As a suggestion, we can consider obstacles in the path of the agents, in this situation, all the agents should communicate with the leader and share their information with the leader, and the leader should use another path to avoid the obstacles by consensus with all the followers.

REFERENCES

- [1] H. Du and S. Li, 'Attitude synchronization for flexible spacecraft with communication delays', *IEEE Transactions on Automatic Control*, vol. 61, no. 11, pp. 3625–3630, 2016.
- [2] Z. Zhang, Y. Zheng, X. Xiao, and W. Yan, 'Improved order-reduction method for cooperative tracking control of time-delayed multi-spacecraft network', *Journal of the Franklin Institute*, vol. 355, no. 5, pp. 2849–2873, 2018.
- [3] P. Li, 'Global finite-time attitude consensus tracking control for a group of rigid spacecraft', *International Journal of Systems Science*, vol. 48, no. 13, pp. 2703–2712, 2017.
- [4] I. Shames, B. Fidan, and B. D. O. Anderson, 'Close target reconnaissance with guaranteed collision avoidance', *International Journal of Robust and Nonlinear Control*, vol. 21, no. 16, pp. 1823–1840, 2011.
- [5] B. D. O. Anderson, B. Fidan, C. Yu, and D. Walle, 'Uav formation control: Theory and application', in *Recent Advances in Learning and Control*, V. D. Blondel, S. P. Boyd, and H. Kimura, Eds., London: Springer London, 2008, pp. 15–33, ISBN: 978-1-84800-155.
- [6] D. van der Walle, B. Fidan, A. Sutton, Changbin Yu, and B. D. O. Anderson, 'Non-hierarchical uav formation control for surveillance tasks', *American Control Conf.*, pp. 777–782, 2008.
- [7] K. Guo, X. Li, and L. Xie, 'Ultra-wideband and odometry-based cooperative relative localization with application to multi-uav formation control', *IEEE Transactions on Cybernetics*, pp. 1–14, 2019.
- [8] W. Ren and Y. Cao, 'Distributed coordination of multi-agent networks: emergent problems, models, and issues'. *Springer Science & Business Media*, 2010.

- [9] V. E. Pryanichnikov, A. A. Ayskin, S. R. Eprikov, K. B. Kirsanov, R. V. Khelemendik, A. Y. Ksenzenko, E. A. Prysev, and A. S. Travushkin, ‘**Technology of multi-agent control for industrial automation with logical processing of contradictions**’, *Annals of D.*
- [10] V. N. Coelho, M. W. Cohen, I. M. Coelho, N. Liu, and F. G. Guimarães, ‘**Multi-agent systems applied for energy systems integration: State-of-the-art applications and trends in microgrids**’, *Applied Energy*, vol. 187, pp. 820–832, 2017.
- [11] O. J. Shukla, A. Joshi, G. Soni, and R. Kumar, ‘**Analysis of critical drivers affecting implementation of agent technology in a manufacturing system**’, *Journal of Industrial Engineering International*, vol. 15, no. 2, pp. 303–313, 2019.
- [12] H. Du, M., Zhao, D., Yang, M., & Chen, “**Nonlinear extended state observer-based output feedback stabilization control for uncertain nonlinear half-car active suspension systems.**” *Nonlinear Dyn.*, vol. 100, pp. 2483–2503, 2020.
- [13] Du, M., Zhao, D., Yang, M., & Chen, H,” **Nonlinear extended state observer-based output feedback stabilization control for uncertain nonlinear half-car active suspension systems**”, *Nonlinear Dynamics*, Vol.100, No.3, pp.2483-2503, 2020.
- [14] Zhao, D., Zou, T., Li, S., & Zhu, Q, ‘**Adaptive backstepping sliding mode control for leader–follower multi-agent systems**’, *IET control theory & applications*, Vol.6, No.8, pp.1109-1117, 2012.

Effect of Absorption Coefficients in Upper Efficiency Limit of Intermediate Band Solar Cells

Mohammad R. Ershadi¹ 

1- Islamic Azad University, Isfahan Branch/Faculty of Skills and Entrepreneurship, Isfahan, Iran.
Email: ershadimr@yahoo.com (Corresponding author)

ABSTRACT:

In this paper, the idea of an intermediate band solar cell which increases the efficiency of solar cells is considered. By using quantum dots the idea of intermediate band solar cell can be achieved at an acceptable level. Actual results of using quantum dots have led to decreased efficiency of solar cells. The effect of absorption coefficients on the upper limit of efficiency in special types of solar cells is the focus of this paper. The main factors that have the most impact on the upper limit of efficiency of our position of intermediate bands and consequently the structure of quantum dots are analyzed. Furthermore, the changes in cell characteristics, quantum dot type, quantum dot structure, and even polarization of the incident light can change the upper limit of efficiency. Changes in distance layers of quantum dots create different results for different polarization of light for the upper limit of efficiency. Using the results of this research can be a way to new research in the field of solar cells with quantum dots and the optimum use of solar cells will be useful..

KEYWORDS: Band Position, Detailed Balance Theory, Output Power Reduction, IBSC.

22. INTRODUCTION

One of the most important methods for increasing the efficiency of solar cells is the application of the intermediate bands because of increasing of output current by absorption of photons with energies below the band gap. By using this technique, the upper limit of efficiency, based on detailed balance theory, is increased from about 40% [1] for the solar cell without an intermediate band to about 60% with one intermediate band [2]. This significant rise has attracted the attention of many researchers. One of the major challenges of this research is the realization of the intermediate band. Some ways to create intermediate band gap energy of the semiconductor solar cell substrate include creating special doping with appropriate energy balance [3-5], quantum wells [6-8], quantum dots [9-12], and highly mismatching alloys [13-15]. However, the creation of energy levels due to the special doping with appropriate energy balance because of low level of concentration does not have the characteristics of a band and despite allowing the absorption of low energy photons does not guarantee a dramatic increase in performance. Using quantum dots is preferable to quantum wells because, in addition to the isotropic nature of the incoming light, the quantization of energy levels in quantum dots is in three dimensions while in quantum wells is in one dimension. Highly mismatched alloys, with convenient features that make the intermediate band, their presence does not cause a dramatic increase in performance. As a result, it appears that the proposed methods achieve an intermediate band using quantum dots that can be a further increase in performance. In the first research, (for example [16]) actual results of using quantum dots were against the expected results because these changes caused to decrease the solar cell efficiency. This reduction is contrary to the goals of the researchers then they decided to examine the reasons for this occurrence. Along with this research, attention was paid to the absorption of photons in these structures, because in addition to solar cells [17-18], have a main effect on the photo-detectors [19-20]. Luque et al proposed a model for the transfer of the central bands of bound states in a solar cell for calculating the absorption coefficient [21]. Luque with regard to the transition between the intermediate band and conduction band completed the previous research [22].

Paper type: Research paper

<https://doi.org/>

Received: 8 June 2024; revised: 14 July 2024; accepted: 17 August 2024; published: 1 September 2024

How to cite this paper: M. R. Ershadi, “**Effect of Absorption Coefficients in Upper Efficiency Limit of Intermediate Band Solar Cells**”, *Majlesi Journal of Telecommunication Devices*, Vol. 13, No. 3, pp. 183-189, 2024.

The structure of this paper is as follows. In sections 2 and 3, the absorption coefficient calculation method and the upper efficiency limit of this type of solar cell are explained. At the end, the results of our work are presented.

23. THEORETICAL BACKGROUND

The relationship between photon absorption coefficients in an absorbing layer containing quantum dots is as follows [23]:

$$\alpha(E) = \frac{2\pi^2 e^2 E}{n_{ref} ch \epsilon_0} \times \frac{|\langle \psi | r \cdot \epsilon | \psi' \rangle|^2}{S} \times FN_l \delta(E - E_{line}) \quad (1)$$

Where E is the photon energy, ϵ is the light polarization vector, n_{ref} is the refractive index of the medium, F is the fractional coverage of the surface with QDs, N_l is the number of QD layers per unit length, S is the Effective cross-sectional area of each quantum dot, and E_{line} is the energy difference between the two states. It should be noted that the density of quantum dots is equal to FN_l / S [23]. δ represents the effect of the statistical distribution dimensions of the quantum dots that is variable and is expressed as a Gaussian [22]:

$$\delta(E - E_{line}) \cong \frac{1}{\sigma\sqrt{\pi}} \exp\left(-\frac{(E-E_{line})^2}{\sigma^2}\right) \quad (2)$$

Where, σ represents the energy dispersion. This dispersion depends on the regularity of the sample, although the integrated values are independent of s . The energy dispersion has been set to 0.025 eV. In addition, $|\langle \psi | \epsilon \cdot r | \psi' \rangle|^2$ expression in equation (1) is called a square matrix element and ψ and ψ' , respectively, are the normalized wave functions of the first and last state.

The pin solar cell structure in this study is the structure of quantum dots on the i region. To calculate the absorption coefficient of the i -only cells containing quantum dots have been satisfied. The i -type GaAs semiconductor material and quantum dots made of $In_{1-x}Ga_xAs$ are assumed. The number and location of the intermediate bands in addition to the size of the quantum dots and the distance between them, by changing the mole fraction x can be changed.

For ease of calculation, the cubic model for quantum dots inside the region of i will be considered. Similar to the method presented in [22], the solution of the Schrödinger equation in quantum wells in three dimensions of the cube and the emergence of wave functions and continuity of the first derivative of the border, inside and outside the energy levels and wave functions of quantum dots are calculated.

To evaluate the effect of polarization in the calculation of absorption coefficients and ultimately upper limit of the efficiency, five different modes of light polarization are considered.

Assuming that the cells are in the z -direction, these five polarization states of light are:

- 1- Z Unpolarized Beam: In this case, the light emitted in the direction z and the light polarization vector that is perpendicular to the light beam can have any direction in the xy plane.
- 2- Y-Polarized Z-Beam: The light emitted in the direction of z and y is a vector in the direction of polarization of light.
- 3- X Unpolarized Beam: The light emitted in the direction of x and light polarization vector can have any direction in the yz plane.
- 4- Y-Polarized X-Beam: The light emitted in the direction of x and y is a vector in the direction of polarization of light.
- 5- Z-Polarized X-Beam: The light emitted in the direction of x and z is a vector in the direction of polarization of light.

To establish the effect of light polarization with respect to the Euler angles (φ, θ) we have defined:

$$r = xi + yj + zk \quad (3)$$

$$\epsilon = (\cos \varphi \sin \theta)i + (\sin \varphi \sin \theta)j + (\cos \theta)k \quad (4)$$

Therefore:

$$\begin{aligned} |\langle \psi | \epsilon \cdot r | \psi' \rangle|^2 &= \cos^2 \varphi \sin^2 \theta |\langle \psi | x | \psi' \rangle|^2 \\ + \sin^2 \varphi \sin^2 \theta |\langle \psi | y | \psi' \rangle|^2 &+ \cos^2 \theta |\langle \psi | z | \psi' \rangle|^2 \end{aligned} \quad (5)$$

According to [22], we can see that a necessary condition for the transition between two energy levels of quantum numbers is only the change of one direction x, y, or z, and other quantum numbers are unchanged. Also, due to the resulting wave functions are simply shown:

$$D_t = |\langle \psi | t | \psi' \rangle| = \int_{-l}^l \psi_t^* t \psi_t' dt =$$

$$A_n B_m \left(\frac{1}{(k_m + k_n)^2} \sin(l(k_m + k_n)) - \frac{l}{k_m + k_n} \cos(l(k_m + k_n)) \right) +$$

$$A_n B_m \left(\frac{1}{(k_m - k_n)^2} \sin(l(k_m - k_n)) - \frac{l}{k_m - k_n} \cos(l(k_m - k_n)) \right) \quad (6)$$

Thus we have:

$$|\langle \psi | \varepsilon \cdot r | \psi' \rangle|^2 = \cos^2 \varphi \sin^2 \theta \times D_x^2 +$$

$$\sin^2 \varphi \sin^2 \theta \times D_y^2 + \cos^2 \theta \times D_z^2 \quad (7)$$

Radiated photon polarization can be different and the latter is obtained by averaging the results. Square matrix element can thus be written as follows:

$$|\langle \psi | \varepsilon \cdot r | \psi' \rangle|^2 = \cos^2 \varphi \sin^2 \theta |\langle \psi | x | \psi' \rangle|^2 +$$

$$\sin^2 \varphi \sin^2 \theta |\langle \psi | y | \psi' \rangle|^2 + \cos^2 \theta |\langle \psi | z | \psi' \rangle|^2$$

$$= A |\langle \psi | x | \psi' \rangle|^2 + B |\langle \psi | y | \psi' \rangle|^2 + C |\langle \psi | z | \psi' \rangle|^2 \quad (8)$$

For all authorized transactions and considering the quantum numbers of each of the energy levels, the coefficients of the matrix elements for the above five types of polarization are shown in Table 1. As can be seen in terms of what quantum number has changed, the coefficients of these 5 modes of polarization are obtained based on the above table. Also, a necessary condition for the transition between the two bands is the change of x or y or z quantum numbers, and transfer to a band is allowed so that the parity of its quantum number is different with respect to the parity of the source band. Thus, as seen in the following table, if the parity of the source band is odd the parity of the destination band is even and vice versa.

The fullness of the intermediate band is effective in the evaluation of the absorption coefficient, so the two modes as [22] have been considered:

In the first case with the FF = 1 in the charts, the lowest intermediate band is half-filled, and other bands are assumed to be empty.

In the latter case with the FF = 2 in the charts, the lowest intermediate band is completely filled and the first excited energy levels are assumed to be half full and others empty.

Using the absorption coefficient obtained, we can obtain the probability of absorption. Absorption probability is equal to the product of the absorption coefficient on the distance traveled by light in the cell. By considering the size of the cell and the path traveled by light photons inside the cell, we can specify the length of the path traveled by the photon, and with it, the probability of photon absorption can be achieved.

24. CALCULATION METHOD

To calculate the upper limit of efficiency based on detailed balance theory and according to [24], the model of Fig. 1 for a cell with three intermediate bands is considered. Obviously, it will be extended to more or less the intermediate band.

In this circuit model, two circuit elements can be seen: the diode and the current source. The current source is used for the production of light by absorption of photons by transmission between the source and destination bands, and the diode is used to show the flow of the radiative recombination (the only mechanism permitted to recombination in detailed balance theory). By changing the place of the intermediate bands, the distance between the energy levels and therefore the production and radiative recombination currents will be changed.

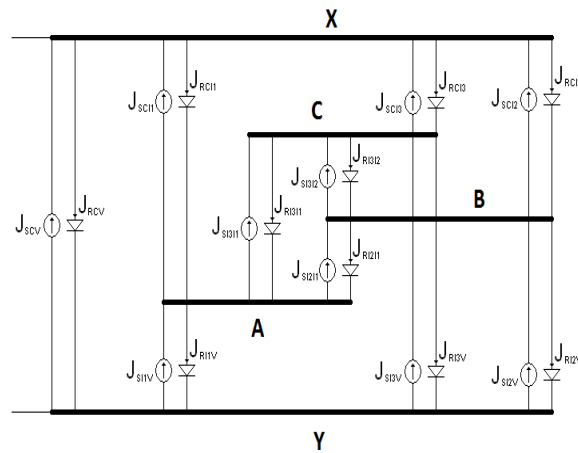


Fig. 1. The equivalent circuit model to simulate the solar cell with three intermediate bands.

To calculate the maximum efficiency for specific locations for intermediate bands, the production and recombination currents at nodes X and Y are calculated and the minimum current as a result of the current production of solar cells has been considered, and finally, the upper limit on the maximum power output and efficiency are achieved.

25. RESULTS AND DISCUSSION

The dimensions of Quantum dots in the direction of x and y (perpendicular to the main cell) are identical and 5.8 nm and for z-direction, it is assumed 3.5 nm. Also, the distance between the quantum dots in the directions x and y is identical to 20 nm and for z direction, between 20 to 300 nm is assumed. The distance between quantum dots along z, actually is the distance between the layers of quantum dots, and its change, due to the limited length of the cell, changes the number of layers of quantum dots. By creating layers of quantum dots, the distance between quantum dots in the direction of solar cell growth from a practical point is specific and dependent on the solar cell manufacturing process and cannot be involved in it, but by assuming that this distance can be changed, calculation of absorption coefficient is done until the impact of possible changes in the distance between the layers of the quantum dots in the upper limit of efficiency may be shown in its simplest form. In addition, the mole fraction for the material of quantum dots is assumed to be zero. To prove the validity of the method of calculation that is used, the absorption coefficient between the intermediate bands of the conduction region is calculated. The following curves show the variation of the absorption coefficient between intermediate bands of the conduction region for different polarization light. As be seen, the results with the results presented in [22] shown in Fig. 4 are similar well, and the validity of computational method is proved.

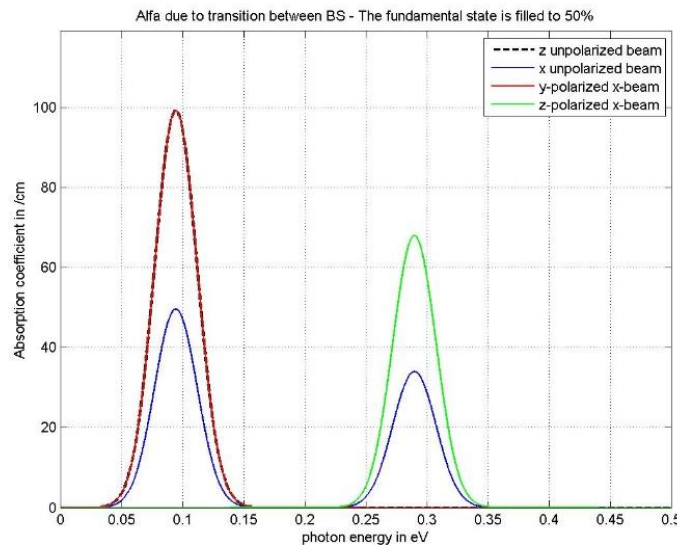


Fig. 2. Changes in the absorption coefficient between intermediate bands of conduction region for FF = 1.

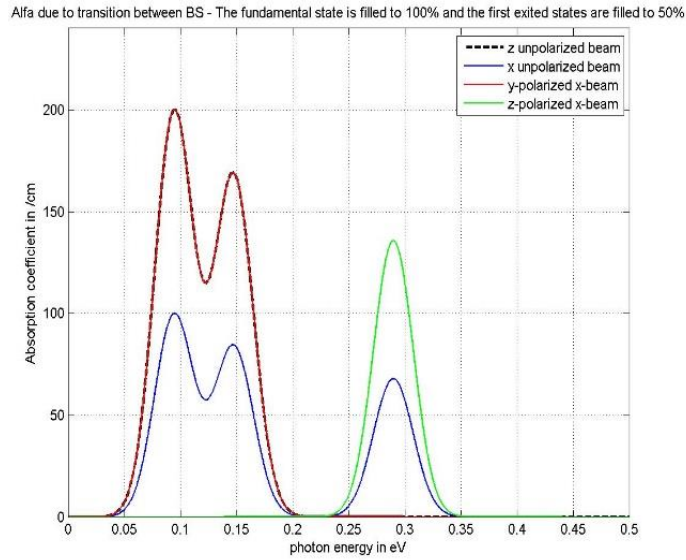


Fig. 3. Changes in the absorption coefficient between intermediate bands of conduction region for FF = 2.

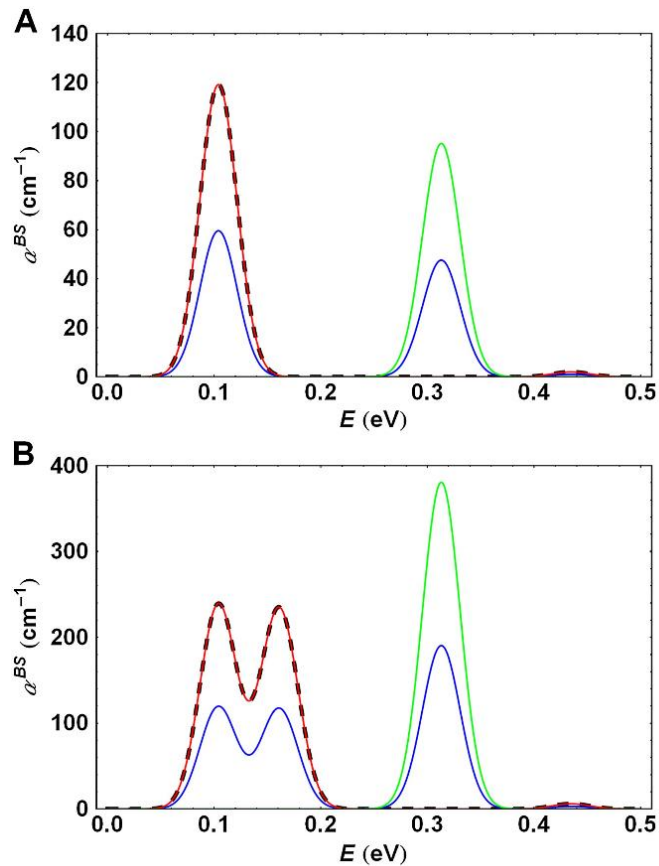


Fig. 4. The curve of the variation for absorption coefficient between the intermediate bands borrowed from [22]

To evaluate the effect of distance between quantum dot layers, we change the L_c parameter, which shows the period in z-direction or direction of light radiation, and for comparison, the sum of absorption coefficient in all desired energy spectrums is calculated and compared with each other.

Results are shown in the following figure:

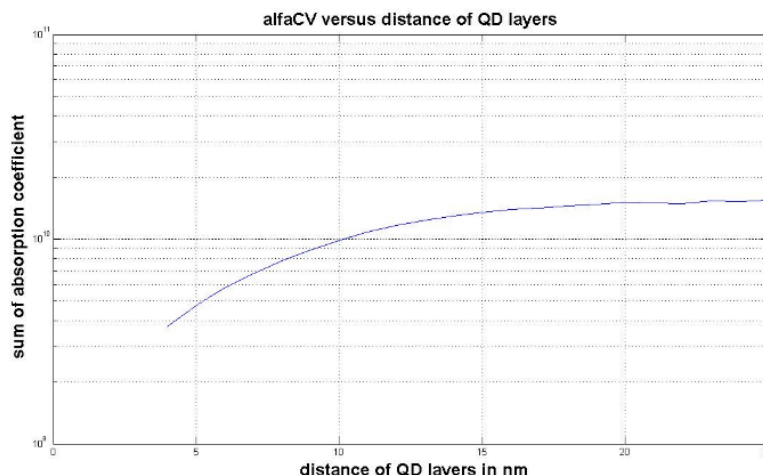


Fig. 5. Changes in the absorption coefficient per changes between quantum dot layers

As can be seen from the above figure, increasing the distance between quantum dot layers causes an increase in the absorption coefficient and follows the increasing efficiency of the solar cell.

Adding quantum dot layers to create intermediate bands in solar cells, results in the absorption of sub-bandgap photons on one hand, but on the other hand, follows the reduction of absorption coefficient in the transition between conduction bands and valance bands.

Therefore, we must balance the place of adding quantum dot layers and the number of them on one hand and the absorption coefficient in the transition between conduction and valance bands on the other hand.

REFERENCES

- [15] Shockley W. & Queisser H. J. “Detailed balance limit of efficiency of p-n junction solar cells”. J. Appl. Phys. 32, 510-519 (1961).
- [16] Luque A. & Martí A. “Increasing the efficiency of ideal solar cells by photon induced transitions at intermediate levels”. Phys. Rev. Lett. 78, 5014-5017 (1997).
- [17] J. Bruns, W. Seifert, P. Wawer, H. Winnicke, D. Braunig, and H. Wagemann, “Improved efficiency of crystalline silicon solar cells due to he+ implantation”. Applied Physics Letters, vol. 64, no. 20, pp. 2700–2, 1994.
- [18] M. J. Keevers and M. A. Green, Sol. Energy Mater. Sol. Cells 41 195 (1996).
- [19] H. Kasai, T. Sato, and H. Matsumura, “Impurity photovoltaic effect in crystalline silicon solar cells”, in Conference Record of the Twenty Sixth IEEE Photovoltaic Specialists Conference - 1997 (Cat. No.97CB36026), 1997, pp. 215–18.
- [20] S. P. Bremner, R. Corkish, and C. B. Honsberg, “Detailed balance efficiency limits with quasi-fermi level variations”, IEEE Transactions on Electron Devices, vol. 46, no. 10, pp. 1932–9, 1999.
- [21] L M. Green, “Prospects for photovoltaic efficiency enhancement using low-dimensional structures”. Nanotechnology, vol. 11, no. 4, pp. 401–5, 2000.
- [22] K. Barnham, B. Braun, J. Nelson, M. Paxman, C. Button, J. Roberts, and C. Foxon, “Short-circuit current and energy efficiency enhancement in a low-dimensional structure photovoltaic device”, Applied Physics Letters, vol. 59, no. 1, pp. 135–7, 1991.
- [23] A. Martí, L. Cuadra, and A. Luque, “Quantum dot intermediate band solar cell”, in Conference Record of the Twenty-Eighth IEEE Photovoltaic Specialists Conference, Anchorage, AK, USA, 2000, pp. 940–3.
- [24] A. Martí, E. Antolín, C. Stanley, C. Farmer, N. López, P. Díaz, E. Cánovas, P. Linares, and A. Luque, “Production of photocurrent due to intermediate-to-conduction-band transitions: A demonstration of a key operating principle of the intermediate-band solar cell”, Physical Review Letters, vol. 97, no. 24, pp. 247 701/1–4, 2006.
- [25] A. G. Norman, M. C. Hanna, P. Dippo, D. H. Levi, R. C. Reedy, J. S. Ward, and M.M. Al-Jassim, “InGaAs/GaAs QD superlattices: MOVPE growth, structural and optical characterization, and application in intermediate-band solar cells”, in Conference Record of the 31st IEEE Photovoltaic Specialists Conference, Orlando, FL, USA, 2005, pp. 43–8.
- [26] M. Y. Levy and C. Honsberg, “Nanostructured absorbers for multiple transition solar cells”, IEEE Transactions on Electron Devices, vol. -, no. -, p. in print, 2008.
- [27] K. Yu, W. Walukiewicz, J.W. Ager III, D. Bour, R. Farshchi, O. Dubon, S. Li, I. Sharp, and E. Haller, “Multiband GaNAsP quaternary alloys”, Applied Physics Letters, vol. 88, no. 9, p. 092110, 2006.
- [28] W. Shan, W. Walukiewicz, J.W. Ager III, E. Haller, J. Geisz, D. Friedman, J. Olson, and S. Kurtz, “Band anticrossing in gannas alloys”, Physical Review Letters, vol. 82, no. 6, pp. 1221 – 4, 1999.

- [29] W. Walukiewicz, K. Yu, J. Wu, J.W. Ager III, W. Shan, M. Scapulla, O. Dubon, and P. Becla, “**Highly mismatched alloys for intermediate band solar cells**”, Thin-Film Compound Semiconductor Photovoltaics. Symposium (Materials Research Society Symposium Proceedings Vol.865), pp. 125–30, 2005.
- [30] Luque, A., and Steven Hegedus. “**Handbook of Photovoltaic Science and Engineering**”. Chichester, West Sussex, U.K.: Wiley, 2011. Print.
- [31] Martí A, Cuadra L, Luque A. “**Quantum dot intermediate band solar cell**”. IEEE: Proc. 28th IEEE Photovoltaics Specialists Conference, New York, 2000.
- [32] Luque A, Martí A, Stanley C, López N, Cuadra L, Zhou D, Mc-Kee A. “**General equivalent circuit for intermediate band devices: potentials, currents and electroluminescence**”. Journal of Applied Physics 2004; 96(1): 903–909.
- [33] Berryman KW, Lyon SA, Segev M. “**Mid-infrared photoconductivity in InAs quantum dots**”. Applied Physics Letters 1997; 70(14): 1861–1863.
- [34] Liu HC, Duboz JY, Dudek R, Wasilewski ZR, Fafard S, Finnie P. “**Quantum dot infrared photodetectors**”. Physica E: Low-dimensional Systems and Nanostructures 2003; 17: 631–633.
- [35] Luque A, Martí A, Antolin E, Garcia-Linares P. “**Intraband absorption for normal illumination in quantum dot intermediate band solar cells**”. Solar Energy Materials and Solar Cells 2010; 94: 2032–2035.
- [36] Luque A, Martí A, Mellor A, Fuertes Marron D, Tobias I & Antolin E. “**Absorption coefficient for the intraband transitions in quantum dot materials**”. Prog. Photovolt: Res. Appl. (2012);
- [37] Luque A, Martí A, Antolín E, Linares PG, Tobias I, Ramiro I, Hernandez E. “**New Hamiltonian for a better understanding of the quantum dot intermediate band solar cells**”. Solar Energy Materials and Solar Cells 2011; 95(8): 2095–2101.
- [38] Nozawa T. & Arakawa Y. “**Detailed balance limit of the efficiency of multilevel intermediate band solar cells**”. Appl. Phys. Lett. 98, 171108 (2011).